NAVAL POSTGRADUATE SCHOOL
Monterey, California

THESIS

INVESTIGATION OF HIGH FREQUENCY
SHIP RADAR CROSS SECTION REDUCTION
BY MEANS OF SHAPING

by

Dimitrios Kouteas

September 1998

Thesis Advisor: David C. Jenn
Co-Advisor: David D. Cleary

Approved for public release; distribution is unlimited.

19980825 018

REPORT DOCUMENTATION PAGE

Form Approved
OMB No. 0704-0188

Public reporting burden for this collection of information is estimated to average 1 hour per response, including the time for reviewing instruction, searching existing data sources, gathering and maintaining the data needed, and completing and reviewing the collection of information. Send comments regarding this burden estimate or any other aspect of this collection of information, including suggestions for reducing this burden, to Washington headquarters Services, Directorate for Information Operations and Reports, 1215 Jefferson Davis Highway, Suite 1204, Arlington, VA 22202-4302, and to the Office of Management and Budget, Paperwork Reduction Project (0704-0188) Washington DC 20503.

1. AGENCY USE ONLY *(Leave blank)*	2. REPORT DATE September 1998	3. REPORT TYPE AND DATES COVERED Master's Thesis

4. TITLE AND SUBTITLE INVESTIGATION OF HIGH FREQUENCY SHIP RADAR CROSS SECTION REDUCTION BY MEANS OF SHAPING	5. FUNDING NUMBERS
6. AUTHOR(S) Kouteas, Dimitrios	

7. PERFORMING ORGANIZATION NAME(S) AND ADDRESS(ES) Naval Postgraduate School Monterey, CA 93943-5000	8. PERFORMING ORGANIZATION REPORT NUMBER

9. SPONSORING / MONITORING AGENCY NAME(S) AND ADDRESS(ES)	10. SPONSORING / MONITORING AGENCY REPORT NUMBER

11. SUPPLEMENTARY NOTES

The views expressed in this thesis are those of the author and do not reflect the official policy or position of the Department of Defense or the U.S. Government.

12a. DISTRIBUTION / AVAILABILITY STATEMENT Approved for public release; distribution is unlimited.	12b. DISTRIBUTION CODE

13. ABSTRACT *(maximum 200 words)*

The objective of this thesis is to investigate and evaluate the effectiveness of ship radar cross section (RCS) reduction in the high frequency (HF) band by means of shaping. The study is based on a computer simulation which uses the method of moments to compute the RCS of a number of conventional and shaped ship geometries. It was found that a ship with canted deckhouse walls and a standard hull had little reduction in RCS relative to a conventional ship. This result shows that shaping is not as effective at these frequencies (3-30 MHz) as it is in the optical region. The hull is the major contributor to RCS near broadside. Shaping the hull did reduce the RCS slightly for the frequencies and elevation angles investigated.

14. SUBJECT TERMS HF Radar, RCS, PATCH, Method of Moments, ACAD			15. NUMBER OF PAGES 115
			16. PRICE CODE

17. SECURITY CLASSIFICATION OF REPORT Unclassified	18. SECURITY CLASSIFICATION OF THIS PAGE Unclassified	19. SECURITY CLASSIFICATION OF ABSTRACT Unclassified	20. LIMITATION OF ABSTRACT UL

NSN 7540-01-280-5500

Standard Form 298 (Rev. 2-89)
Prescribed by ANSI Std. 239-18

INVESTIGATION OF HIGH FREQUENCY SHIP RADAR CROSS SECTION REDUCTION BY MEANS OF SHAPING

Dimitrios Kouteas
Lieutenant, Hellenic Navy
Hellenic Naval Academy, 1988

Submitted in partial fulfillment
of the requirements for the degrees of

MASTER OF SCIENCE IN ELECTRICAL ENGINEERING
MASTER OF SCIENCE IN APPLIED PHYSICS

from the

## NAVAL POSTGRADUATE SCHOOL
September 1998

Author: _____
Dimitrios Kouteas
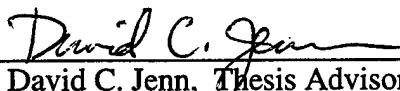
Approved by: _____
David C. Jenn, Thesis Advisor

_____
David D. Cleary, Thesis Co-Advisor

_____
William B. Maier, Chairman
Department of Physics
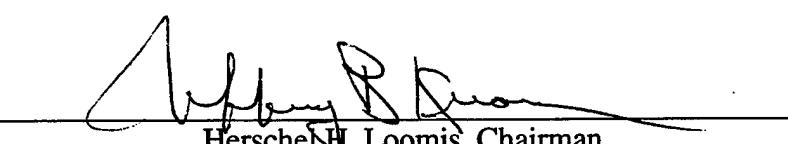
_____
Herschel H. Loomis, Chairman
Department of Electrical and Computer Engineering

iii

ABSTRACT

The objective of this thesis is to investigate and evaluate the effectiveness of ship radar cross section (RCS) reduction in the high frequency (HF) band by means of shaping. The study is based on a computer simulation which uses the method of moments to compute the RCS of a number of conventional and shaped ship geometries. It was found that a ship with canted deckhouse walls and a standard hull had little reduction in RCS relative to a conventional ship. This result shows that shaping is not as effective at these frequencies (3-30 MHz) as it is in the optical region. The hull is the major contributor to RCS near broadside. Shaping the hull did reduce the RCS slightly for the frequencies and elevation angles investigated.

TABLE OF CONTENTS

vii

ACKNOWLEDGMENT

I. INTRODUCTION

The word *radar* was coined during the World War II and stands for radio detection and ranging. Radar has played an important role in both military and civilian applications. Radar operates by radiating electromagnetic energy and detecting the echo returned from targets. Beyond-the-horizon ranges of up to thousands of nautical miles can be achieved by radars operating in the high-frequency (HF) band (3 to 30 MHz). Long-range detection is achieved by using sky-wave propagation via refraction by the ionosphere. Ground-wave propagation is possible for shorter over-the-horizon detection ranges.

HF radar development over the past several decades has led to several operational systems being deployed. Because of the low frequency involved, the radar system components are large and only ground based systems are practical. HF radars are used to defend large land masses from invading forces. The targets of interest include aircraft, missiles, and ships, similar for microwave radar. However, HF radar has the advantage of early detection compared to microwave radar. This is a crucial advantage in today's military operations.

Although HF radar is capable of the detection of targets at very large ranges, it has several disadvantages. First the military targets of interest are small compared to the wavelength of the radar wave. Thus the radar cross section (RCS) is moderate or small at HF. For example, the RCS of an auxiliary ship at 3 GHz could be as high as $10^5 \, m^2$. However at 10 MHz it may be only $10^2 \, m^2$. Second, the radar must be able to detect the target in extreme clutter conditions. Large returns from the earth's surface and atmosphere can easily mask a target. Signal processing and clutter suppression techniques have been used successfully to detect targets in the presence of strong clutter. A third disadvantage of HF radar is that it relies on the conductivity of the ionosphere, which can change quickly and unpredictably.

In an attempt to defeat HF radars much effort has been expended on finding methods of reducing the RCS in order to increase survivability. Low observable (LO) platforms, which are designed to have low signature for all sensors, not just RCS, have become common over the last several decades. In general, there are four basic techniques for radar cross section reduction (RCSR):

1.   shaping,

2.   application of radar absorbing material (RAM),

3. active cancellation, and

4. passive cancellation.

Each method has advantages and disadvantages. The two most commonly applied RCSR techniques are shaping and radar absorbing materials. Usually shaping techniques are employed as a first step to create a platform design with inherently low RCS in the primary threat sectors. Only then is RAM used to treat areas where the shape could not be optimized, or to reduce the effects of creeping or traveling waves on the signature.

The objective of shaping is to orient the target surfaces and edges to deflect scattered energy in directions away from the radar. Since this cannot be done for all viewing angles, the success of shaping depends on the existence of angular sectors over which low radar cross section is less important than over others. For structures such as ships and ground vehicles, the major RCS contributors are internal dihedral and trihedral corners. For ships in particular, these are the vertical bulkheads and masts. The scattering·from vertical target surfaces also can be reflected from the earth's surface (multipath) providing an enhanced return under some conditions. One way to reduce RCS is to tilt the bulkheads away from the vertical. Of course it is impractical to retrofit or upgrade

3

an existing vessel with a shaped superstructure, but even with new designs the amount of bulkhead tilt is a trade-off between RCS reduction and other issues.

Radar absorbing materials reduce the energy reflected to the radar by means of absorption. The loss mechanisms involve the dielectric or magnetic properties of the material. The loss arises from the conversion of radio frequency energy into heat. At radio and microwave frequencies, the loss is due to the finite conductivity of the material. Carbon was the basic material used in the fabrication of early absorbers because of its high loss, and it continues to be an important constituent in modern absorbers. The major penalty for using absorbent materials is a reduction in range or payload due to increased weight. It also complicates the maintenance and sea keeping functions.

Active and passive cancellation refer to the addition of secondary scatterers with precisely controlled phases and amplitudes so that they cancel with the 'skin return' from the target. Cancellation techniques are not generally used for large platforms that have hundreds of individual echo sources with random scattering characteristics.

The RCS of an object can be attributed to a combination of specular and non-specular scattering components.

Specular scatterers refer to any part of an object where surfaces are relatively flat in terms of wavelength and, in the case of monostatic RCS, perpendicular to the incident electromagnetic wave. A flat and smooth surface is a very strong scatterer at normal incidence, but the echo reduces rapidly as the angle of incidence moves away from the surface normal. The larger the surface area in terms of wavelength, the higher the maximum RCS, and the narrower the angular region of the lobe. Thus effective shaping techniques are associated with electrically large targets. At the low HF frequencies the wavelength is 100 m, and therefore even physically large targets like ships are only a few wavelengths long. Large specular reflections do not occur and the scattering is dominated by non-specular contributions.

The objective of this thesis is to investigate and evaluate the effectiveness of ship RCS reduction in the HF band by means of shaping. Shaping has already been used to reduce the RCS of aircraft and ships and has lead to unconventional platform shapes such as the *NORTHROP B-2* and *LOCKHEED F-117A* aircraft shown in Figures 1-1 and 1-2. The *SEASHADOW* is an extreme example of ship RCS control by shaping, as shown in Figure 1-3.
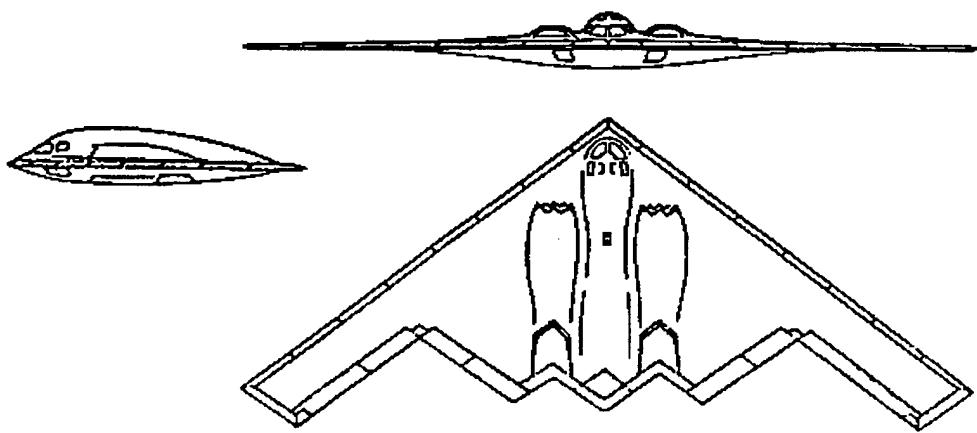
Figure 1-1. The NORTHROP B-2 (from [1]).
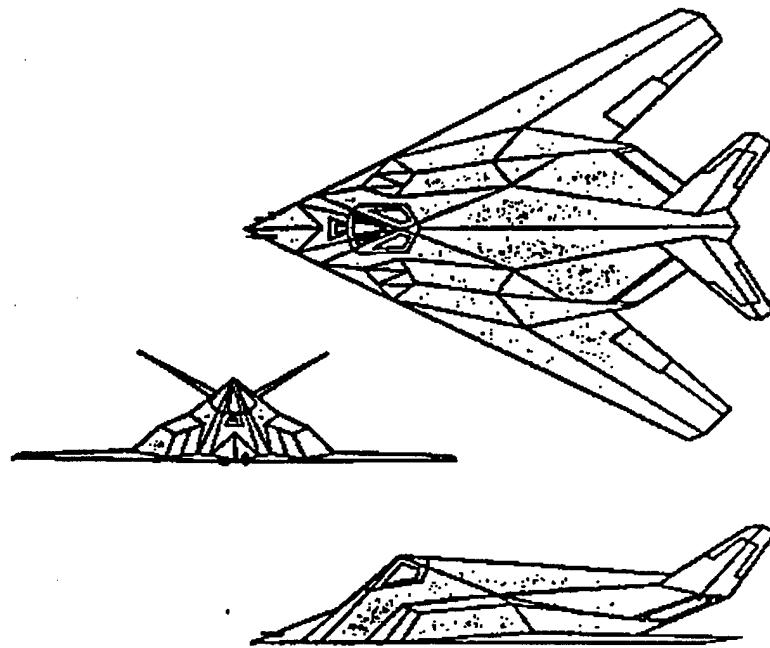
**Figure 1-2.** The LOCKHEED F-117A (from [1]).

(a)
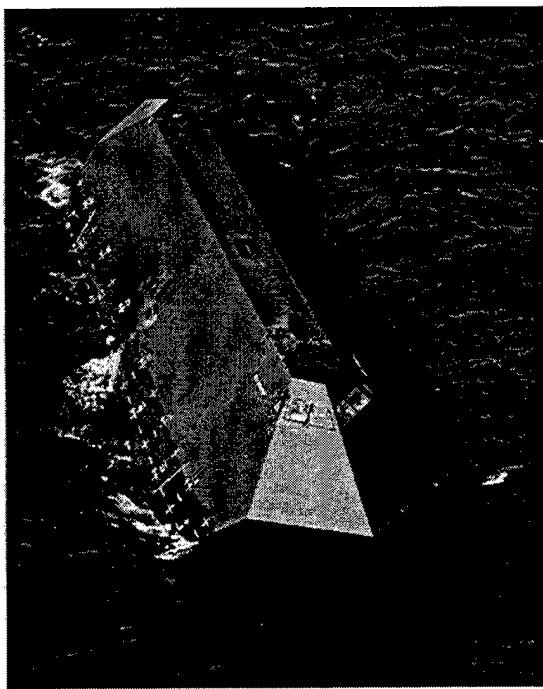
(b)

Figure 1-3. The SEASHADOW (from [2]).

Another example of shaping for RCS control is illustrated by the Swedish ship *YTSTRIDSFARTYG 2000 (SURFACE COMBATANT 2000)*, shown in Figure 1-4. It is a fully stealthy design with weapons and workspaces behind hatches, low concealed exhaust pipes to minimize the infrared (IR) signature, and an nonmagnetic hull. All work with weapons and mines is conducted inside the ship and it is impossible to see which weapons are carried from the outside. Construction started in autumn 1996, the first ship is expected to enter operational service in 2002.
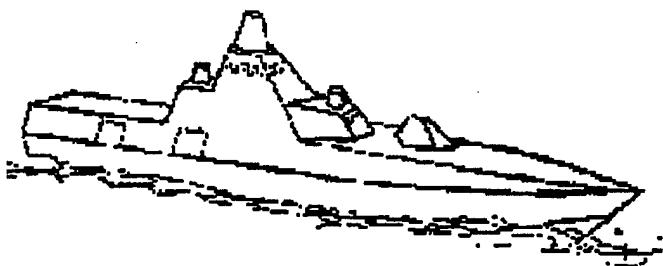
Figure 1-4. YTSTRIDSFARTYG 2000 (from [3]).

Finally the Swedish stealth ship *HMS SMYGE* (shown in Figure 1-5) was built as a test platform for developing stealth technology, and testing new weapon systems, sensors, communications systems, and navigation equipment. It was

first shown publicly in 1991. The configuration is a side-keel hovercraft, manufactured mostly of kevlar and glass fiber. It is designed to have low radar, IR and noise signatures. All structures consist of angled flat surfaces and all inlets and outlets are screened or fitted with radar absorbent material. The engine exhausts are cooled, using three different methods to dissipate heat. The use of water jets makes for a small noise signature. It has conformal and retractable antennas, including an elevating radar mast.
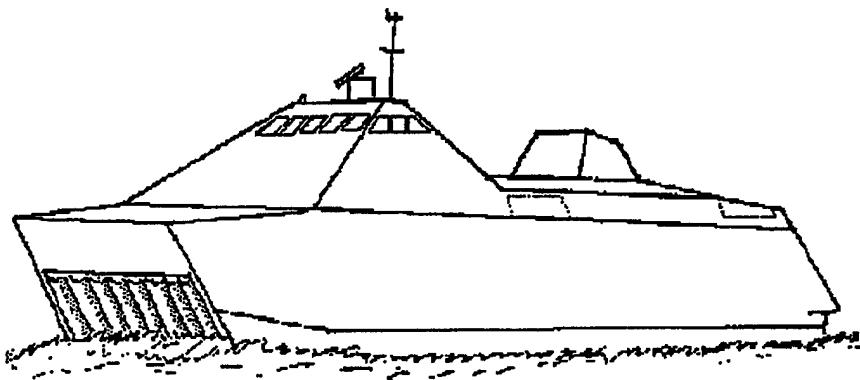
**Figure 1-5.** HMS SMYGE (from [4]).

These LO designs are effective at microwave frequencies where specular scattering dominates. However it is not clear that shaping provides any advantage in the HF band.

Before addressing the question of ship HF RCS reduction the important concepts of RCS and HF radar are introduced. Chapter II discusses the basic characteristics of HF radars and the different modes of over-the-horizon propagation. Chapter III introduces the RCS concept and briefly describes the most common methods for its prediction. The RCS of several ships was computed using the numerical electromagnetics code named PATCH. Chapter IV contains a description of the PATCH code and information on the numerical calculations it performs. Chapter V provides RCS data for several stealthy (shaped) and conventional ships. Finally, Chapter VI presents the summary, conclusions, and recommendations for future research.

II. HF OVER-THE-HORIZON RADAR

A.   INTRODUCTION

Ranges up to thousands of nautical miles (beyond-the-horizon) can be achieved by radar operation in the High-Frequency (HF) band (3 to 30 MHz). Both sky-waves refracted from the ionosphere and ground-waves diffracted around the curvature of the earth can be used, as shown in Figure 2-1. As depicted in the figure, the longest ranges
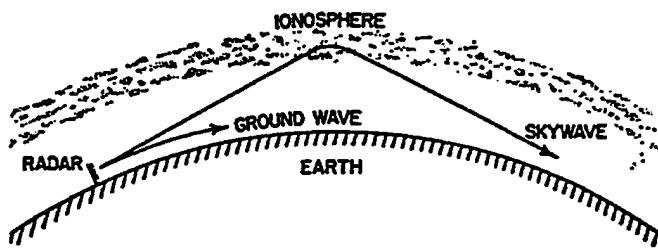
Figure 2-1. Illustration of sky wave and ground wave propagation (from [5]).

are achieved by using sky-wave propagation. The range of a ground wave HF radar is on the order of 200-400 km, and the coverage of a sky-wave radar might extend from 1000 to perhaps 4000 km or even more. HF radars can be used for

11

detecting the same type of point targets as microwave radars, such as aircraft, missiles, and ships. The ability of HF radiation to propagate beyond the line-of-sight also allows HF radar to be used for tracking distributed targets such as surface winds and ocean currents. [6]

HF radars have several disadvantages that arise from the frequency employed. The wavelengths are too long to provide good spatial resolution compared to higher frequency radars. Radars at HF frequencies suffer from limited bandwidth, wide beamwidths, and high ambient noise. Another limiting factor is the magnitude and doppler distribution of the earth-surface backscatter, which must be taken into consideration in setting system dynamic-range and signal-processing characteristics.

One of the most challenging problems is the extremely large clutter echo returned from the ground, from which the target signal must be extacted. For example, the echo from the ground might easily be 40-80 dB greater than an aircraft echo, depending upon the antenna beamwidth and pulsewidth. [5] To increase the target-to-clutter ratio requires high resolution in range and angle and excellent Doppler-frequency discrimination as in a moving target indicator (MTI) or pulse Doppler radar. At HF, sufficient resolution in angle and/or range to adequately suppress the clutter echo is difficult to achieve. For example, a 1°

12

beamwidth requires an antenna of the order of 2 km. [6] Range resolution requires a wide signal bandwidth, but it is seldom that the ionosphere can effectively support an instantaneous bandwidth greater than about 100 kHz, which corresponds to a range resolution of roughly 1.5 km.

B.   RADAR EQUATION

The radar equation gives the received signal-to-noise ratio (SNR) in terms of the system and enviromental factors such as frequency, waveform type, radar cross section, path losses, multipath effects, noise, interference, antenna gain, spatial resolution, and clutter characteristics. For HF frequencies the radar equation can be written as [6]

$$\frac{S}{N} = \frac{P_{av}G_tG_rT\lambda^2\sigma F_p}{N_oL(4\pi)^3R^4} \qquad (2.1)$$

where:

$\dfrac{S}{N}$ = output signal-to-noise ratio

P_{av} = average transmitted power, W

G_t = transmitter antenna gain

G_r = receiver antenna gain

T = effective processing time, s

13

λ = wavelength, m

σ = target radar cross section, m^2

F_p = propagation-path factor

N_o = noise power spectral density, W/Hz

L = transmission-path and system losses(≥ 1)

R = distance between radar and target, m

A typical OTH radar designed for the detection of aircraft at ranges of approximately 4000 km can have an average transmitted power on the order of several hundreds of kilowatts, and antenna gains of 20-30 dB. The antenna must be large enough to provide as narrow a beamwidth as possible. A typical horizontal length is 300 m. The transmitted waveform can be either continuous wave (CW), a simple pulse, frequency modulated continuous wave (FM-CW), a chirped pulse, or other waveforms.

There are special points that should be made about the quantities in the radar equation with regard to HF:

1. Gain of Antennas (G_t and G_r): HF-band radars are coupled to the earth, which affects their performance. Therefore, the earth's conductivity and dielectric constant are important factors in determining antenna performance. The electrical properties of the earth, terrain features and

14

surface roughness are important factors for horizontal and vertical polarizations. Large vertical apertures are difficult to construct.

2. *Coherent processing time (T):* HF radar must contend with earth backscatter at the same range as the target. Doppler processing is used to separate moving targets from earth backscatter. The propagation environment must be stable over a sufficiently long time to collect coherent pulse returns.

3. *Wavelength (λ):* The operating frequency is very important for two reasons. First, proper frequency selection results in efficient refraction of waves by the ionosphere. Secondly, the frequency affects the interference with other sources, including clutter. Specifically for HF radar design, clutter levels play an important role since they are large relative to most target returns.

4. *Radar cross section (RCS) (σ):* The radar cross section of targets depends on the frequency, polarization, and aspect angle. Aircraft and ships have dimensions that put them in the resonant scattering region at HF. The smallest aircraft and cruise missiles are in the *Rayleigh* scattering region for the lower half of the HF band. At these frequencies the cross section decreases rapidly with decreasing frequency as shown for a sphere in Figure 2-2.

The RCS has only small aspect sensitivity, but depends

strongly upon the target's gross dimensions. For an aircraft
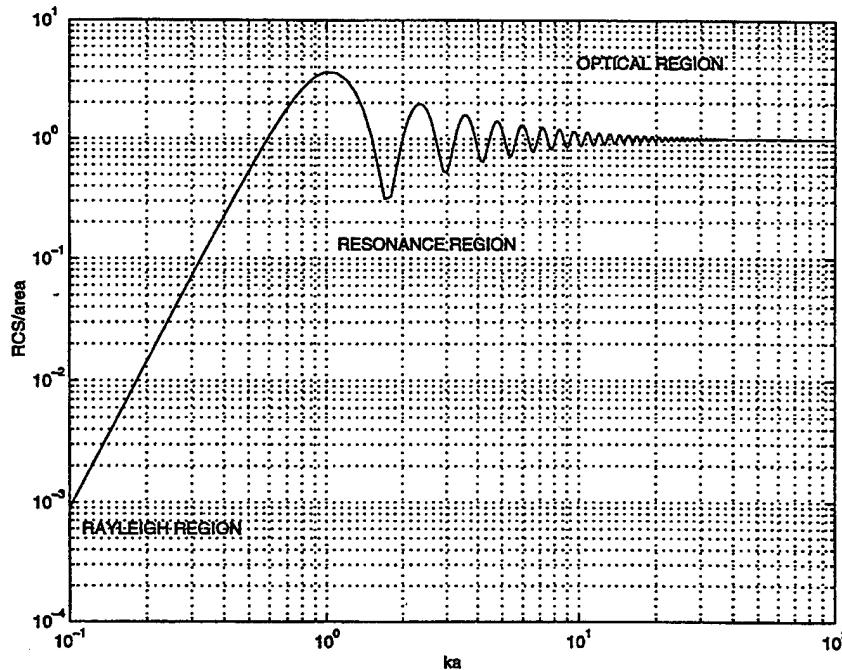
Figure 2-2. RCS and frequency regions of a sphere
where κ is wave number and a is radius of sphere
(from [7]).

the span of the wings, fuselage length, tail and elevator

span, vertical stabilizer and rudder height, and their

relative locations are the features that determine the RCS.

Shaping a target that has dimensions much less than a

wavelength will have little effect on RCS.

5. *Propagation factor* (F_p). Propagation phenomena,

such as multipath and Faraday polarization rotation, must be

16

taken into account in the radar equation. Faraday rotation results in a polarization mismatch varying with distance and time. In other words, the polarization of the incident wave will rotate as distance changes. This phenomenon is more severe for linearly polarized radiation.

6. *Noise* (N_o): For HF-band radars, external noise due to atmospherics (lightning), cosmic noise, and other environmental noise are dominant. This is in contrast to microwave radar, for which the internal noise generated within the receiver itself is usually more important.

7. *Losses* (L): The loss term contains the two-way propagation losses along the path, ionospheric absorption, ground-reflection losses, and all radar system losses.

8. *Range* (R): The range is the great-circle ground distance between the target and radar.

Some typical HF radar system parameters are listed in Table 2-1. [8]

C.   SURFACE CLUTTER

HF radars operate in both the land and sea environment. In contrast to the backscattered energy from land which is topography-dependent, the seascattering coefficient, or RCS per unit surface area, σ^o in m^2/m^2, is fairly uniform. That

Table 2-1. Typical HF Radar System Parameters.

PARAMETER	TYPICAL VALUES
Operating Frequency	3-30 MHz, electonically tuned
Peak Output Power	2 Kw to 1 Mw
Pulse Repetition Frequency	CW- 50Hz (Russian Woodpecker, 10.5 Hz)
Pulse Width	10 μs to 200 μs or CW
Antenna Gains	15 to 30 dBi
Antenna Beamwidths Horizontal Vertical	 $0.5° - 20°$ $10° - 60°$
Antenna Steering Horizontal Vertical	Transit and receive antennas are usually different. Sometimes multiple beams, V or H are used. $20° - 150°$ $0° - 30°$
Dwell Time	10 seconds or more

is, it changes gradually with range and azimuth. The surface scattering coefficient, is much larger for vertical polarization than for horizontal polarization. The echo from the sea for horizontal polarization can be neglected at the

18

smaller grazing angles. For ground waves the grazing angle is 0°. For sky waves the grazing angles range from 20° to 60°. The sea echo power is approximately proportional to the resolution cell area [3]. For the seascattering coefficient to be approximately constant, time averaging on the order of minutes is required. [6]

The sea is only slightly rough compared to the size of HF-band wavelengths. Backscatter from the sea can be considered a resonant interaction. The random-looking ocean waves can be considered the sum of an infinite number of Fourier surfaces, each being a sinusoidal corrugated sheet with a different wavenumber and direction. For a grazing-incidence electromagnetic wave, the principal backscatter is the component sheet that has a wavelength equal to one-half of the radar wavelength and that is either directly approaching the radar or receding from it.

Ocean waves are mostly excited by the surface winds. In order for a steady-state condition to be achieved, in an area where a wind blows for a long time at a constant velocity, the wind must provide just enough energy to the water to supply that lost in breaking and other dissipation. The wind will generate water waves with a phase velocity nearly equal to the wind speed, as well as the ocean waves of lower velocities.

In summary: (1) the sea echo power in a resolution cell is generally the largest in-band echo signal; (2) a significant return exists in the open ocean even in relative calm; (3) the return varies as the square of resonant waveheight, which is frequently limiting at the higher frequencies; and (4) it varies with direction, being greatest for seas running toward or away from the radar. [6]

D. HF SKY-WAVE PROPAGATION

Sky-wave propagation provides transmission paths between two points on earth even if they are very far apart. Solar ultraviolet radiation and energetic electron impact cause ionization in the earth's upper atmosphere (altitudes ≥ 60 km). The ionosphere persists at night even though there is no intense radiation source, because the time constant for ion recombination can be quite long for these altitudes.

Over-the-horizon ground illumination is enabled by refraction in the ionosphere. When an oblique-incidence radio or high-frequency EM wave is launched it bends away from the vertical as it travels into a region of increased electron density, as shown in Figure 2-3. If the electron density is sufficient, the wave will bend completely back to the earth, providing the desired long-distance illumination.

The lower the radio-wave frequency, the smaller the required electron density. That is, the magnitude of this bending
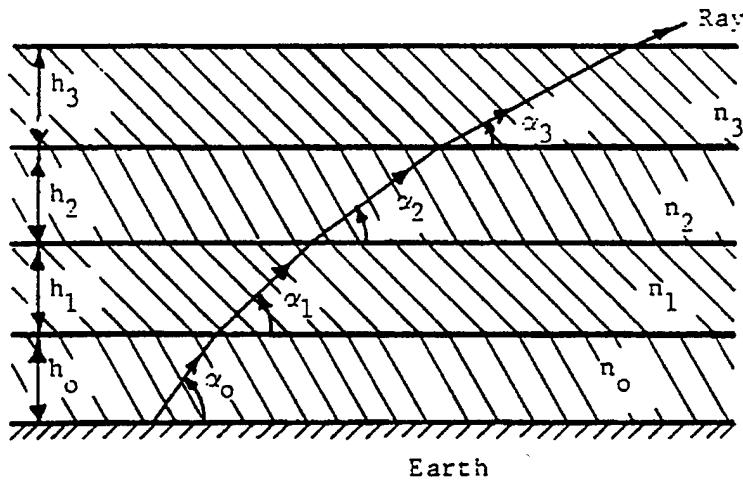
Figure 2-3. Path of a ray through a horizontally stratified atmosphere. (n is the index of refraction, α the transmission angle and h the thickness) (from [9]).

increases with decreasing radio frequency. Ionization in the upper atmosphere always exists, and by choosing the appropriate frequency for the existing electron density distribution, is always possible to illuminate the earth over the horizon. This is illustated in Figure 2-4.

The ionosphere can be considered to be divided into the following regions (see Figure 2-5):

1. D region: This region is the lowest charged layer.
It ranges from 60 to 90 km, where electron density rapidly
increases with altitude in the daytime. In this region,
energy is adsorbed, since free electrons (excited by the
radio waves) collide with neutral particles. This is called
nondeviative absorption.
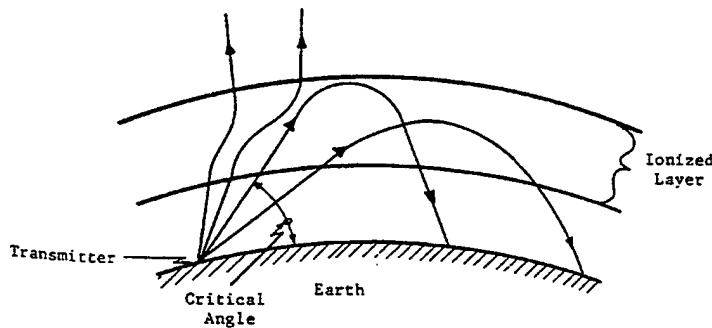
Figure 2-4. Typical behavior of rays passing
through an ionized layer (from [9]).

2. E region: This ionization region extends between
about 90 and 120 km in altitude with a maximum near 110 km
when sunlit. This is the region where an anomalous
ionization referred to as sporadic E can occur. Sporadic E
is the existence of thin patch of high-density ionization
which gives obscuration to the higher ionosphere.

3. F Region: This is the highest-altitude region with the greatest electron density. During daytime, especially in summer, there are two distinguishable components to this region. The F1 region lies between 120 and 160 km and is directly dependent upon solar radiation. The F2 region is
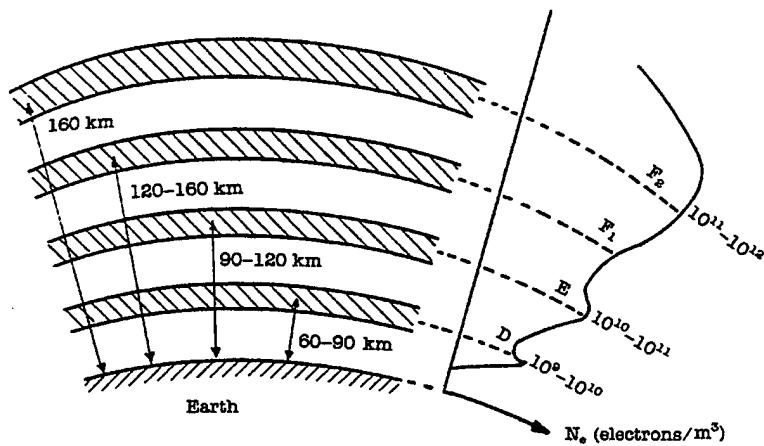
Figure 2-5. The layers of the ionosphere. Electron densities are typical of noontime values (from [9]).

variable in both time and geographical location. The altitudes of the F2 region peaks are considered to lie between 250 and 350 km in the middle latitudes.

Now that we have examined the HF radar equation, and how RCS affects the received signal and detection range, the next chapter investigates how RCS can be reduced.

III. RADAR CROSS SECTION

A. RADAR CROSS SECTION DEFINITION

Radar cross section (RCS) or *echo area* has been defined in order to characterize radar target scattering. It is a measure of the scattered power in a specific direction when the target is illuminated by an incident wave. In order to make RCS independent of the distance between the target and the source, RCS is normalized to the power density of the incident wave at the target. A formal definition for RCS is given in [10]:

> RCS is a measure of reflective strength of a target defined as *4π* times the ratio of the power per unit solid angle scattered in a specified direction to the power per unit area in a plane wave incident on the scatterer from a specified direction.

Mathematically RCS can be expressed as [1]

$$\sigma(\theta,\phi,\theta',\phi') = \lim_{R \to \infty} 4\pi R^2 \frac{|E^{scat}(\theta,\phi)|^2}{|E^{inc}(\theta',\phi')|^2} \tag{3.1}$$

where

$E^{scat}(\theta,\phi)$ is the scattered electric field in the direction θ, ϕ measured at a distance R from the target

$E^{inc}(\theta',\phi')$ is the incident plane wave electric field at the target from the direction θ', ϕ'

This thesis deals entirely with the monostatic case for which the directions of excitation and observation are the same in the target coordinate system ($\theta = \theta'$ and $\phi = \phi'$).

A physical interpretation of RCS is illustrated in Figure 3-1. The incident power density at the target is P^{inc} (W/m^2). The target intercepts power equal to σP^{inc} (W), which is reradiated back to the receiver as well as all other angles within a sphere. Therefore, the scattered power density (W/m^2) on a sphere of radius R is given by

$$P^{scat} = \frac{\sigma P^{inc}}{4\pi R^2}. \tag{3.2}$$

Solving the above equation for σ, and considering long ranges R, gives:

$$\sigma = 4\pi R^2 \frac{P^{scat}}{P^{inc}}. \tag{3.3}$$

26
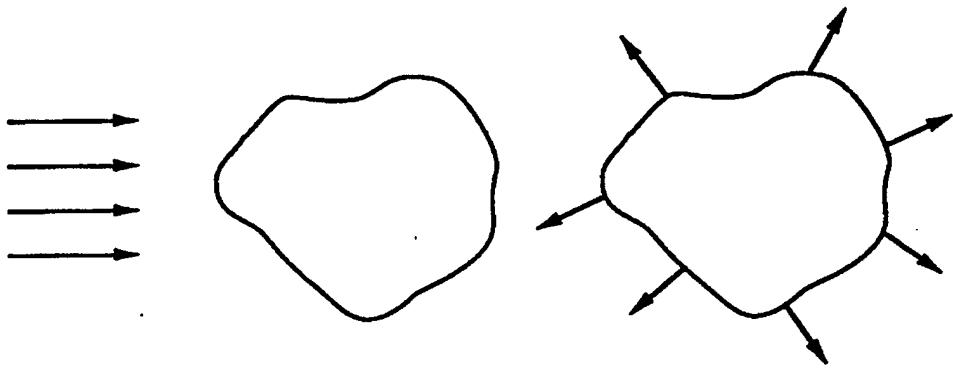
P^{inc} (W/m^2) $\qquad\qquad \sigma P^{inc}$ (W) $\qquad\qquad P^{scat} = \dfrac{\sigma P^{inc}}{4\pi R^2}$ (W/m^2)

Incident Power   Target With Cross   Target Re-radiates
Flux From   Section σ Captures   Captured Energy
Transmitter   Energy = σP^{inc} "Isotropically"

Figure 3-1. Physical interpretation of RCS (after [11]).

Since the power is proportional to the square of the electric or magnetic field, Equation 3.3 can be written as

$$\sigma = 4\pi R^2 \frac{|E^{scat}|^2}{|E^{inc}|^2} = 4\pi R^2 \frac{|H^{scat}|^2}{|H^{inc}|^2} . \qquad (3.4)$$

RCS is frequently expressed in decibels relative to a square meter (dBsm), which is defined as

$$\sigma_{dBsm} = \sigma_{dBm^2} = 10\log_{10}(\frac{\sigma_{m^2}}{\sigma_{ref}}) = 10\log_{10}(\frac{\sigma_{m^2}}{1}) . \qquad (3.5)$$

27

Typical values of RCS vary from 10^{-5} m^2 for insects to 10^6 m^2 for large ships.

B.   TARGET SCATTERING MATRICES

The fields scattered from a body depend on the polarization of the incident field. For RCS computation the reference for polarization is usually with respect to the coordinate system of the body as shown in Figure 3-2.   In
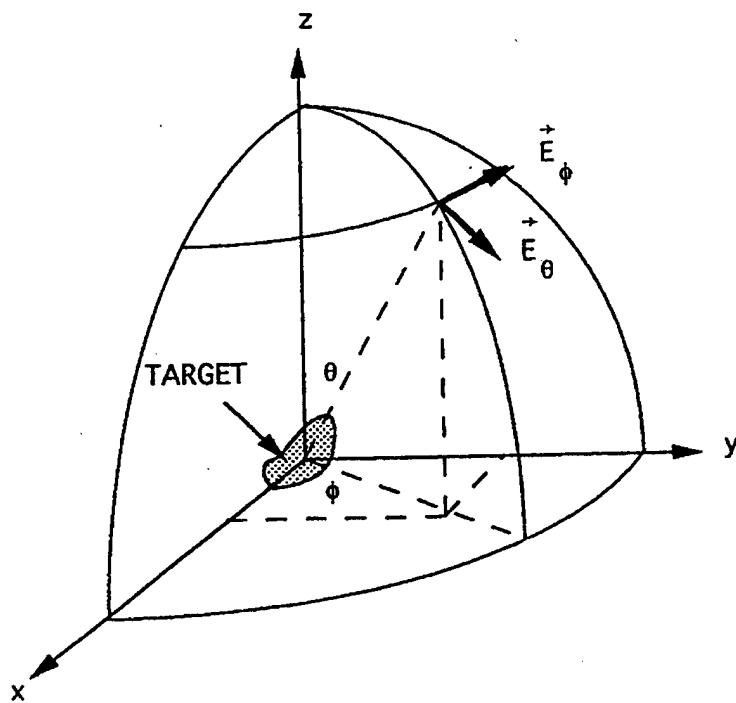
Figure 3-2. Incident wave polarization in the target coordinate system   (from   [1]).

28

most cases it is necessary to decompose the polarization of the incident wave into two orthogonal components, usually chosen to be the θ and ϕ components of a spherical system centered at the target. Then the general expression for an incident wave is

$$\vec{E}^{inc} = E_\theta^{inc}\hat{\theta} + E_\phi^{inc}\hat{\varphi} \qquad (3.6)$$

where $\hat{\theta}$ and $\hat{\varphi}$ are unit vectors. [1]

It should be pointed out that the polarization of the scattered field is not necessarily the same as the polarization of the incident field. For a complex target a *cross-polarized* scattering component is generally created. This phenomenon is called *depolarization*. This can arise from the curvature of the surface or multiple diffractions and reflections. A complete representation of the incident and scattered fields is obtained by using a *scattering matrix* defined by [1]

$$\begin{bmatrix} E_\theta^{scat} \\ E_\phi^{scat} \end{bmatrix} = \begin{bmatrix} S_{\theta\theta} & S_{\theta\phi} \\ S_{\phi\theta} & S_{\phi\phi} \end{bmatrix} \begin{bmatrix} E_\theta^{inc} \\ E_\theta^{inc} \end{bmatrix}. \qquad (3.7)$$

The S_{pq} are the scattering parameters, which are related to the components of RCS by

29

$$S_{pq} = \frac{\sqrt{\sigma_{pq}}}{\sqrt{4\pi R^2}} e^{j\Psi_{pq}} \qquad (3.8)$$

where Ψ_{pq} depends on the phases of E_p^{scat} and E_q^{inc}, and

$$\sigma_{pq} = \lim_{R \to \infty} 4\pi R^2 \frac{|E_p^{scat}|^2}{|E_q^{inc}|^2} . \qquad (3.9)$$

The indices p and q can be either θ or ϕ. The first index specifies the polarization of the receiving antenna and the second the polarization of the incident wave. [1]

C.   SCATTERING MECHANISMS

Complex targets support several scattering mechanisms, which interact with each other to yield an RCS which is a complicated function of frequency and angle. The basic scattering mechanisms include:

a.   *Reflections*, which give the highest RCS peaks. In the presence of multiple surfaces, multiple reflections can occur.

b. *Diffractions* arise from discontinuities such as edges and tips. These waves, although less intense than reflected waves, can emerge over a wide range of angles. In the limit of vanishing wavelength the diffracted field behavior is predicted by the geometrical theory of diffraction (GTD). For the case of non-normal incidence, an

edge-diffracted ray can lie anywhere along a forward cone whose half-angle is subtended by the edge and the incident ray. This cone, shown in Figure 3-3, is called the *Keller cone* after J. B. Keller, where β_i and β_s are the angles between the edge and the incident and scattering rays, respectively.

c. *Surface waves* are of several types. They include *creeping waves* which creep around the back of a curved body, and *leaky waves* which are radiating surface waves supported by flat bodies. Travelling waves appear on curved bodies and along edges and suffer little attenuation as they propagate. If the waves reach a discontinuity such as a corner, then they are reflected back toward the source, producing high monostatic RCS lobes.

d. *Ducting* occurs when a wave is trapped in a partially closed structure. The rays can take many paths and, therefore, rays will emerge at almost all angles, creating a large, broad RCS lobe. [11]

D.   APPROACH TO SHAPING

As stated previously one of the four basic techniques for radar cross section reduction is shaping. Shaping is usually the first step in radar cross section reduction. The

31
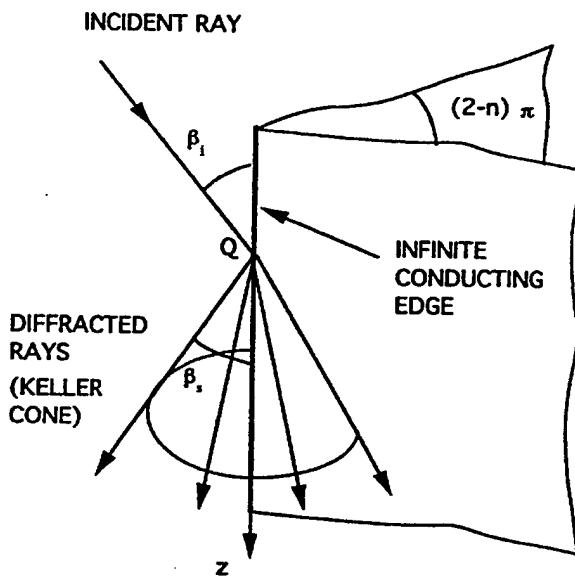
Figure 3-3. Diffracted ray geometry for an "infinite" knife edge (after [1]).

goal of shaping is to redirect incident radar energy away from the threat receiver into non-threat regions. In the case of monostatic radar, shaping attempts to minimize the reflection in the back direction by increasing scattering in the forward direction.

There are two assumptions implicit in the use of shaping. First, it is based on the specular behavior of scattered fields, and therefore the target dimensions should be much greater than the wavelength (i.e. the target should be in the optical region). Figure 3-4 demonstrates how the beamwidth of the specular reflection, for a plate, decreases
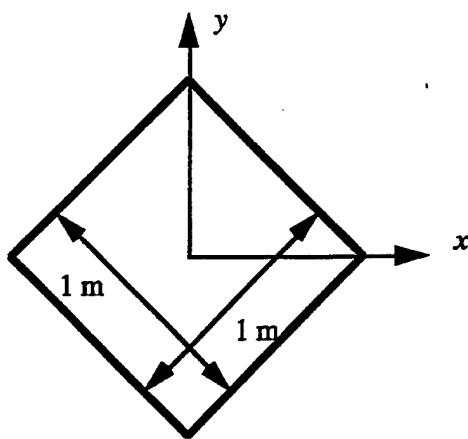
(a)
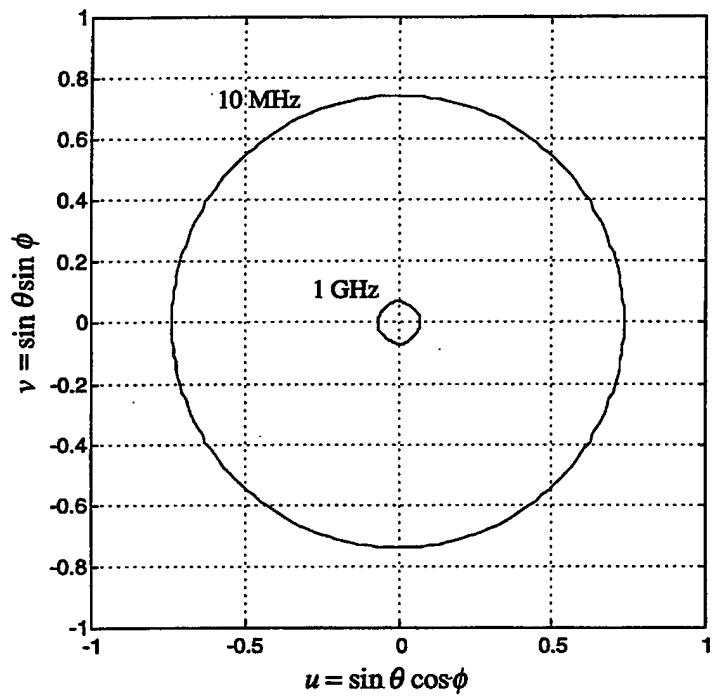
(b)

Figure 3-4. Contours of $\sigma = 10$ dBsm for a 1 m square plate at 10 MHz and 1 GHz.

with increasing frequency. The contours for $\sigma = 10$ dBsm are plotted for a 1 m square plate at frequencies of 10 MHz and 1 GHz. Clearly the region of RCS below 10 dBsm (areas enclosed by the respective contours) is much smaller at 1 GHz than at 10 MHz.

The second assumption is that shaping can not reduce RCS at all aspect angles for a target. Because shaping merely redirects the scattered field, there is a presumption that "low priority" spatial sectors exist where the RCS can be higher than in the "high priority" sectors. The "high priority" regions that must have low RCS are determined by mission requirements, such as locations and types of radars, detection ranges frequencies, and radar polarization. For example, the required low RCS sector for air targets is typically nose on in the azimuth plane and $\pm 15°$ in elevation. Threats usually do not exist from directly above or below. For ships and ground targets threat sectors are usually 360° in azimuth, but limited to 20° to 30° in elevation.

E.   SHAPING GUIDELINES

The concept of shaping can be applied to both surfaces and discontinuities such as edges and corners. Specular scattering from surfaces satisfies Snell's law. Specular RCS

contributions are greatest for large flat or gently curved surfaces. For curved surfaces the peak RCS is less than that for a flat surface, but significant returns exist over a wider angular sector.

Multiple reflections exist when the target is composed of several large flat or gently curved surfaces. For a ship this could be the surfaces of two separated deckhouses or gun turrets. If several surfaces are grouped to form a partial enclosure, then cavity modes may be supported. An example of a cavity is a cylindrical smoke stack as shown in Figure 3-5. If a radar wave arrives at a high elevation then it enters the cylindrical cavity where multiple reflections occur. Cavity structures have significant RCS over a much broader angular region than a flat surface.
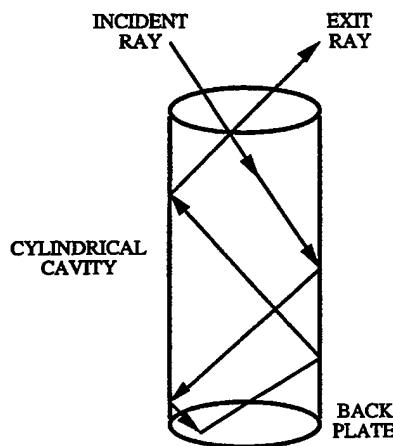
Figure 3-5. Duct cavity design for multiple bounce.

Scattering from discontinuities such as edges is caused by the abrupt change in current from a finite value on the conductor to zero off of the conductor. The abrupt transition is a scattering center. For flat plates it dominates the RCS pattern away from the specular direction. This return is in addition edge diffraction effects. [8] In Figure 3-6 a plate is viewed either in a principal plane or along the diagonal, where four end regions occur at the four corners of the plate. In this case the four end-region discontinuities are much smaller than the discontinuities when the plate is viewed in a principal plane. Thus, from a RCS point of view, it is more beneficial to rotate a square surface so that an observer sees a diamond.

Diffraction also occurs at discontinuities. However it is of second or third order in propagation constant κ which is defined as

$$\kappa = \frac{2\pi}{\lambda} \qquad (3.10)$$

where λ is the wavelength. It is only greater than the specular return at near grazing incidence angles. Diffraction fields from edges can be redirected by proper orientation of edges. This has led to the trailing edge

"zig-zags" that appear on the F-117A and B-2 aircraft discussed in Chapter I.

a) Viewed perpendicular to edge.　　　　　b) Viewed along diagonal
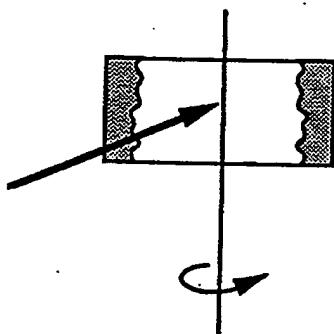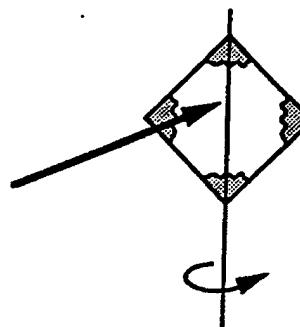
Two end regions　　　　　　　Four end regions

Figure 3-6. End-region discontinuities are scattering centers creating sidelobes for plate scattering (after [11]).

Surface waves also appear at discontinuities on long slender bodies. The scattering structure acts as a transmission line. The surface wave is usually reflected at the end of the body, and radiates as it propagates in the reverse direction. Surface wave reflection can be reduced by

shaping the terminated end of the body as illustrated in Figure 3-7 for an ogive and S curve.

Ogive   *S Curve*
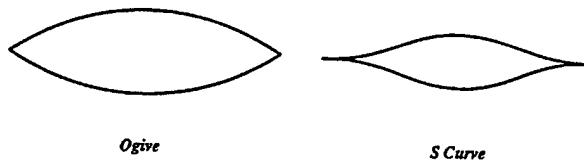
Figure 3-7. Tip scattering is proportional to included angle   (from [11]).

In light of the possible scattering mechanisms and their characteristics it is possible to compile a set of RCS design guidelines: [11]

1. Tilt large flat surfaces so that the threat radar never views the surface near normal aspect angles.

2. Avoid surfaces joined at 90° angles, which forms a strong retroreflector (multiple reflections are strong in the direction of incidence).

3. View surfaces as close to grazing angle as possible, since sidelobe scattering centers attenuate as the end regions are viewed closer to grazing angle.

4. View planar facet end regions along the diagonal to minimize the end region area and hence scattering center magnitude.

5. If it is necessary to view planar facet corners, try to make the included corner angle as small as possible.

6. Try to avoid abrupt changes in either geometry or materials.

7. Terminate long slender (in terms of wavelength) bodies with tapered or blended shapes to avoid surface wave reflections.

These guidelines will be applied to the design of ships in Chapter V. The next chapter discusses the analytical methods and computer codes used to predict RCS.

IV. COMPUTER CODES

A.   INTRODUCTION

PATCH is a method of moments (MoM) triangular subdomain code that was developed by Sandia Labs [9]. It is a FORTRAN computer code that calculates electromagnetic radiation and scattering. It is based on a MoM solution of the E-field integral equation (EFIE). It models a continuous surface by discrete triangular patches in order to handle arbitrary body shapes easily and accurately. This chapter presents a brief summary of the method of moments and its implementation in PATCH.

B.   THE EFIE AND METHOD OF MOMENTS

The EFIE is derived from the radiation integrals and the boundary conditions for a perfect electric conductor. [1] One form of the EFIE is:

$$\vec{E}_i(\vec{r})\mid_{\tan} = \{ j\omega\mu_o \iint_s \vec{J}_s(\vec{r}')G(\vec{r},\vec{r}')ds' + \frac{j}{\omega\varepsilon_o}\nabla[\nabla \bullet \iint_s \vec{J}_s(\vec{r}')G(\vec{r},\vec{r}')ds']\}_{\tan} \quad (4.1)$$

where $\vec{J}_s$ is the surface current density and the term on the left hand side is the tangential component of the incident field. Primed quantities refer to the source point and

41

unprimed quantities to the observation point, both of which lie on the surface of the conductor. The Green's function is [1]

$$G(\vec{r},\vec{r}') = \frac{e^{-jk|\vec{r}-\vec{r}'|}}{4\pi|\vec{r}-\vec{r}'|} \qquad (4.2)$$

where $\vec{r}$ and $\vec{r}'$ are position vectors to the observation and source points, respectively. Other quantities in Equation 4.1 are the permittivity of free space ε_o, the permeability of free space μ_o and the angular frequency $\omega = 2\pi f$ (f is the frequency in Hz).

The unknown quantity in the EFIE is the surface current distribution $\vec{J}_s$. The method of moments is a numerical technique that reduces the EFIE to a set of linear equations which can be solved by matrix methods. To apply the method of moments, $\vec{J}_s$ is represented by a series with unknown coefficients [1]

$$\vec{J}_s = \sum_{n=1}^{N} I_n \vec{J}_n \qquad (4.3)$$

where $\{\vec{J}_n\}$ are the basis functions. The selection of the basis functions is important. Basis functions should be

42

mathematically convenient (easy for integration and differentiation) and also be consistent with the behavior of the current. The formulation used by PATCH is based on overlapping triangular basis functions that span a triangular subdomain as shown in Figure 4-1. The current at a point on a triangle is the vector sum of the currents crossing the edges weighted by their distances from the edge.
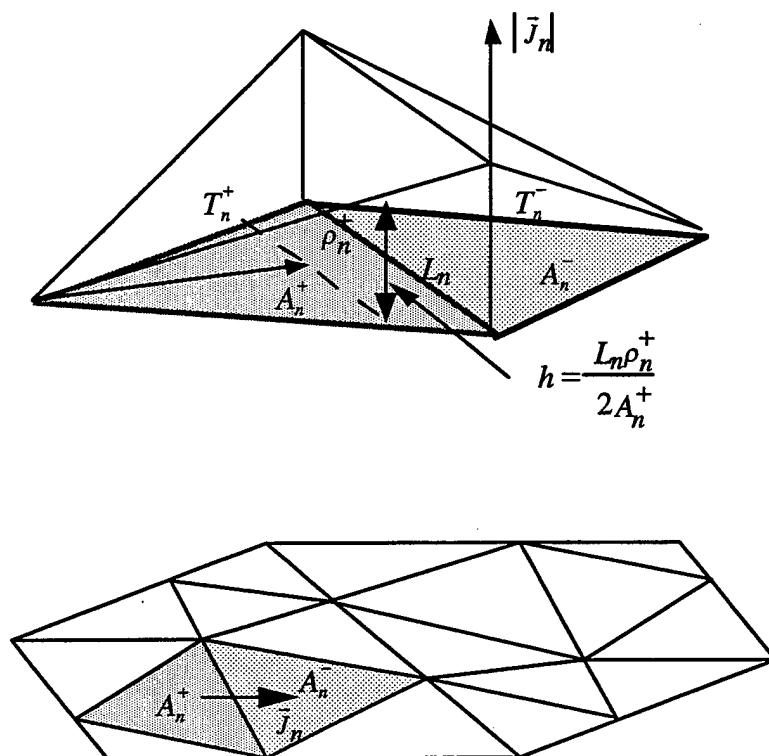
Figure 4-1. Overlapping triangular basis functions that span a triangular subdomain.

Subsectional basis functions are the best choice when the scattering body contains discontinuities. In general, there is no advantage to using basis functions more complicated than overlapping triangles.

In order to determine the unknown coefficients $\{I_n\}$, a matrix of N linear equations is formed. By using a testing procedure which exploits the properties of the basis functions, the $\{I_n\}$ can be determined and thus $\bar{J}_s$ is also determined. After the determination of the current coefficients, the scattered fields can be computed using the radiation integral. [12] The MoM is a rigorous method, that is, the actual current series representation will converge to the true value of the current as the number of basis functions is increased or as the trianglular subdomains become smaller.

The size of the matrix, which is the same as the number of basis functions, depends on the number of triangular patches that are used to represent the body. A three-dimensional body is represented by series of planar triangular faces, or *facets*. If a body is closed, all patches share edges with three other patches. For bodies with edges, however, there are two types of triangles: 1) internal and 2) edge. A triangle that sits at an edge of the

surface has only two of its edges in common with other patches and is therefore spanned by only two basis functions. An internal triangle has three edges in common with adjacent patches, so it is spanned by three basis functions. In general, the more triangles used to represent the body, the shorter the edge lengths and the more accurate the current expansion. A common guideline is that the edge lengths should not exceed 0.1λ.

It should be noted that the area between edges which form the triangle facets are solid material, not air gaps, which would be the case for a wire grid model. Therefore, current flows over the entire surface of the object, not just along wires approximating the surface.

Because of the maximum edge length restriction of 0.1λ for convergence, bodies with a large number of triangles generate matrices that are too large for a computer to handle, or large enough so that the computer processing time is too long for practical applications.

C.   PATCH

PATCH is a FORTRAN code which computes the induced surface current density and scattered field using the MoM technique. PATCH requires geometry data as an input (triangle node locations and edge connections). Obviously

for a large scattering object, the process of triangularizing the body requires substantial effort. Thus automated meshing algorithm must be applied to make trade-off studies practical. The meshing can be accomplished using a combination of Computer Aided Design (CAD) software and additional preprocessing to translate the input data into required PATCH format.

The input file for PATCH is an ASCII file that contains all of the geometry information and calculation parameters. The file can be generated using the preprocessing code BUILD which is a geometry builder that is distributed along with PATCH. BUILD is a program that generates faceted target bodies by joining a set of simple three-dimensional shapes. BUILD is capable of generating five basic geometries: quadrilaterals, cylinders, cones, disks and spheres. BUILD is not useful for generating complex high fidelity geometry models.

In addition to the geometry information, BUILD can be used to input the frequency, range of the observation angles and excitation conditions. Upon execution, PATCH looks for a file named "inpatch" in the same directory and after performimg the required calculations it generates an ASCII output file named "outpatch" that contains all of the output

data in readable form. An output file of current coefficients is also generated.

In addition to the geometry input, PATCH provides some options to the user, such as the introduction of symmetry planes. In some cases this option enables the user to reduce the number of edges and thus the time required by using image planes placed at $x=0$, $y=0$ or $z=0$. The image planes can be either perfect electric conductors (PEC) or perfect magnetic conductors (PMC). Other quantities such as voltage sources or distributed impedances follow the image properties and are taken into account automatically. The code capabilities are summarized in Table 4-1.

PATCH also has the option of entering a number of impedance loads, specifying faces with surface impedance, and computing the field at near observation points. All these options make PATCH a powerful and useful tool in the calculation of RCS for a variety of structures.

D.   ACAD

The Advanced Computer Aided Design (ACAD) [13,14] application is capable of performing the auto-meshing that allows the computational EM codes to be practical engineering tools. Databases from other CAD programs can be imported into ACAD, meshed and then output in a special

"facet" format. The ASCII facet file contains the node and facet information required by PATCH, although it is not in the proper format. An ACAD-to-PATCH translator was used to reformat the facet file into one that is recognized by PATCH.

ACAD provides users with the ability to create and modify geometry in two or three dimensions. Users can choose to model geometry with wireframes, surfaces, or solids. Data entry to ACAD is accomplished through one of many input modes available to the designer. ACAD models can be viewed orthographically or in perspective. Users can specify view orientation and choose to display geometry in multiple window configurations. Window operations such as panning, zooming, and auto extents are accomplished at any time providing instream capability. The ACAD user can also control the display of surfaces or solids with options as wireframe, hidden line removal, flat, or Gouraud shading.

At the heart of the ACAD system is the associative database. In an associative database, geometry is linked together in a relational structure that remembers parent/child dependencies. This type of database enables rapid modifications of geometry, since modifying one geometric element automatically adjusts its dependencies based on a set of predefined rules. For instance, changing an edge of a

wing will automatically regenerate any surface(s) built with the edge spline. In turn, all the geometry that is associated with the modified wing (i.e., plane/curve and surface intersections, fillets) will automatically be regenerated. The relationships between codes are summarized in Figure 4-2.

Table 4-1. Summary of PATCH Capabilities.

Arbitrary Shape
 Open/Closed objects
 Modeled by triangular "patches"
   Variable patch density
   Front end for graphical composition
 Arbitrary edge multiplicity
 Non-orientable surfaces
 Symmetry planes may be included
 Multiple bodies

Surface
 Basis functions yield surface currents
   Type: Wilton Rau
   Free of line and point charges
 Equivalent Thevenin circuits
 Lumped and surface impedance loading

Excitation
 Voltage sources
 Plane waves
 Both

Calculated Quantities
 Surface currents
 Far field patterns
 Radar cross section
 Field calculations at
 general observation
 points

Frequency Domain
 Pattern loops
 Frequency loops
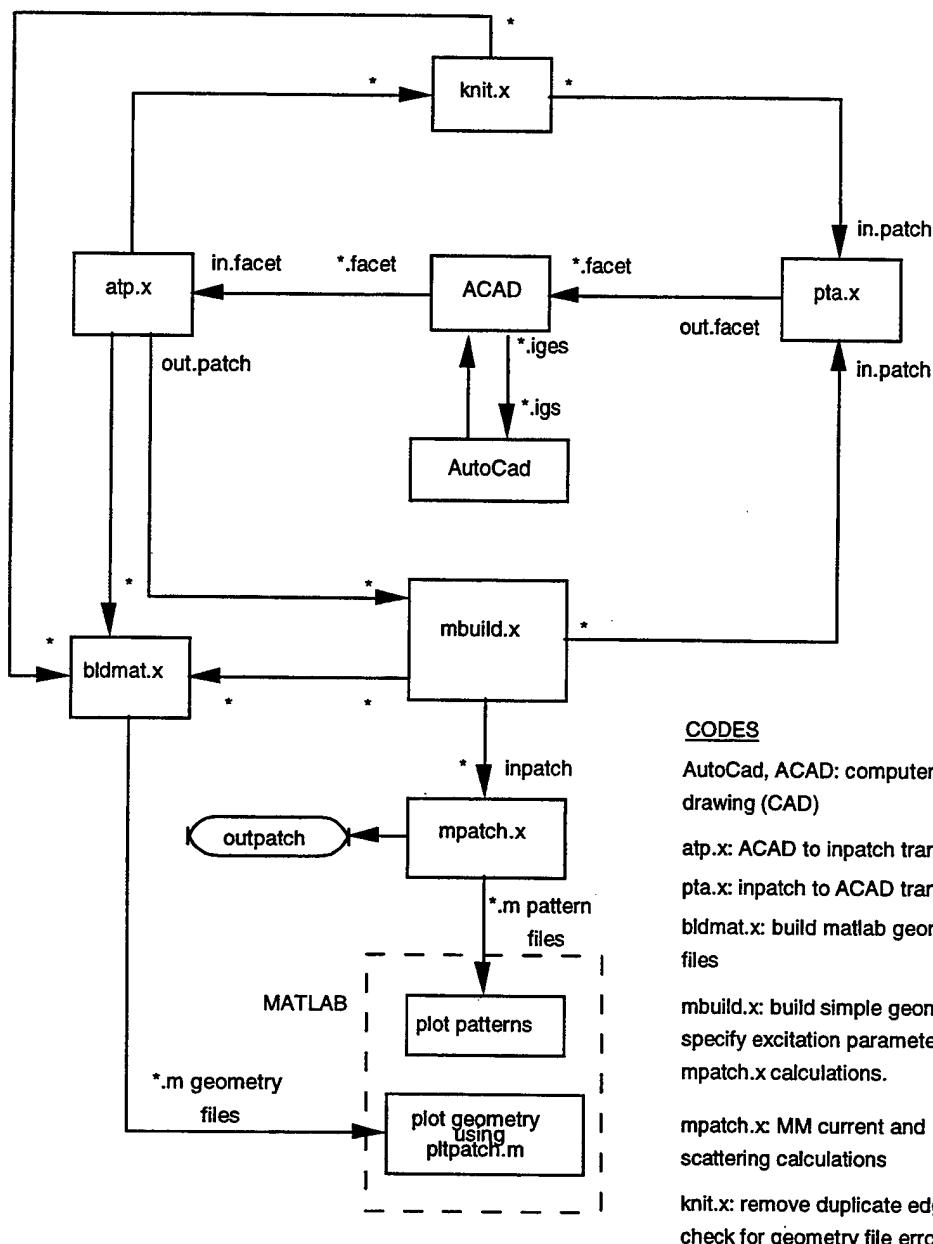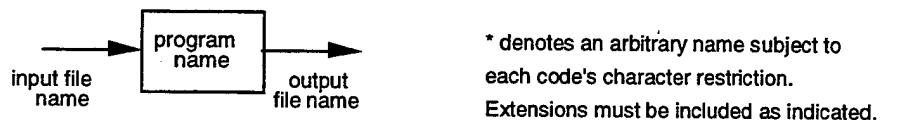
Figure 4-2. Flow chart illustrating the relationships between the various computer codes (from [12]).

V. RESULTS AND ANALYSIS

The objective of this thesis, as stated in Chapter I, is to investigate and evaluate the effectiveness of ship RCS reduction in the HF band by means of shaping. The approach taken is to compare the RCS of shaped ships to that of a conventional baseline. The RCS is compared for elevation angles from 10 to 30 degrees and frequencies of 5, 10, 15 and 20 MHz. The ship coordinate system is defined in Figure 5-1. The baseline used is a *DDG-51 AEGIS CLASS DESTROYER*, shown in Figure 5-2.

The shaped ship designs were generated using the program ACAD, which is discussed in Chapter IV. Shaping primarily involved changing the superstructure. Sloped deckhouse walls were used and the mast removed. The first iteration, referred to as Mod 1, is shown in Figure 5-3. It has a DDG-51 hull and deckhouse walls tilted back 27° from the vertical. The second iteration (Mod 2) is shown in Figure 5-4. It has deckhouse walls tilted back 45°. In order to isolate the effect of superstructure changes on RCS, the scattering from the hull itself was computed. The hull with a solid deck is shown in Figure 5-5.

Initial calculations for Mods 1 and 2 did not show any improvement over the baseline. This was not entirely unexpected because the height of the deckhouse is near one wavelength in the HF band. This is too small for shaping to be effective because the specular lobe is so wide. In an attempt to enhance forward scattering and reduce backscattering a rounded structure was added. This design is Mod 3, which is shown in Figure 5-6.

Before proceeding with RCS calculations the conditions for convergence were established. The previously stated rule of thumb is that the maximum edge length should not exceed 0.1λ. However, ACAD generates a variable mesh which is more dense near corners and edges than it is in smooth surface areas. This characteristic is clearly visible in Figure 5-3. Thus all edge lengths do not have to be less than 0.1λ for convergence as long as edges near discontinuities, where current variation is greatest, are less than 0.1λ. The minimum acceptable number of edges is desired because of the long computation times involved. Table 5-1 summarizes the ship designs and the number of edges for convergence. Convergence was tested by increasing the number of edges and looking for a significant change in RCS. If no change was observed then the model with the smaller number of edges was used.

Table 5-1. Ship designs and the number of edges for convergence.

Model	Number of edges for convergence
Baseline	3,635
Mod 1	3,175
Mod 2	2,402
Mod 3	2,474
Hull	2,372

Data were generated over a range of frequencies and elevation angles. Azimuth angle was varied from 0° to 180°.
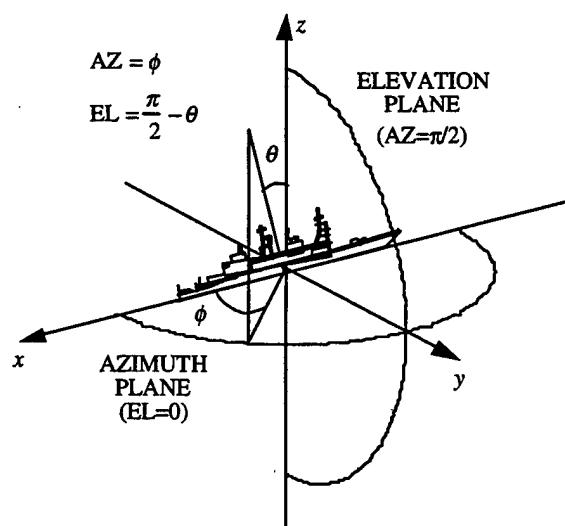
Figure 5-1. Ship's Coordinate System.

Since the ships are nearly symmetrical with respect to the center line, the RCS for azimuth angles between 180° and 360° are similar to those between 0° and 180°. For all cases the monostatic RCS for both polarizations was computed, $\sigma_{\theta\theta}$ and $\sigma_{\phi\phi}$. An infinite perfectly conducting ground plane is used to represent the ocean surface. Azimuth plots of calculated $\sigma_{\theta\theta}$ and $\sigma_{\phi\phi}$ with the infinite perfectly conducting ground plane are included in Figures 5-9 through 5-20.

A comparison of the data shows that shaping the superstructure does not necessarily reduce RCS in the HF frequency band. In fact, the major RCS contributor is the hull. At ship grazing angles (low elevation angles near bow or stern incidence) the baseline and all of the mods had higher RCS than the hull alone. This is probably due to surface waves that are guided along the superstructure and then reflect at the end walls. This phenomenon only occurs for vertical polarization ($\sigma_{\theta\theta}$). Appendix A contains data for ships in free space (without the infinite perfectly conducting ground plane). As it can be seen, the resulting RCS is smaller in all cases when the ground plane is not included.
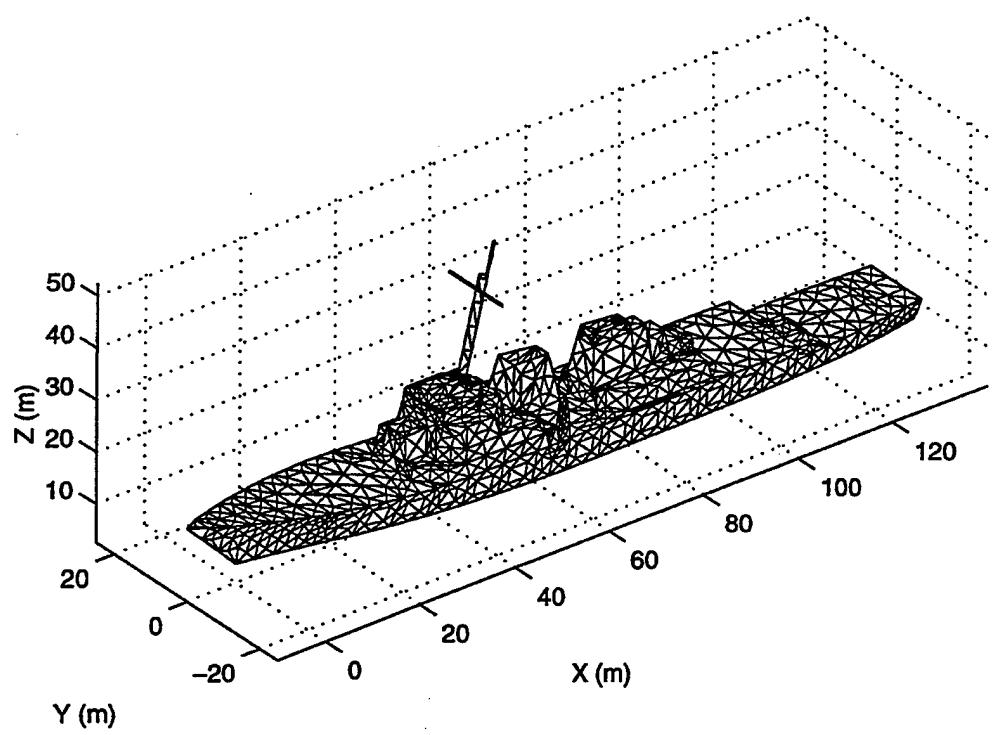
(a)
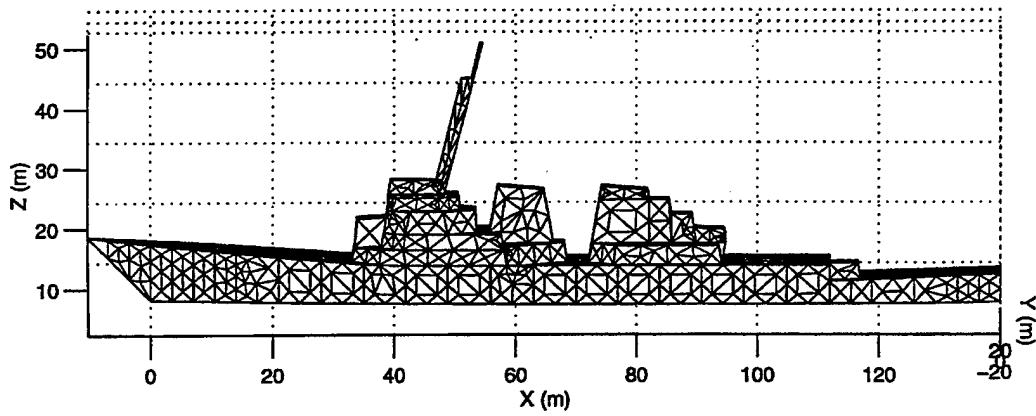
(b)

Figure 5-2. Baseline ship (DDG-51)
(a) 3D view (b) Side view.
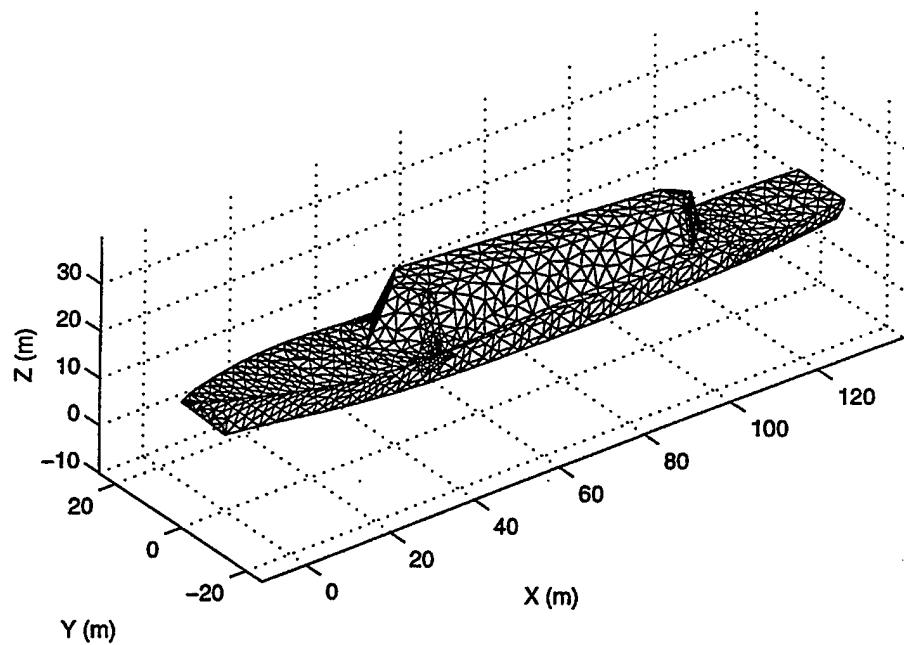
(a)
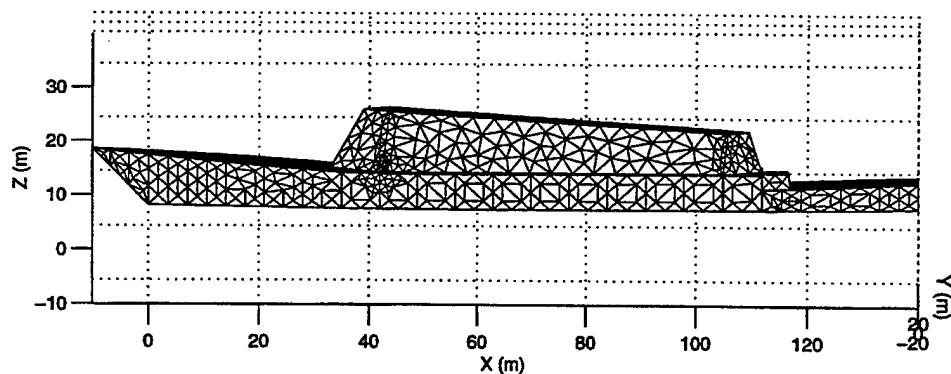
(b)

Figure 5-3. First Modification (Mod 1)
(a) 3D view (b) Side view.
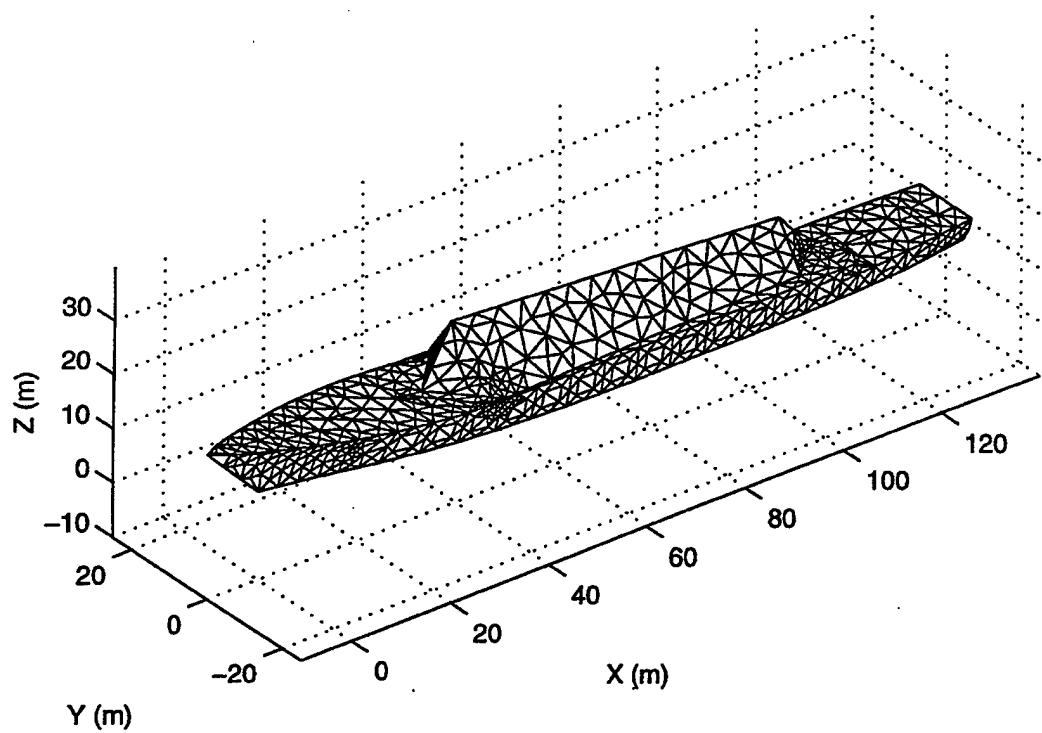
(a)
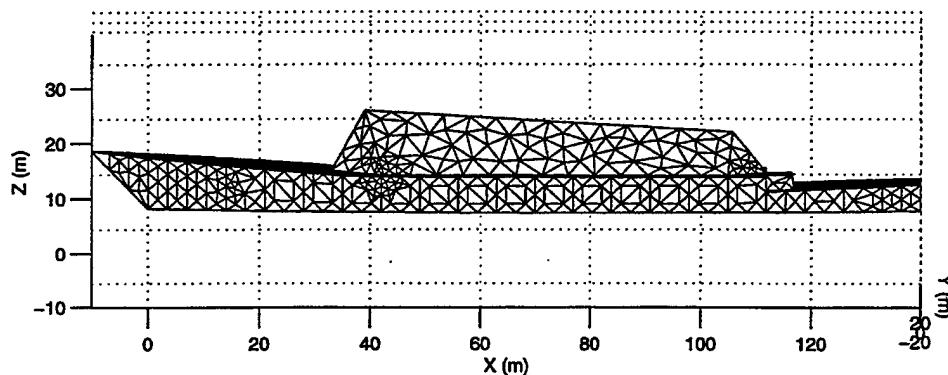
(b)

Figure 5-4. Second Modification (Mod 2)
(a) 3D view (b) Side view.

57
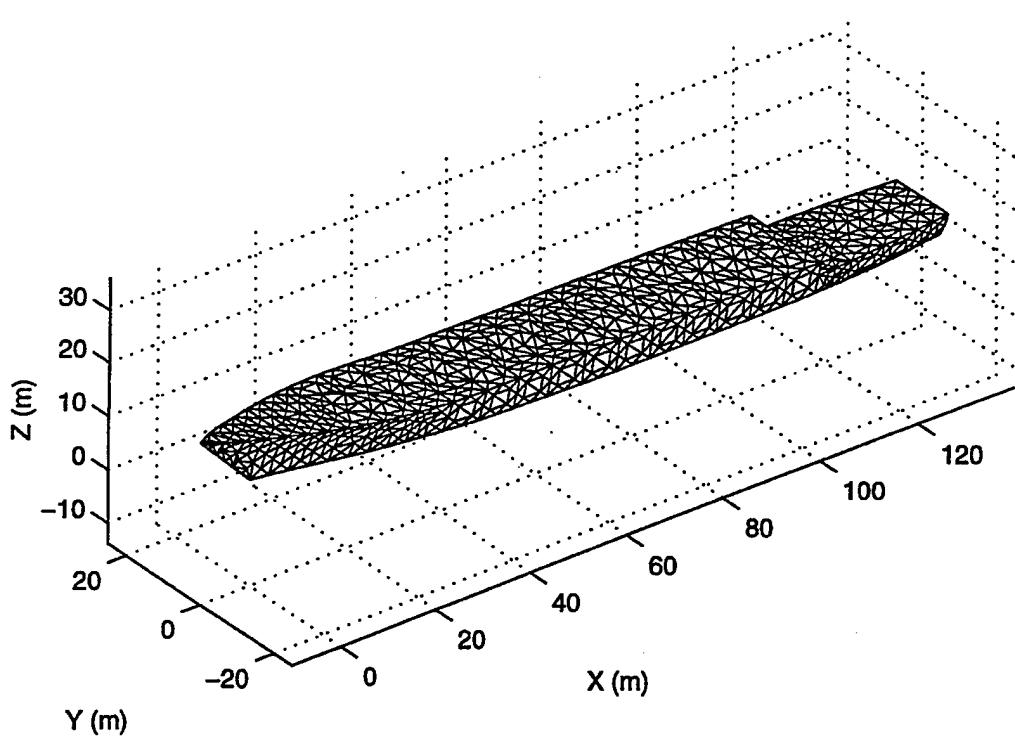
(a)
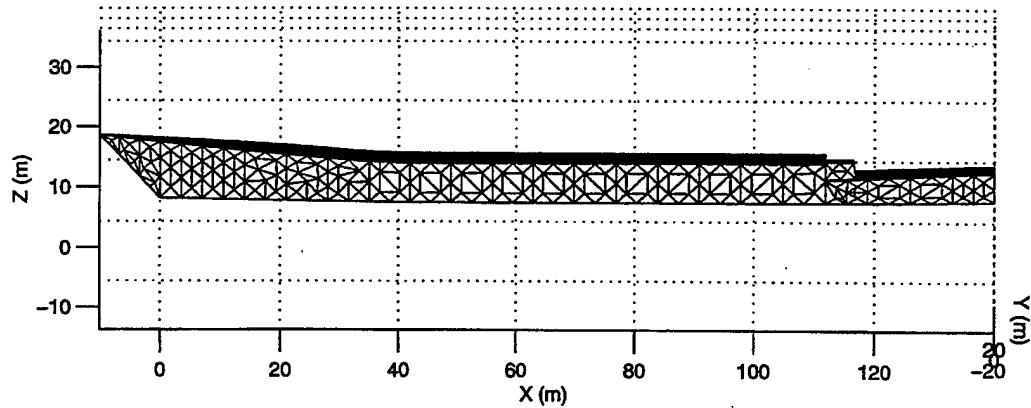
(b)

Figure 5-5. DDG-51 Hull (a) 3D view (b) Side view.
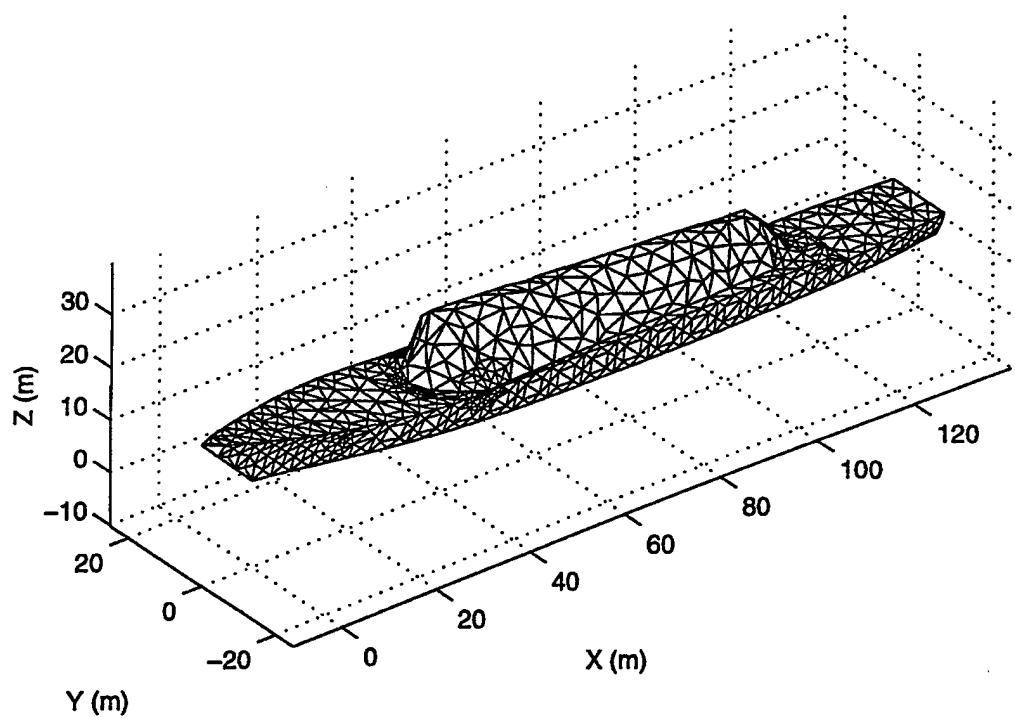
(a)
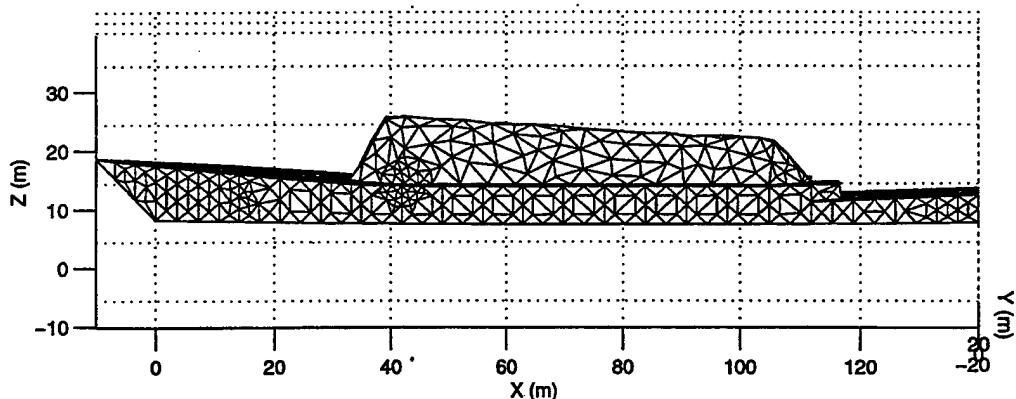
(b)

Figure 5-6. Third Modification (Mod 3)
(a) 3D view   (b) Side view.

In an effort to access the impact of a shaped hull on the RCS, an inverted (Tumblehome) hull was generated using ACAD. The hull walls are tilted back as they rise above from the water line as shown in Figure 5-7. This type of hull design has been seen frequently in NAVSEA presentations and literature [15]. Figure 5-8 shows the patch model of a Tumblehome hull. The RCS of both the new and old hull is shown in Figures 5-21 through 5-32. The reduction in RCS for azimuth angles near the bow and stern is probably due to the Tumblehome's tapered width, which allows traveling waves to scatter in the forward direction.
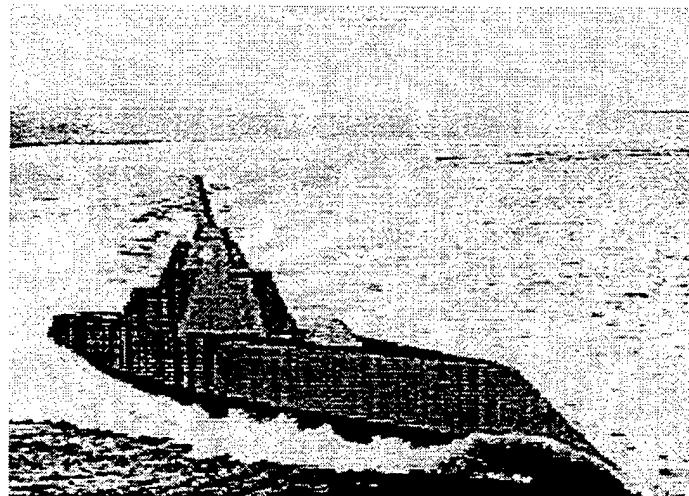
Figure 5-7. DD-21 Destroyer with a
Tumblehome Hull (from [15]).
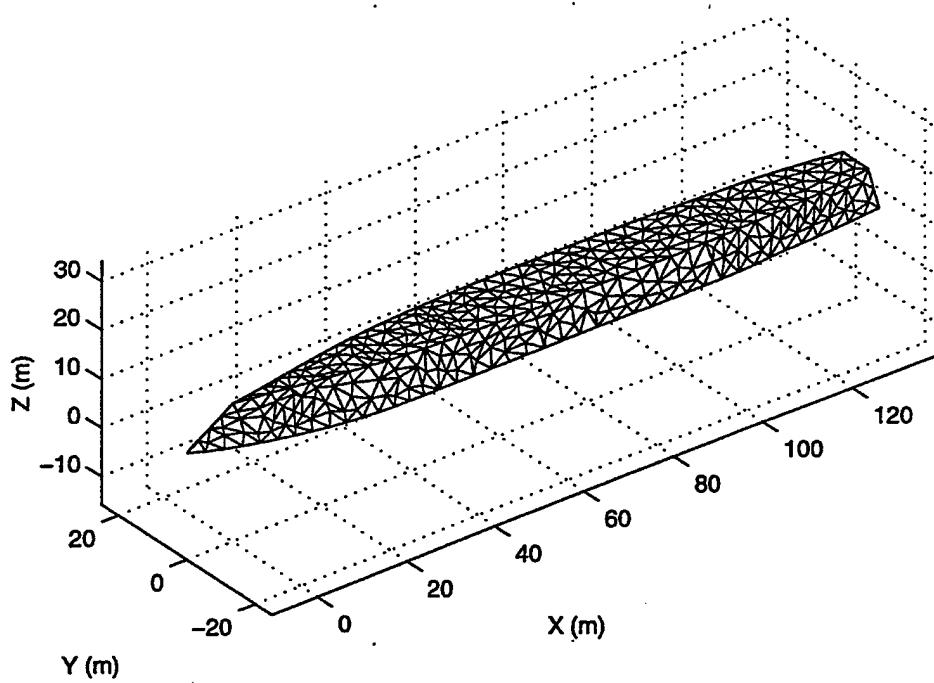
(a)
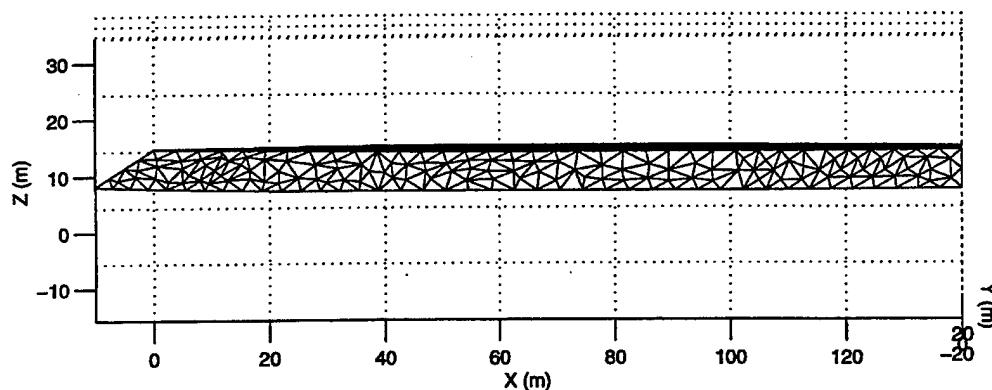
(b)

Figure 5-8. New Hull (a) 3D view (b) Side view.

61
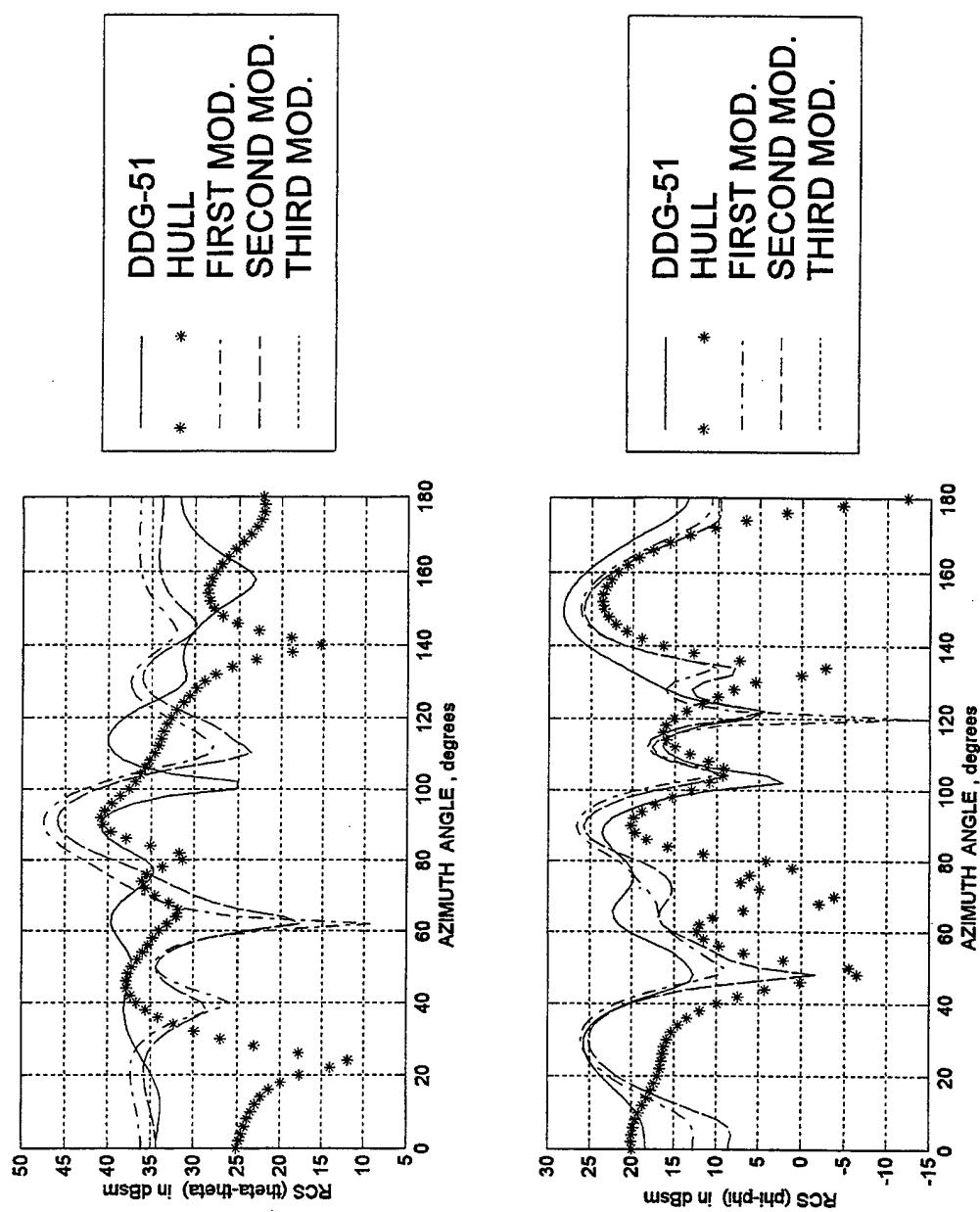
Figure 5-9. Computed RCS for frequency of 5 MHz and elevation angle of 10 degrees including infinite ground plane.
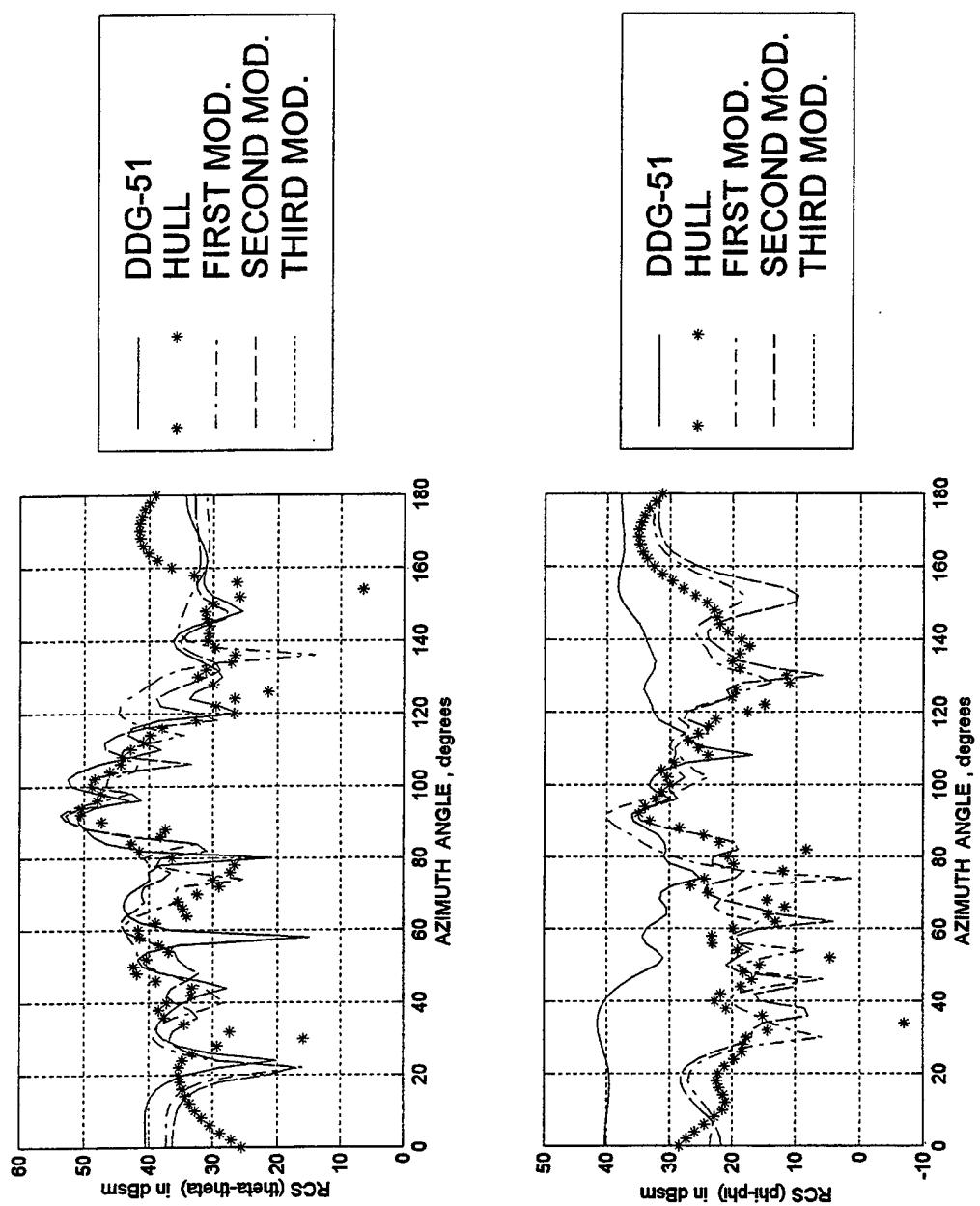
Figure 5-10. Computed RCS for frequency of 10 MHz and elevation angle of 10 degrees including infinite ground plane.
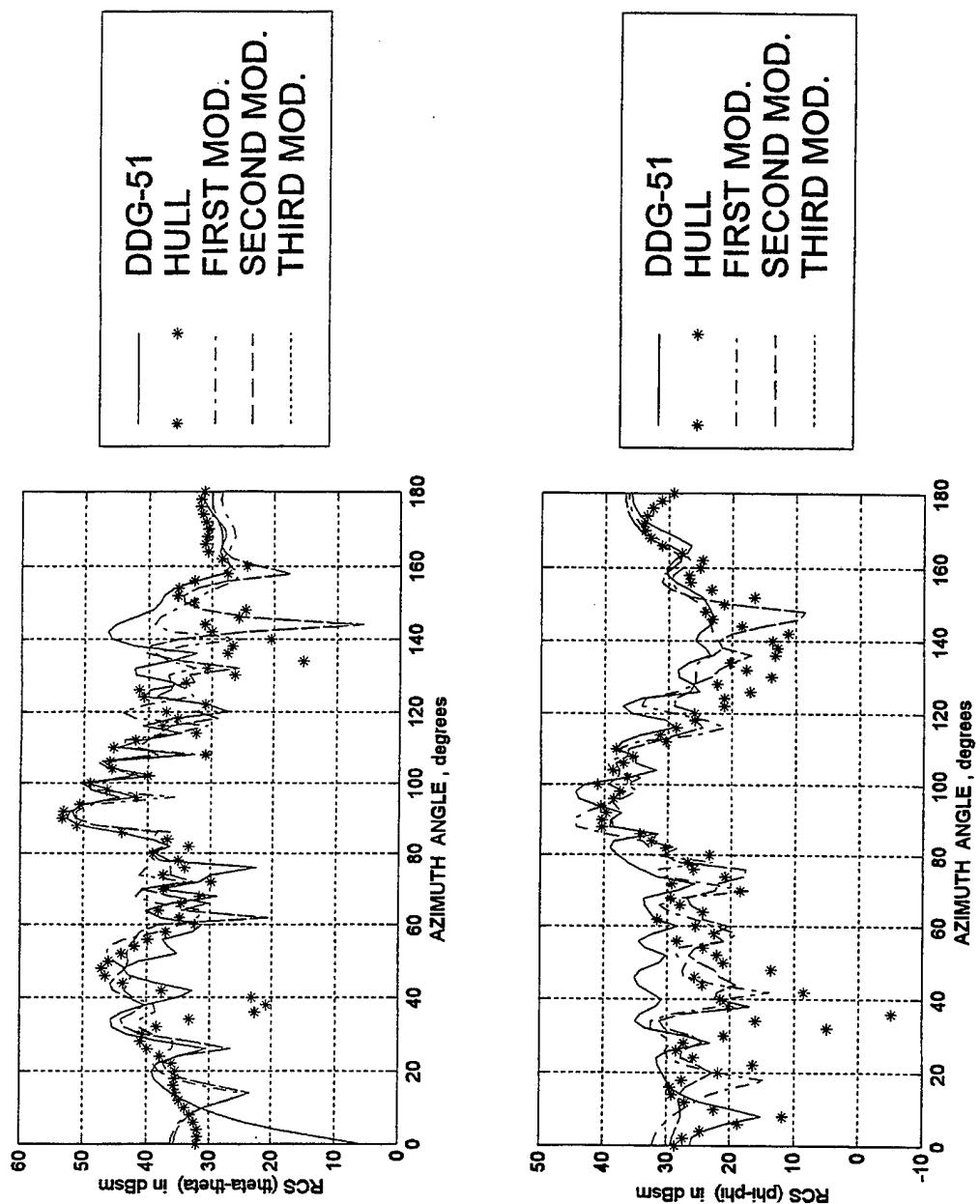
**Figure 5-11**. Computed RCS for frequency of 15 MHz and elevation angle of 10 degrees including infinite ground plane.

64
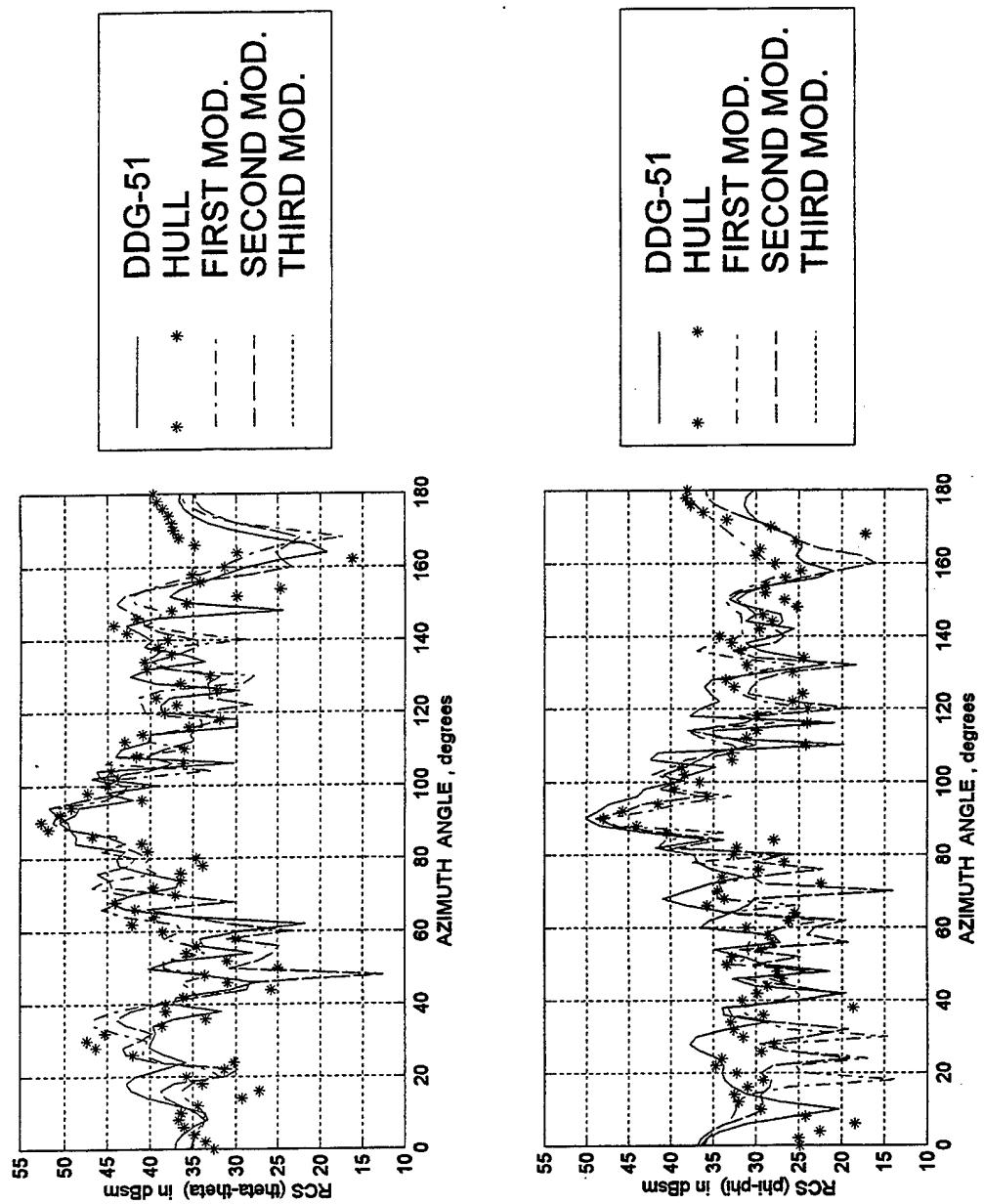
Figure 5-12. Computed RCS for frequency of 20 MHz and elevation angle of 10 degrees including infinite ground plane.
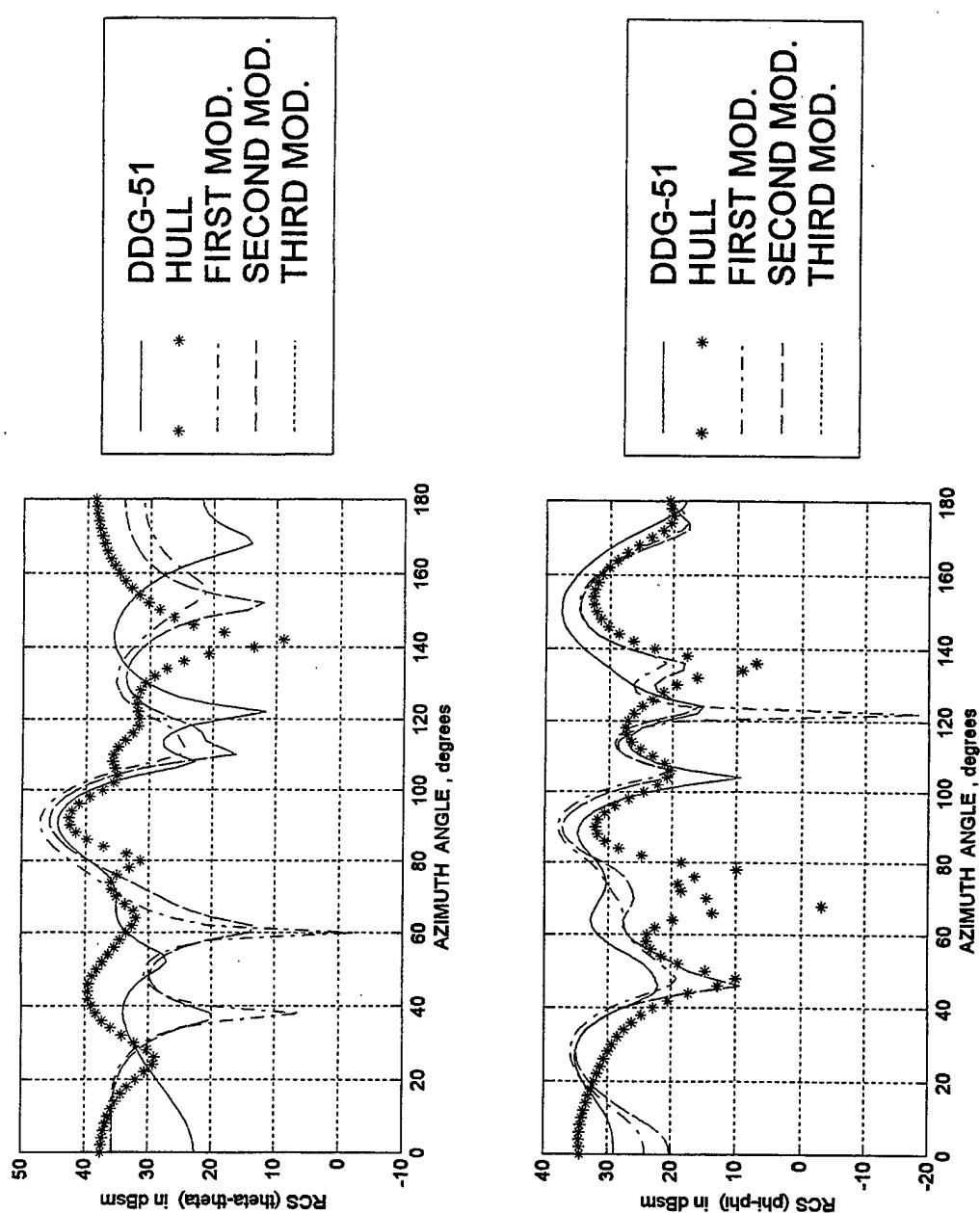
Figure 5-13. Computed RCS for frequency of 5 MHz and elevation angle of 20 degrees including infinite ground plane.
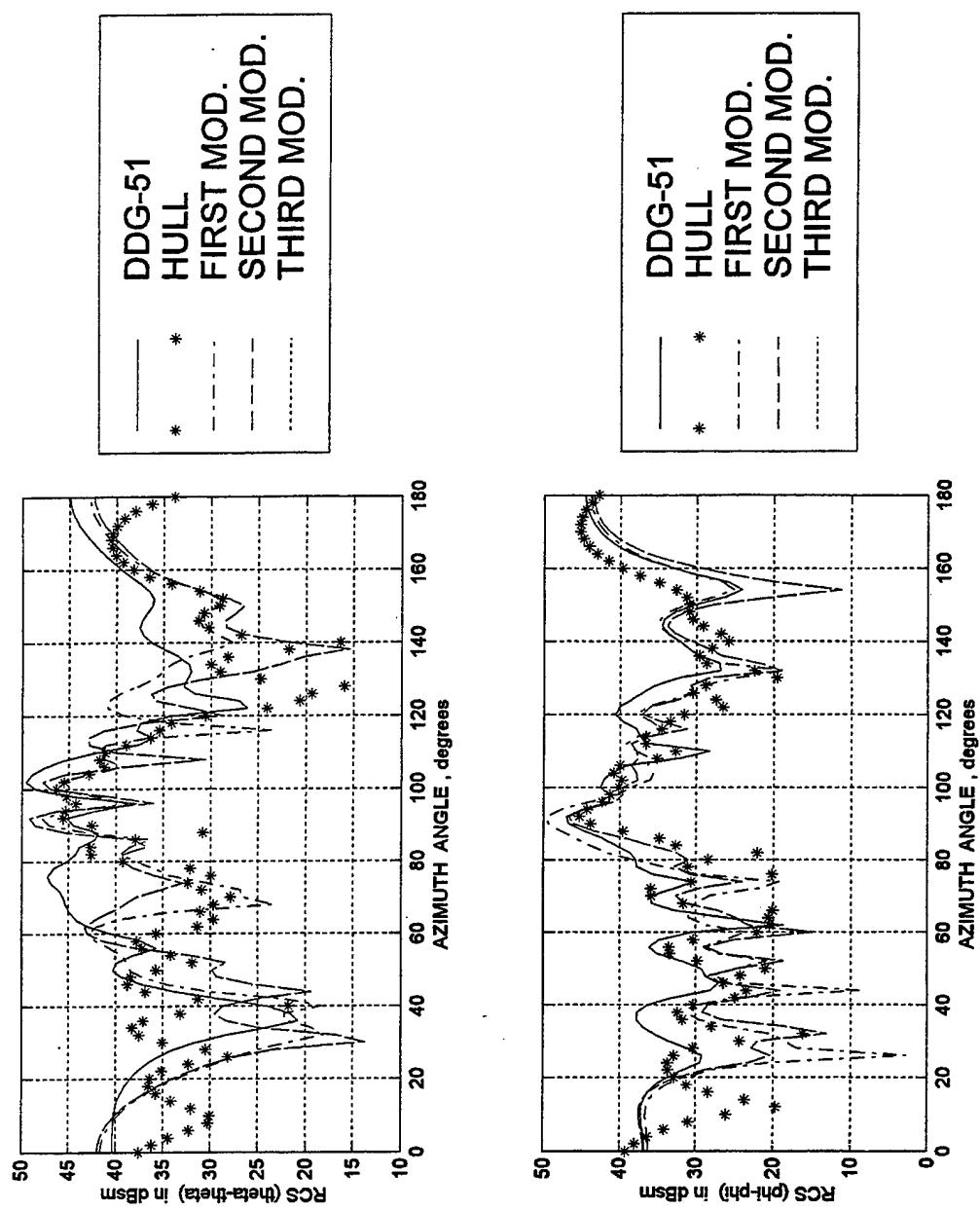
Figure 5-14. Computed RCS for frequency of 10 MHz and elevation angle of 20 degrees including infinite ground plane.
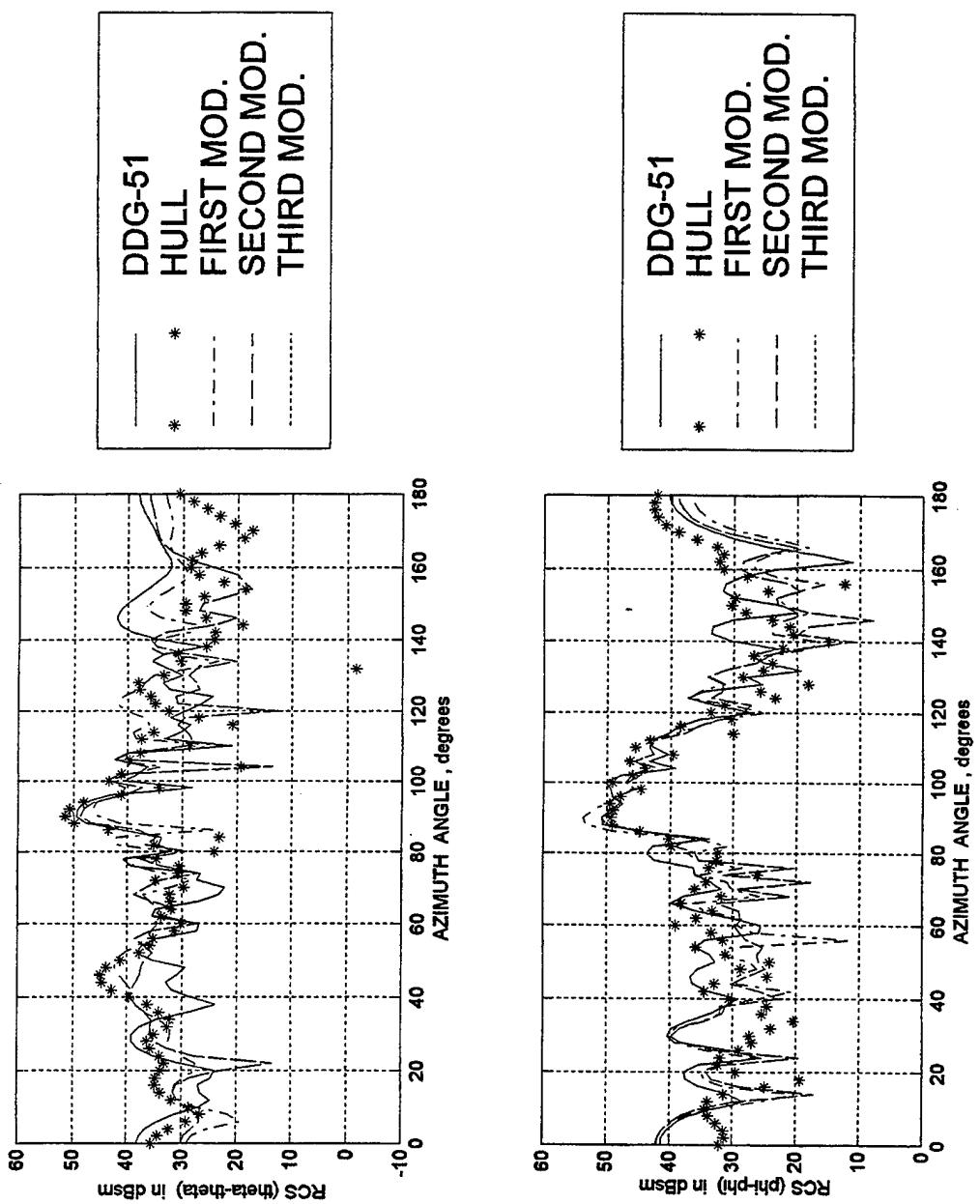
Figure 5-15. Computed RCS for frequency of 15 MHz and elevation angle of 20 degrees including infinite ground plane.
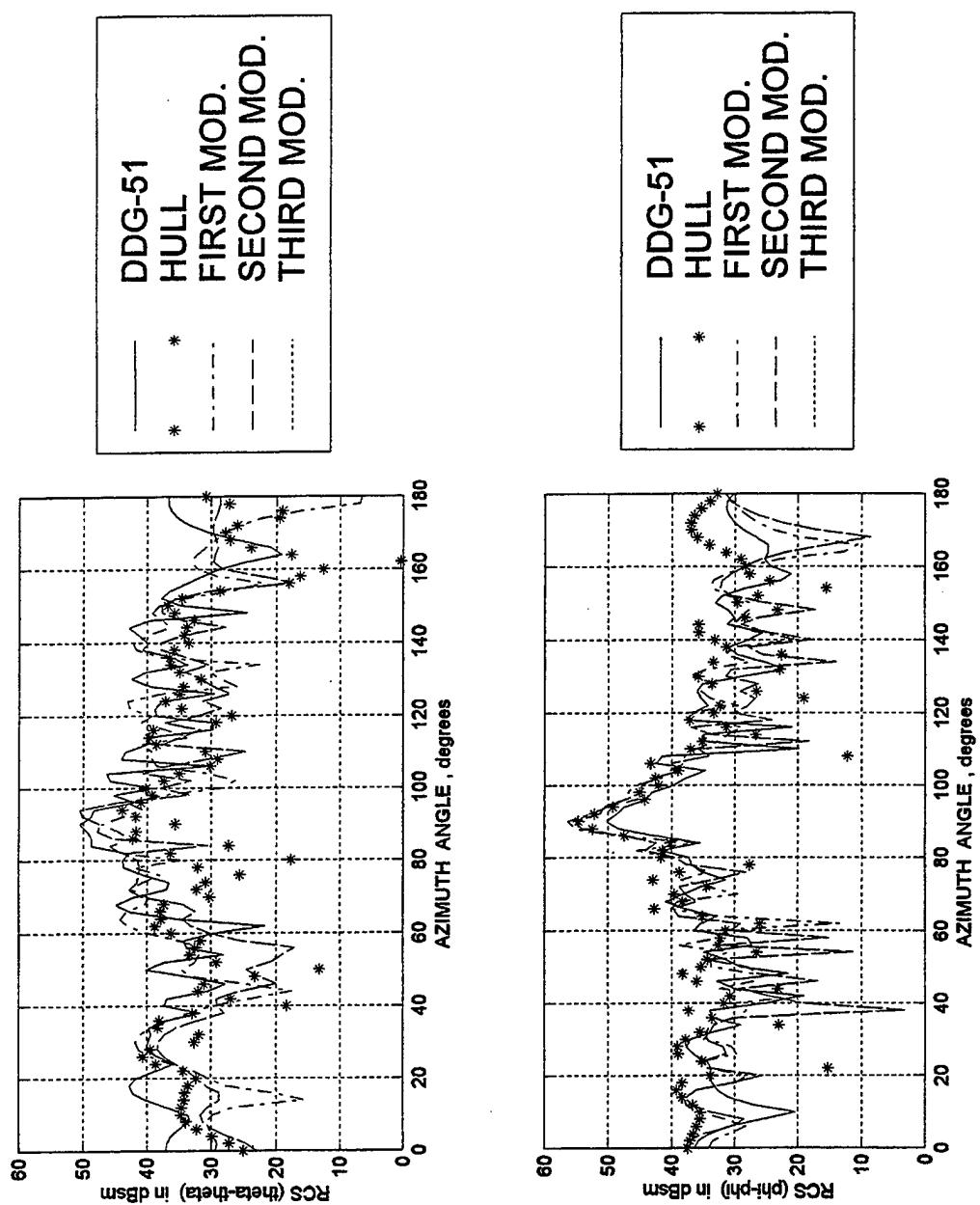
Figure 5-16. Computed RCS for frequency of 20 MHz and elevation angle of 20 degrees including infinite ground plane.
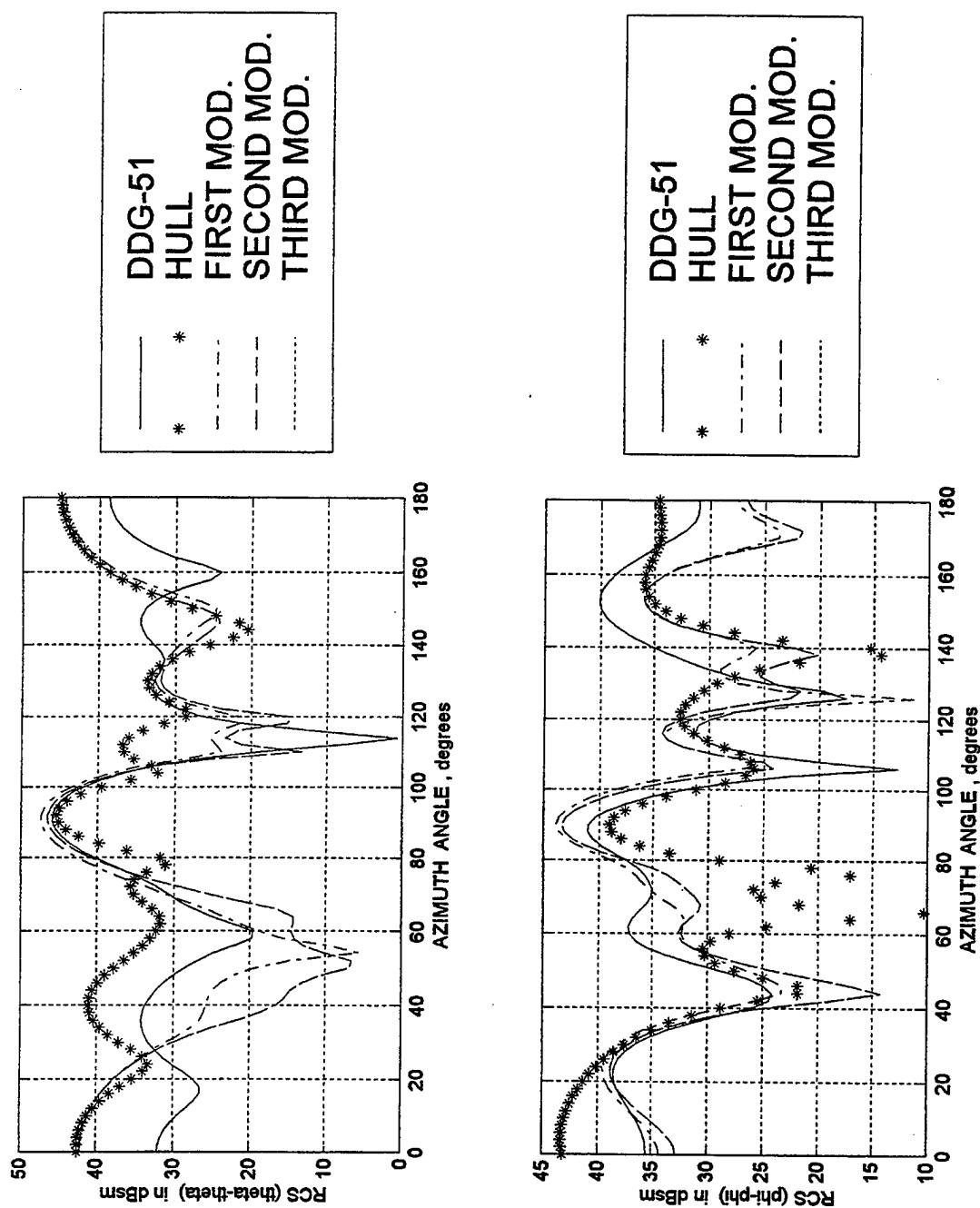
Figure 5-17. Computed RCS for frequency of 5 MHz and elevation angle of 30 degrees including infinite ground plane.

70
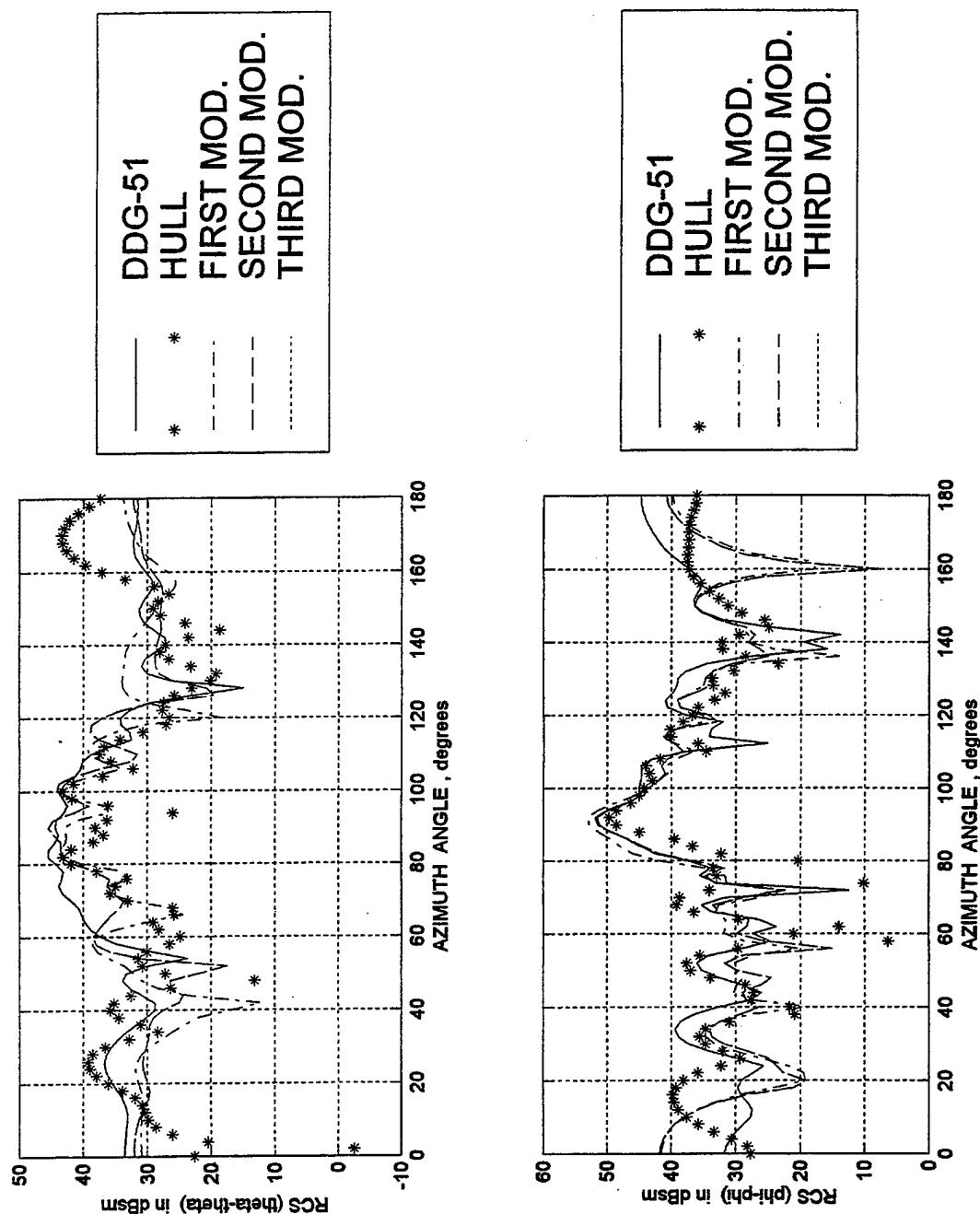
Figure 5-18. Computed RCS for frequency of 10 MHz and elevation angle of 30 degrees including infinite ground plane.

71
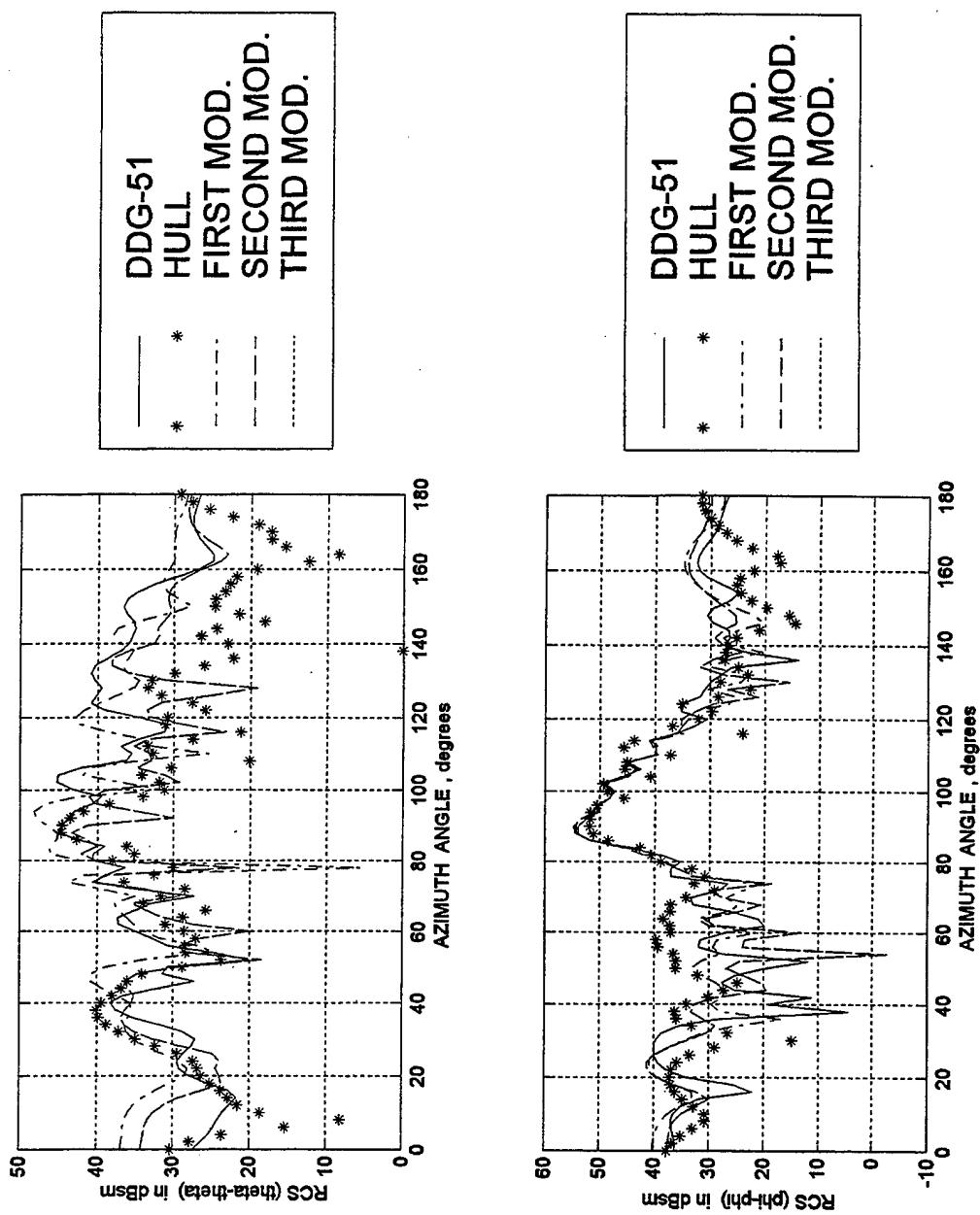
Figure 5-19. Computed RCS for frequency of 15 MHz and elevation angle of 30 degrees including infinite ground plane.
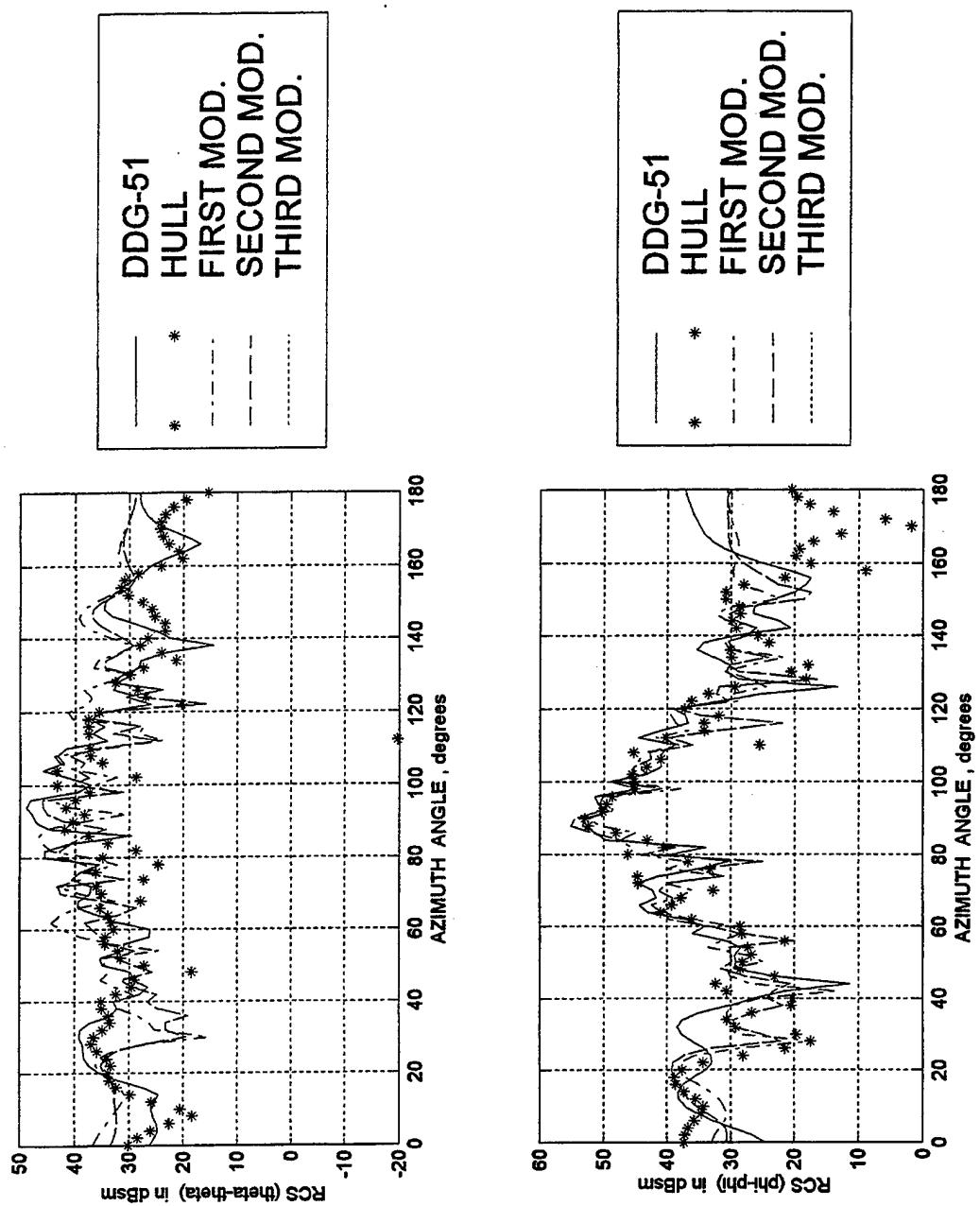
Figure 5-20. Computed RCS for frequency of 20 MHz and elevation angle of 30 degrees including infinite ground plane.

73
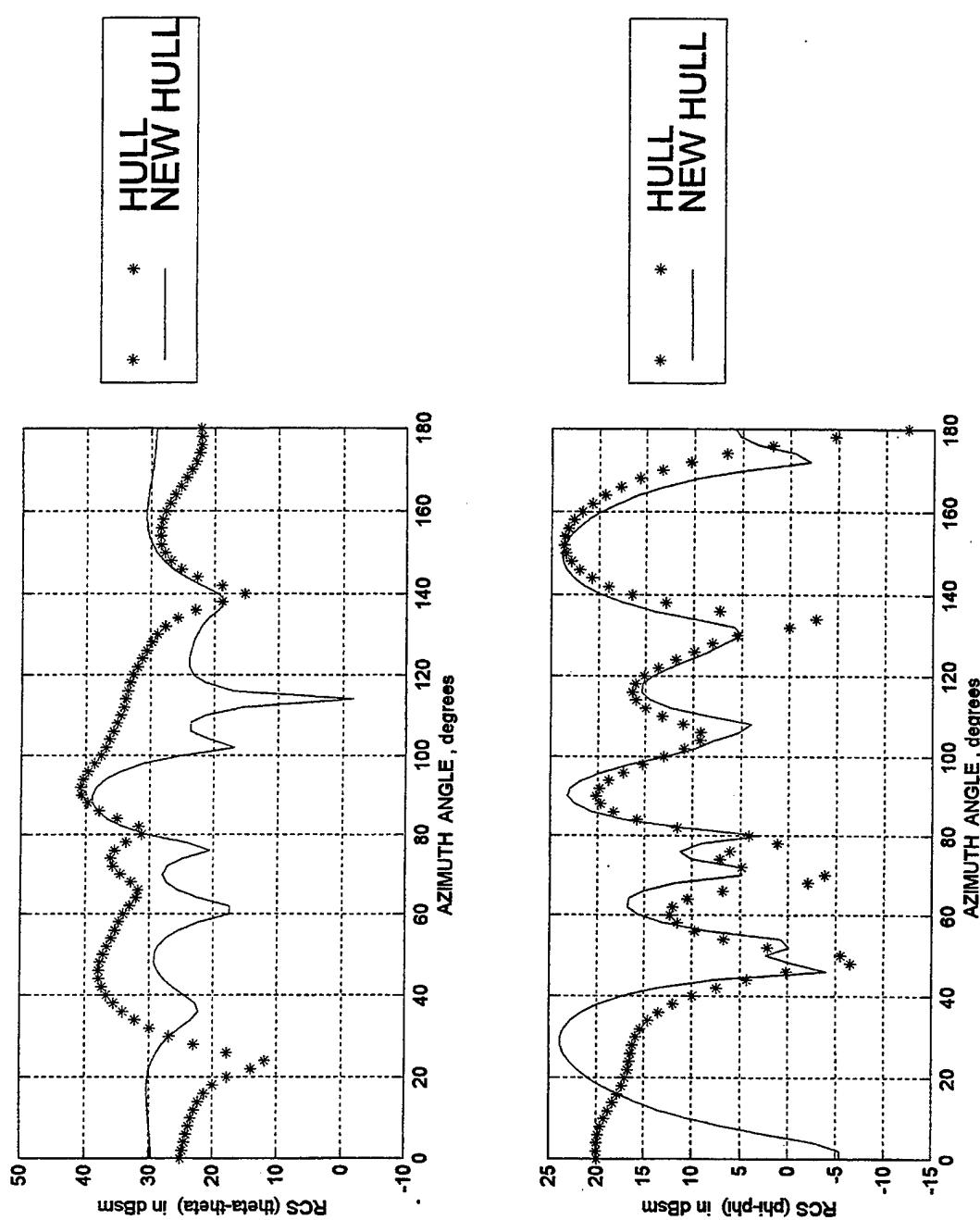
Figure 5-21. Computed RCS of the two different hull designs for frequency of 5 MHz and elevation angle of 10 degrees including infinite ground plane.

74
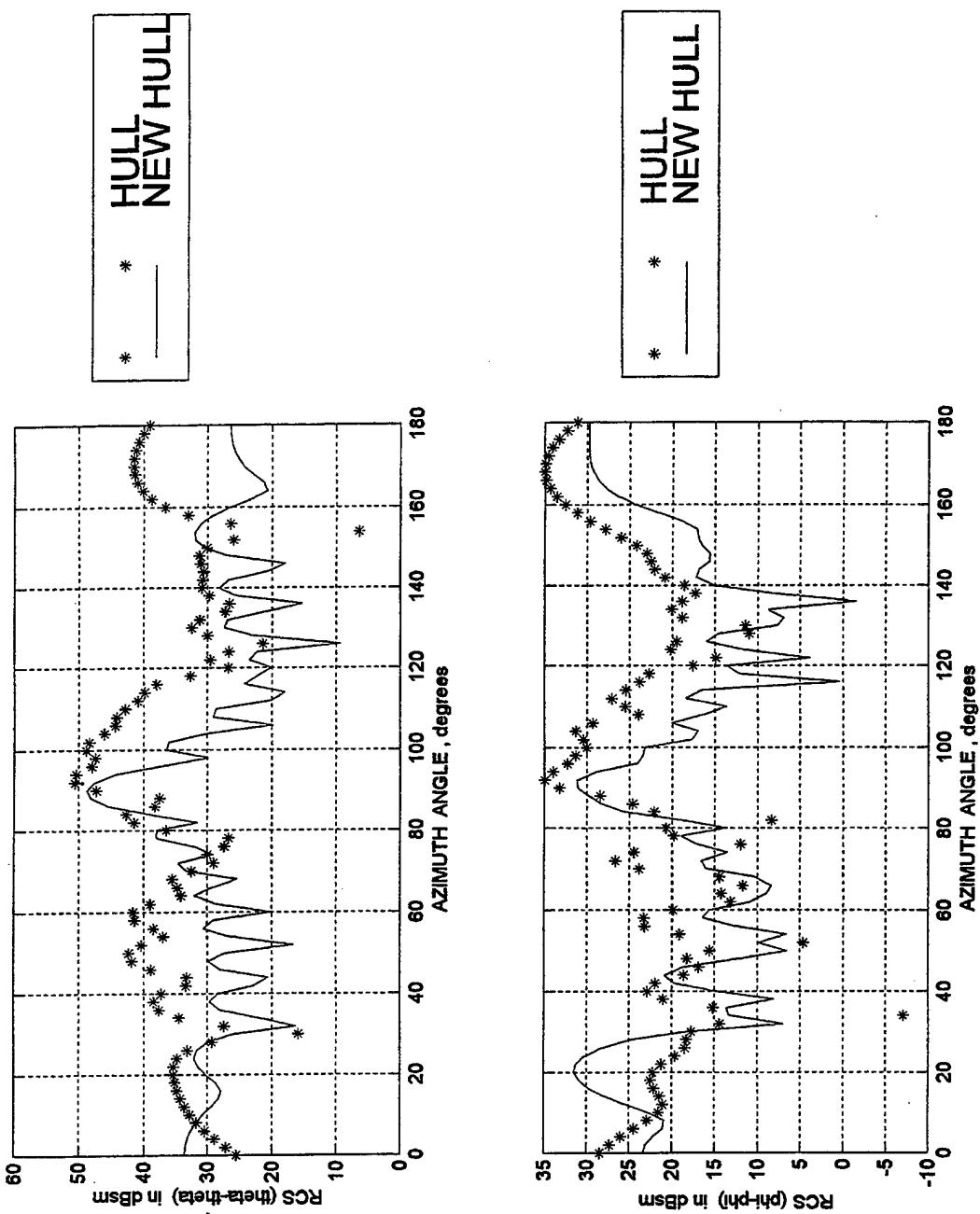
Figure 5-22. Computed RCS of the two different hull designs for frequency of 10 MHz and elevation angle of 10 degrees including infinite ground plane.

75
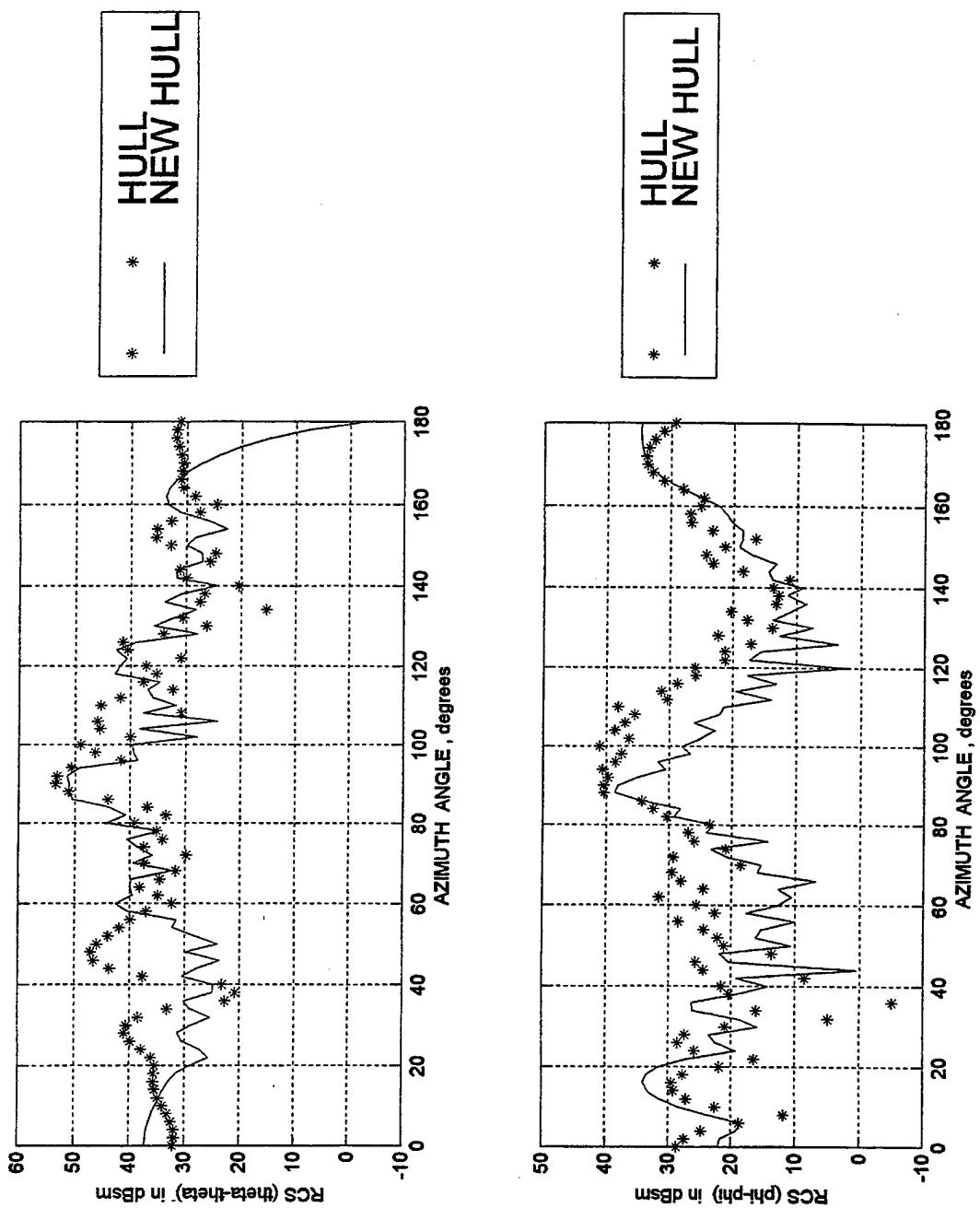
Figure 5-23. Computed RCS of the two different hull designs for frequency of 15 MHz and elevation angle of 10 degrees including infinite ground plane.
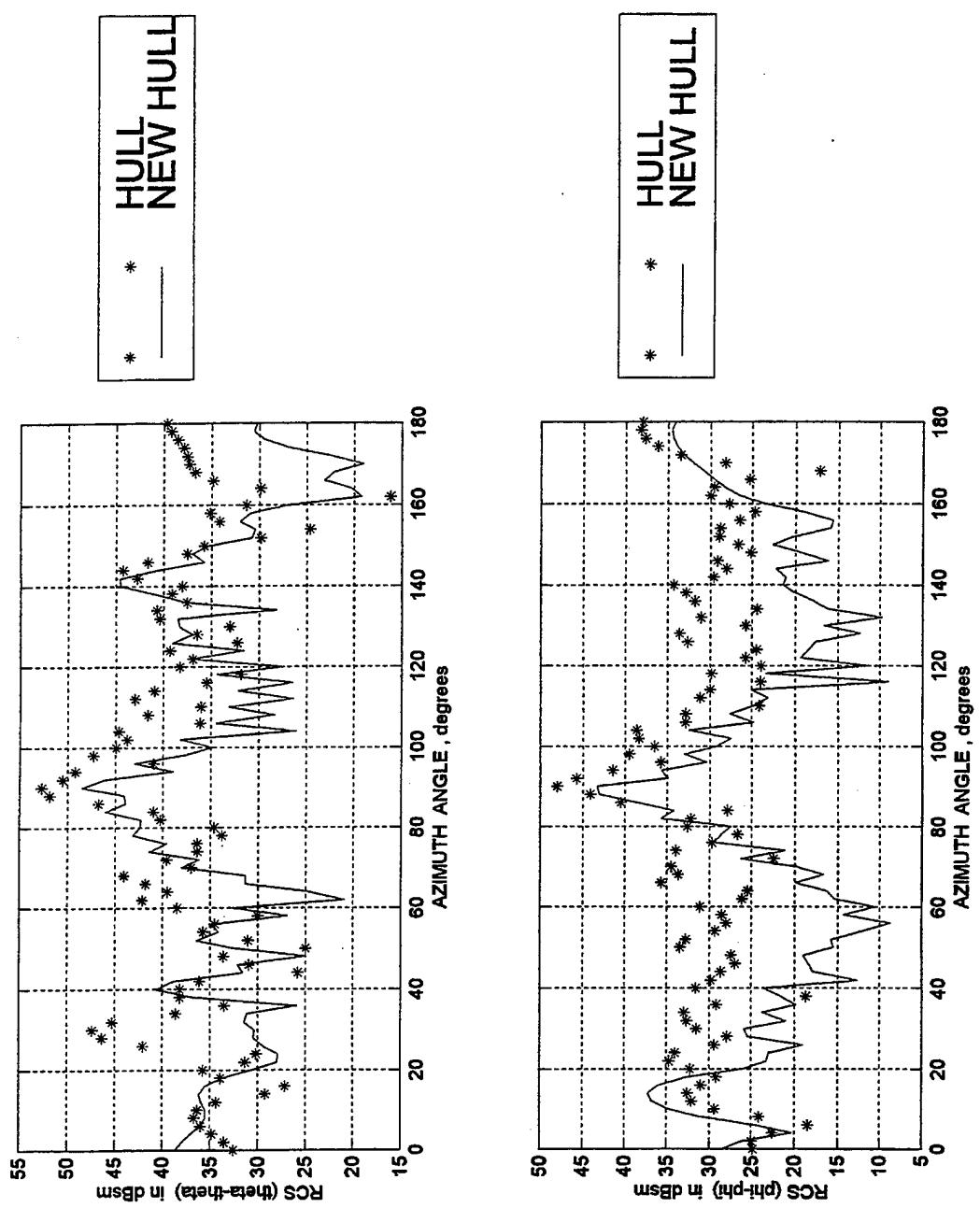
Figure 5-24. Computed RCS of the two different hull designs for frequency of 20 MHz and elevation angle of 10 degrees including infinite ground plane.

77
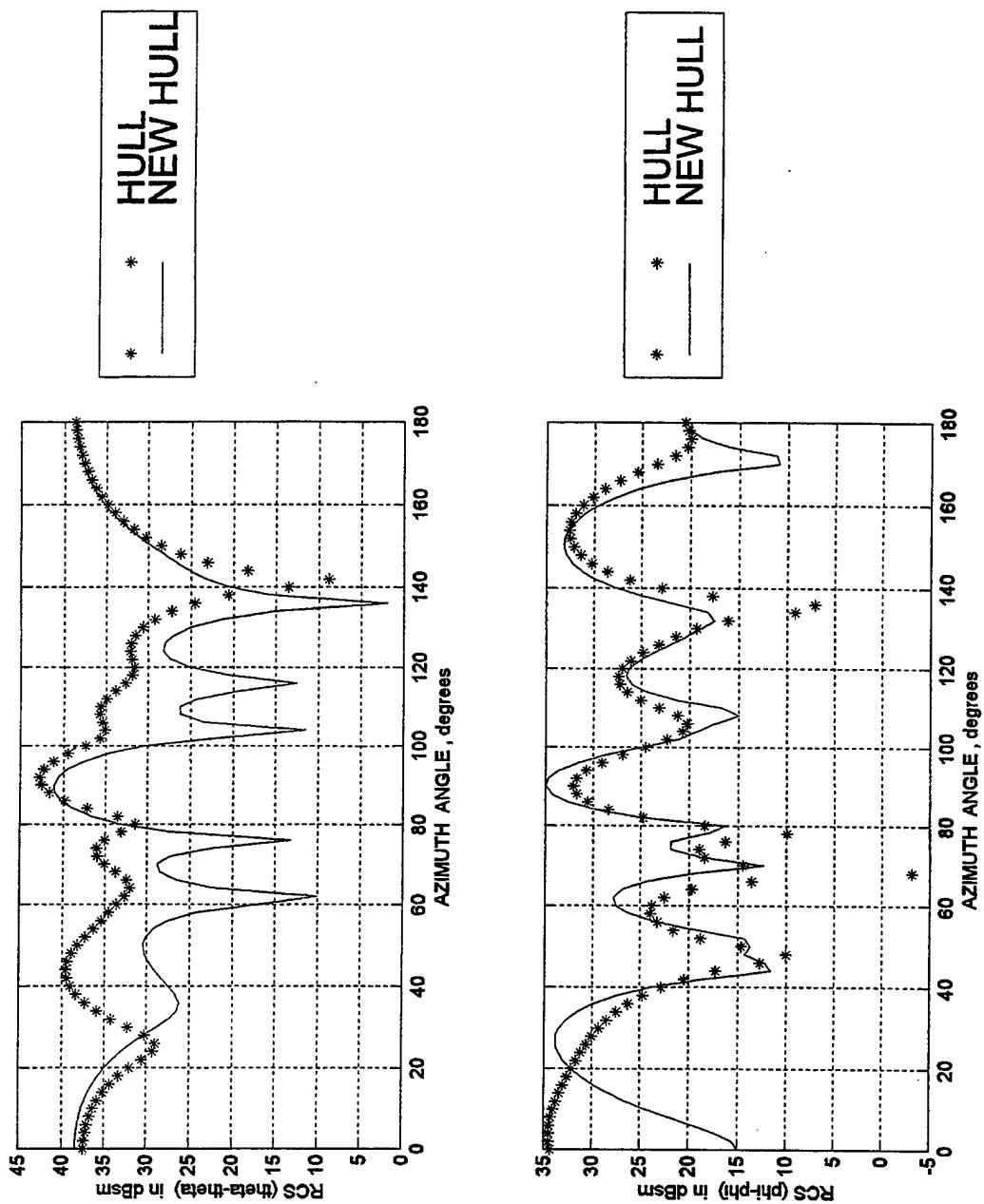
Figure 5-25. Computed RCS of the two different hull designs for frequency of 5 MHz and elevation angle of 20 degrees including infinite ground plane.
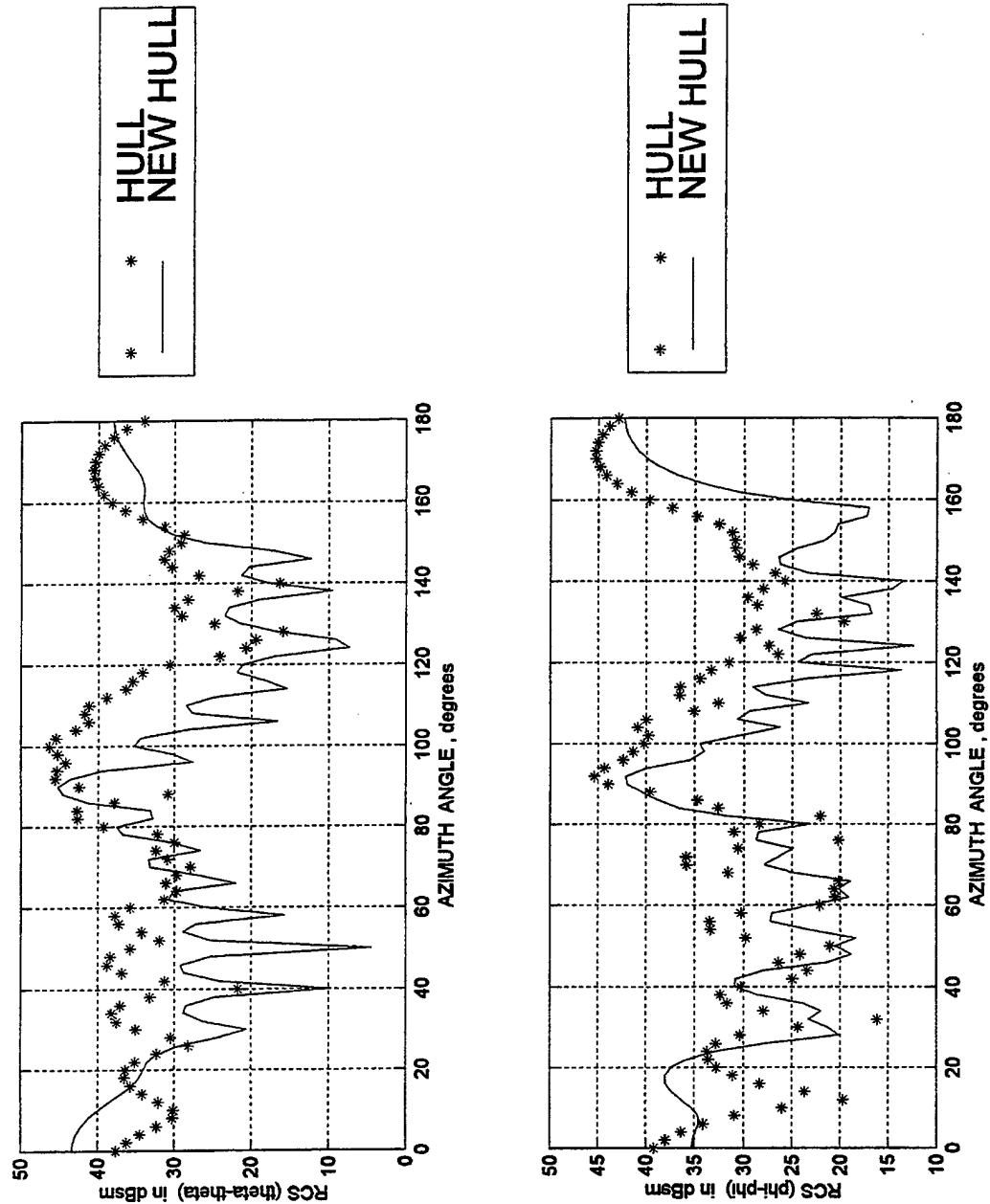
Figure 5-26. Computed RCS of the two different hull designs for frequency of 10 MHz and elevation angle of 20 degrees including infinite ground plane.
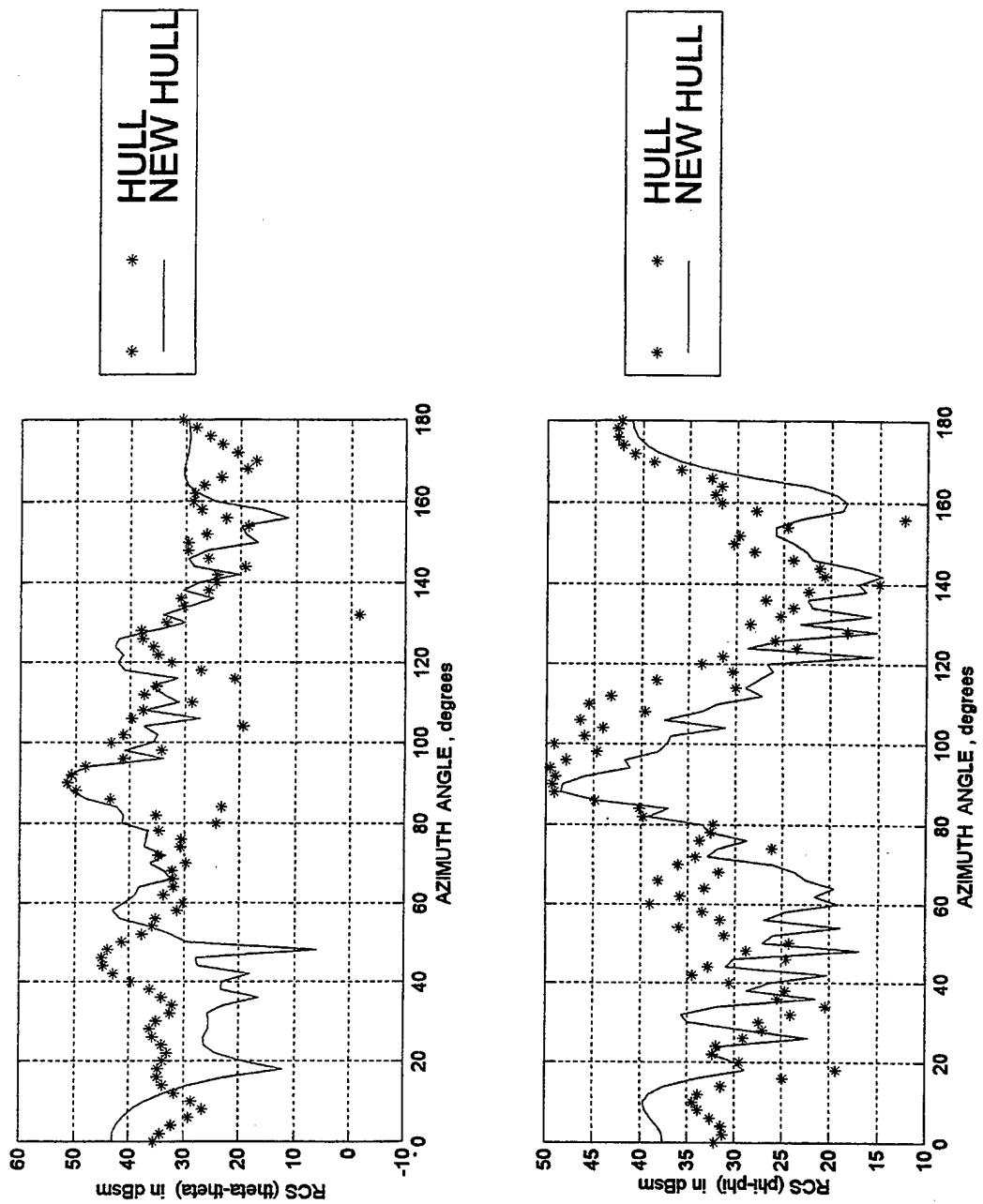
Figure 5-27. Computed RCS of the two different hull designs for frequency of 15 MHz and elevation angle of 20 degrees including infinite ground plane.
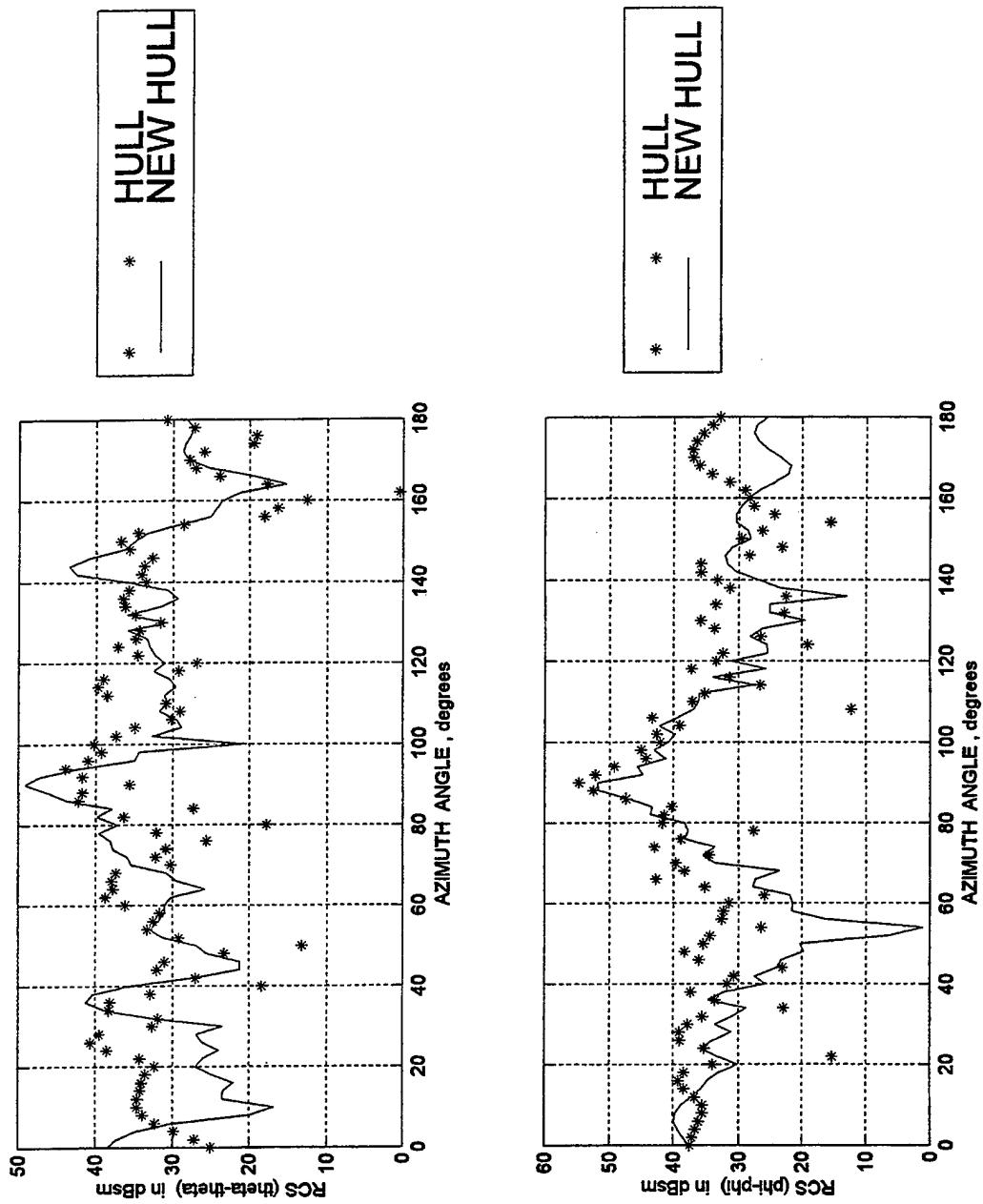
Figure 5-28. Computed RCS of the two different hull designs for frequency of 20 MHz and elevation angle of 20 degrees including infinite ground plane.

81
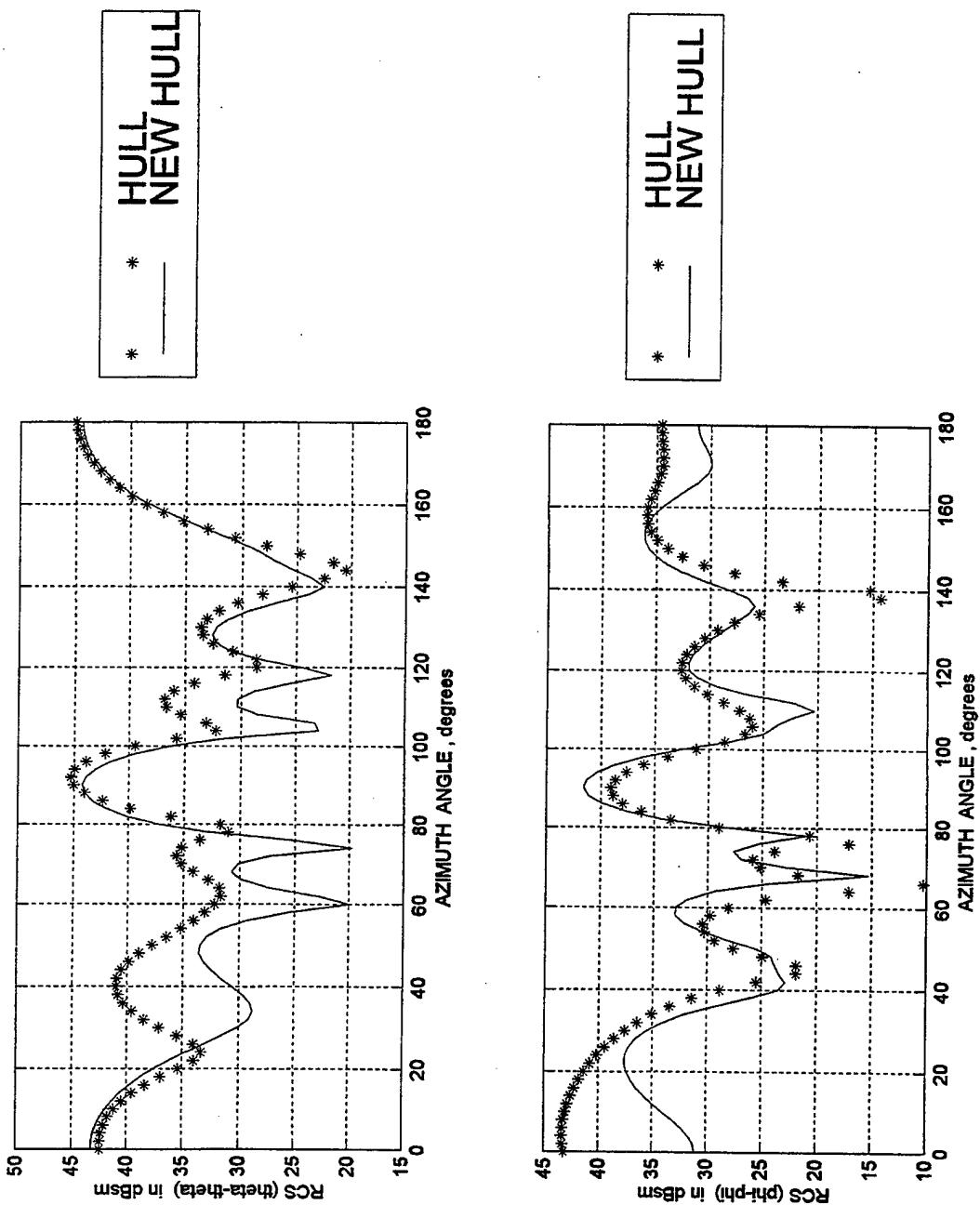
Figure 5-29. Computed RCS of the two different hull designs for frequency of 5 MHz and elevation angle of 30 degrees including infinite ground plane.
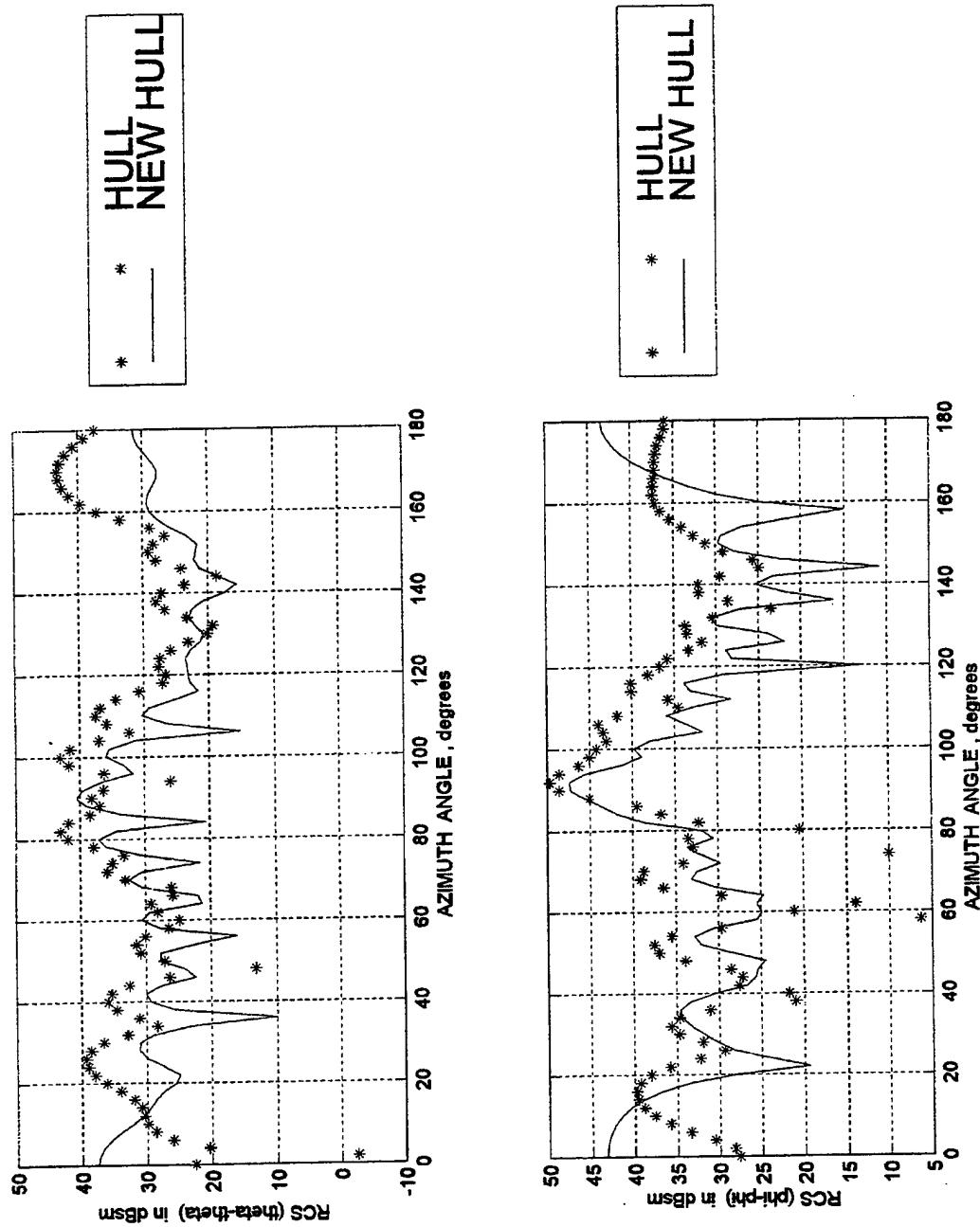
Figure 5-30. Computed RCS of the two different hull designs for frequency of 10 MHz and elevation angle of 30 degrees including infinite ground plane.

83
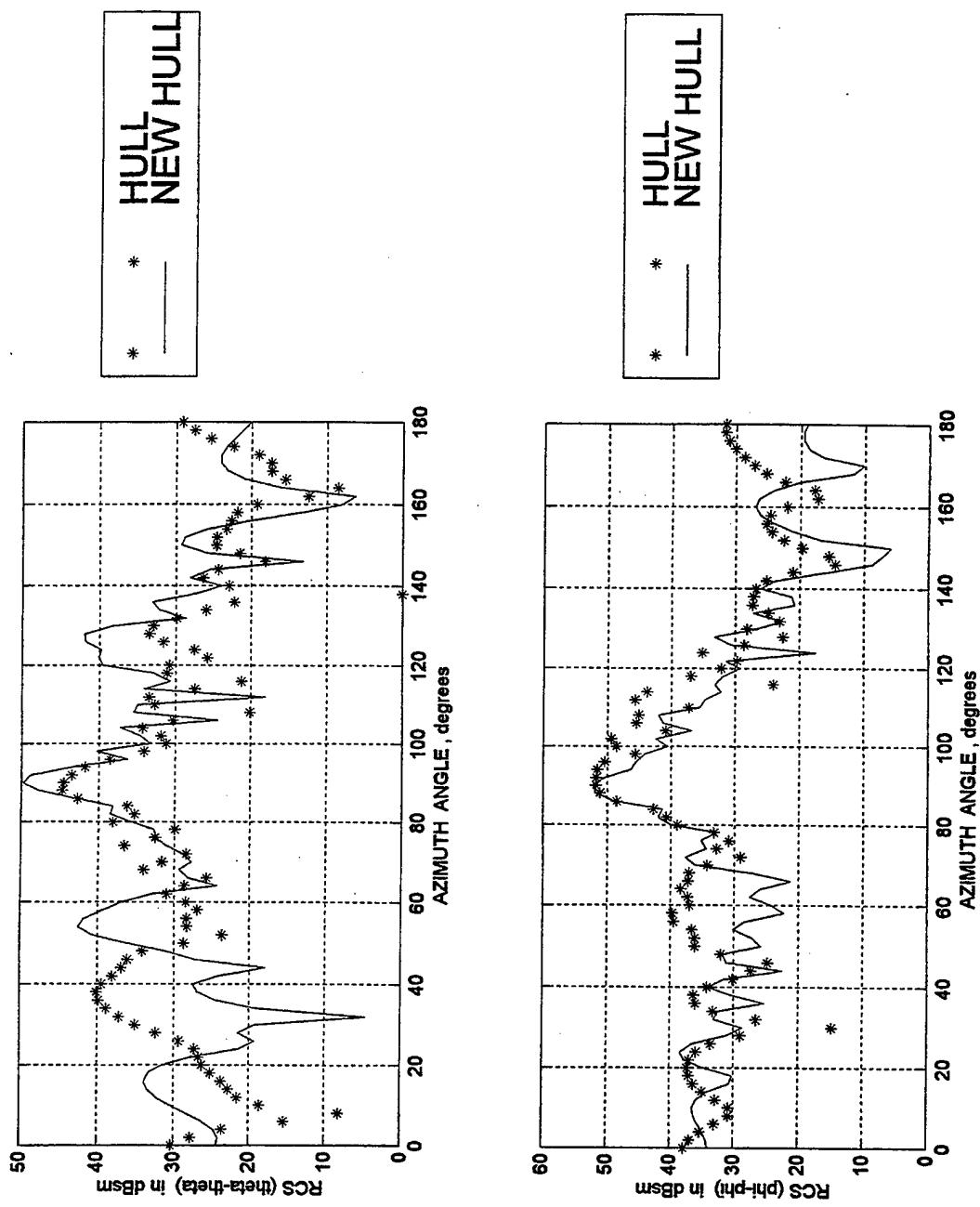
Figure 5-31. Computed RCS of the two different hull designs for frequency of 15 MHz and elevation angle of 30 degrees including infinite ground plane.

84
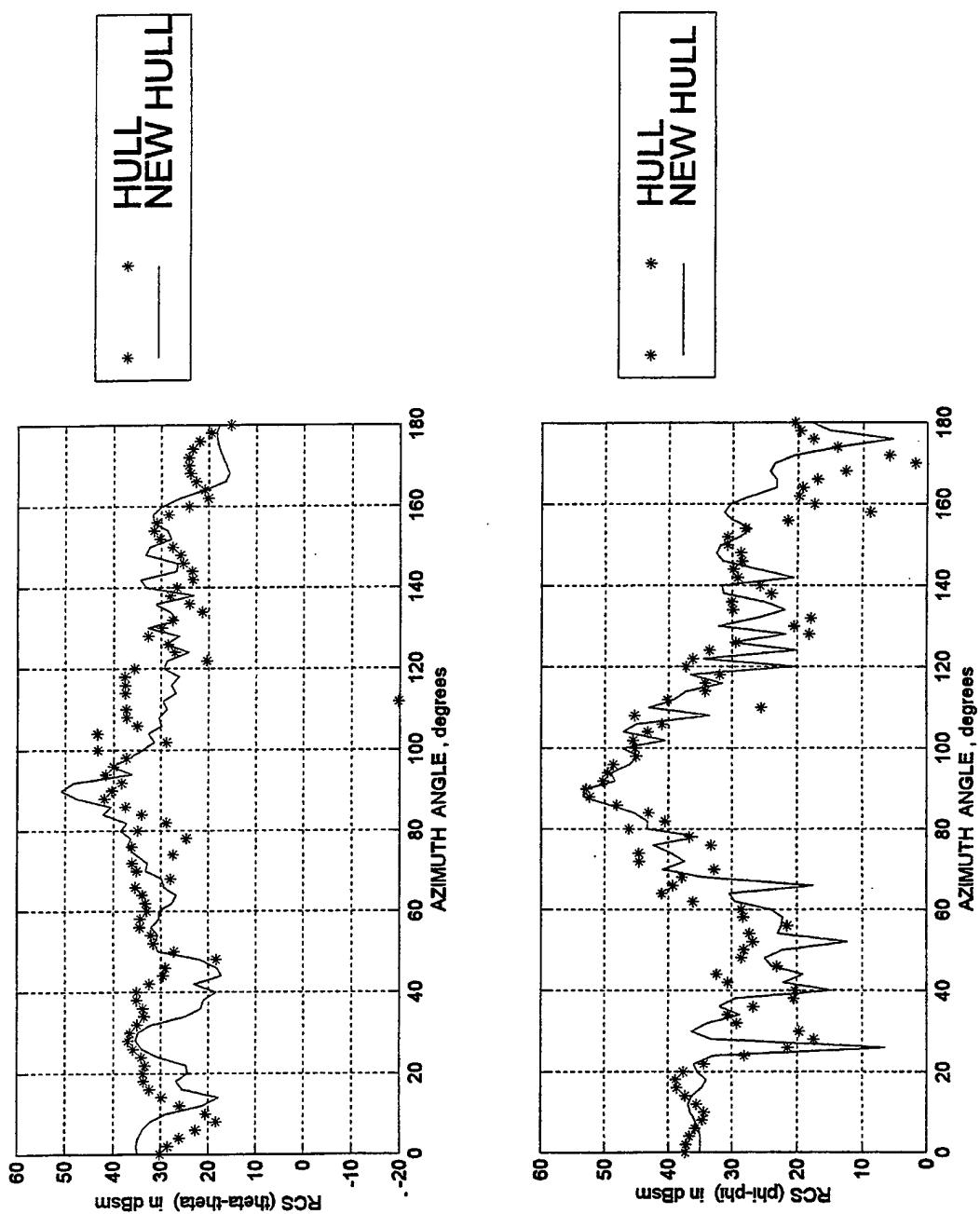
Figure 5-32. Computed RCS of the two different hull designs for frequency of 20 MHz and elevation angle of 30 degrees including infinite ground plane.

85

VI. CONCLUSIONS

Radar cross section reduction plays one of the most important roles in the survivability of all vessels, both ships and aircraft, in the modern theatre of operations. The four basic techniques which are employed in RCS reduction (shaping, radar absorbing materials, active and passive cancellation) have been presented. The significance of shaping, and its effectiveness at optical frequencies has been discussed. The relevant principles of HF radar and propagation have also been introduced.

The objective of this thesis was to investigate and evaluate the effectiveness of HF RCS reduction by means of shaping of a ship superstructure and hull. The results and analysis have been presented in Chapter V. The DDG-51 was used as a baseline to which modifications of the superstructure were made. The ocean surface was represented by an infinite perfect electric conducting plane. Elevation angles from 5° to 30° were considered, which would cover both ground wave and sky wave incidence.

It was found that a ship with canted deckhouse walls similar to the *SEASHADOW* had little reduction in RCS relative to a conventional ship. The explanation is that first, the hull was the major source of scattering at

azimuth angles near broadside and therefore superstructure shaping will not significantly reduce RCS. Second, the deckhouse surfaces are electrically small (on the order of a wavelength). Therefore, the beamwidth of the specularly reflected field is too wide to provide a reduction in RCS. This was illustrated by the RCS of the plate structure in Figure 3-4.

The results clearly indicate that shaping does not improve HF RCS. However, at higher frequencies (S-band through Ku band), it is known that shaping is extremely effective in reducing RCS, and that is sufficient motivation for applying shaping principles to ship design. Almost as important is the conclusion that shaping does not degrade the ship's HF RCS. Note that although in a few instances the RCS of the Mods were greater than the baseline, the Mods have a much larger deckhouse surface area. The Mods are not realistic; the superstructures would be much smaller, which would reduce their RCS. Finally the use of radar absorbing materials (RAM) was not investigated because the objective of the research was to evaluate shaping. The use of RAM would significantly reduce RCS at the HF frequencies.
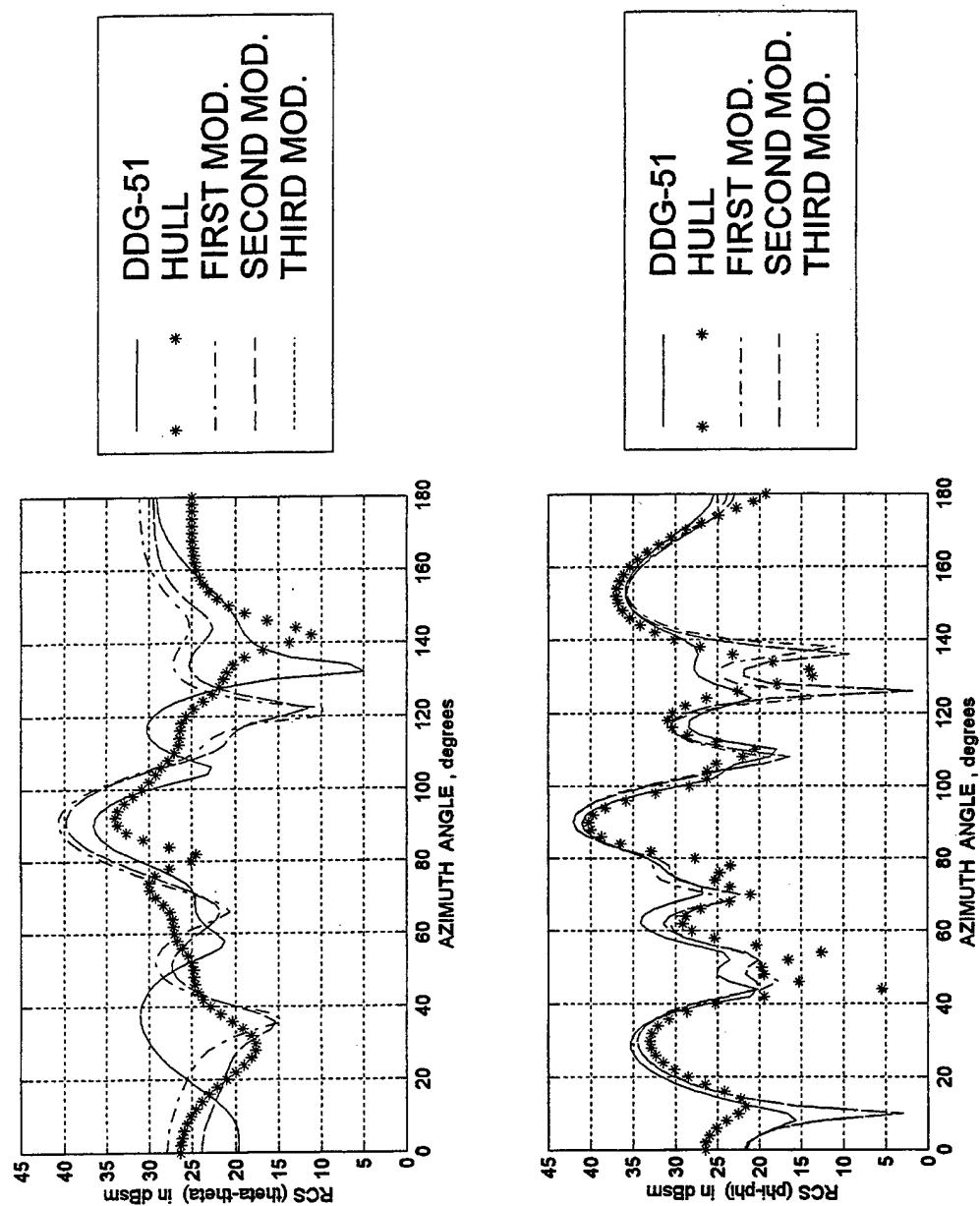
Figure A-1. Computed RCS for frequency of 5 MHz and elevation angle of 10 degrees in free space.
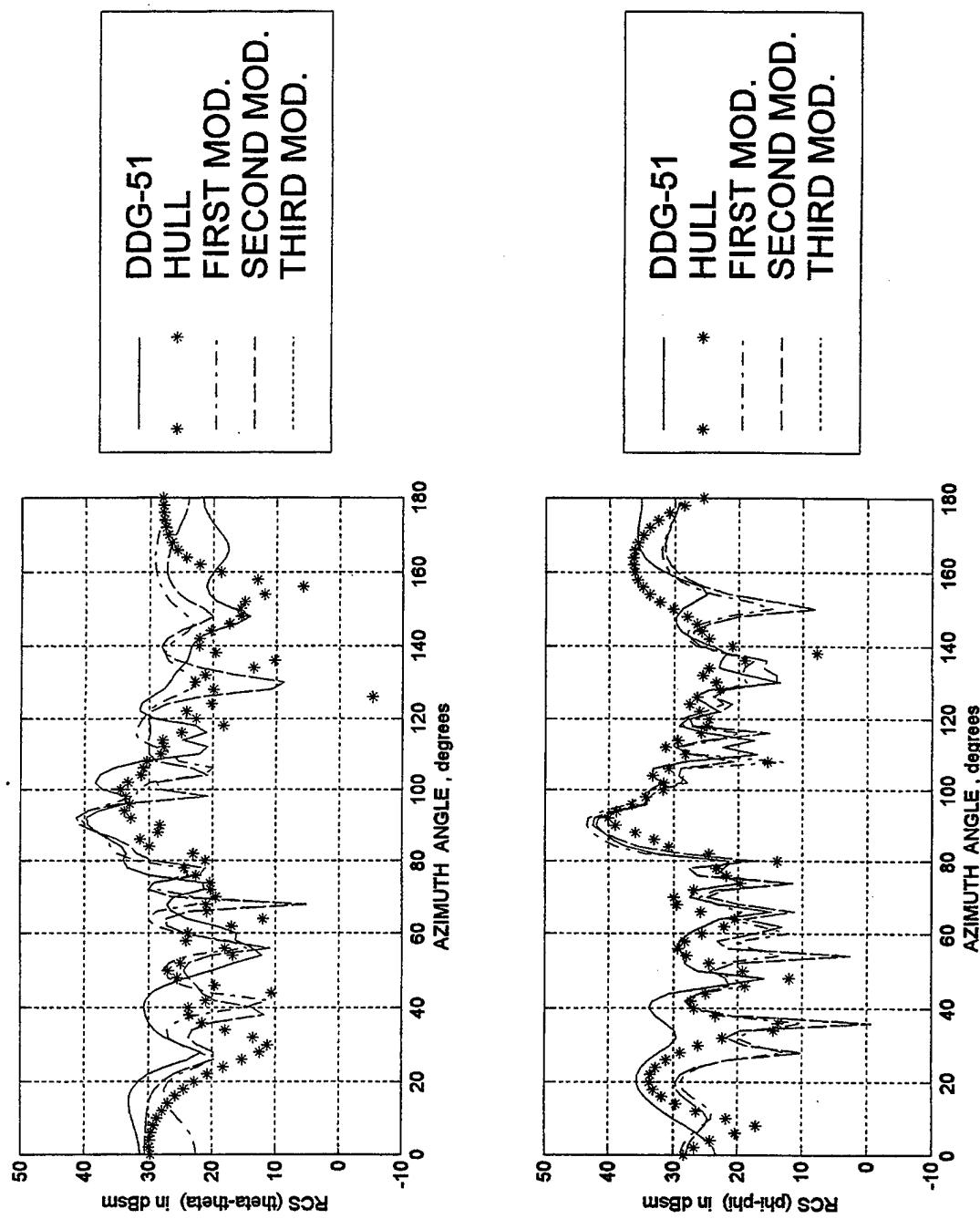
Figure A-2. Computed RCS for frequency of 10 MHz
and elevation angle of 10 degrees in free space.

90
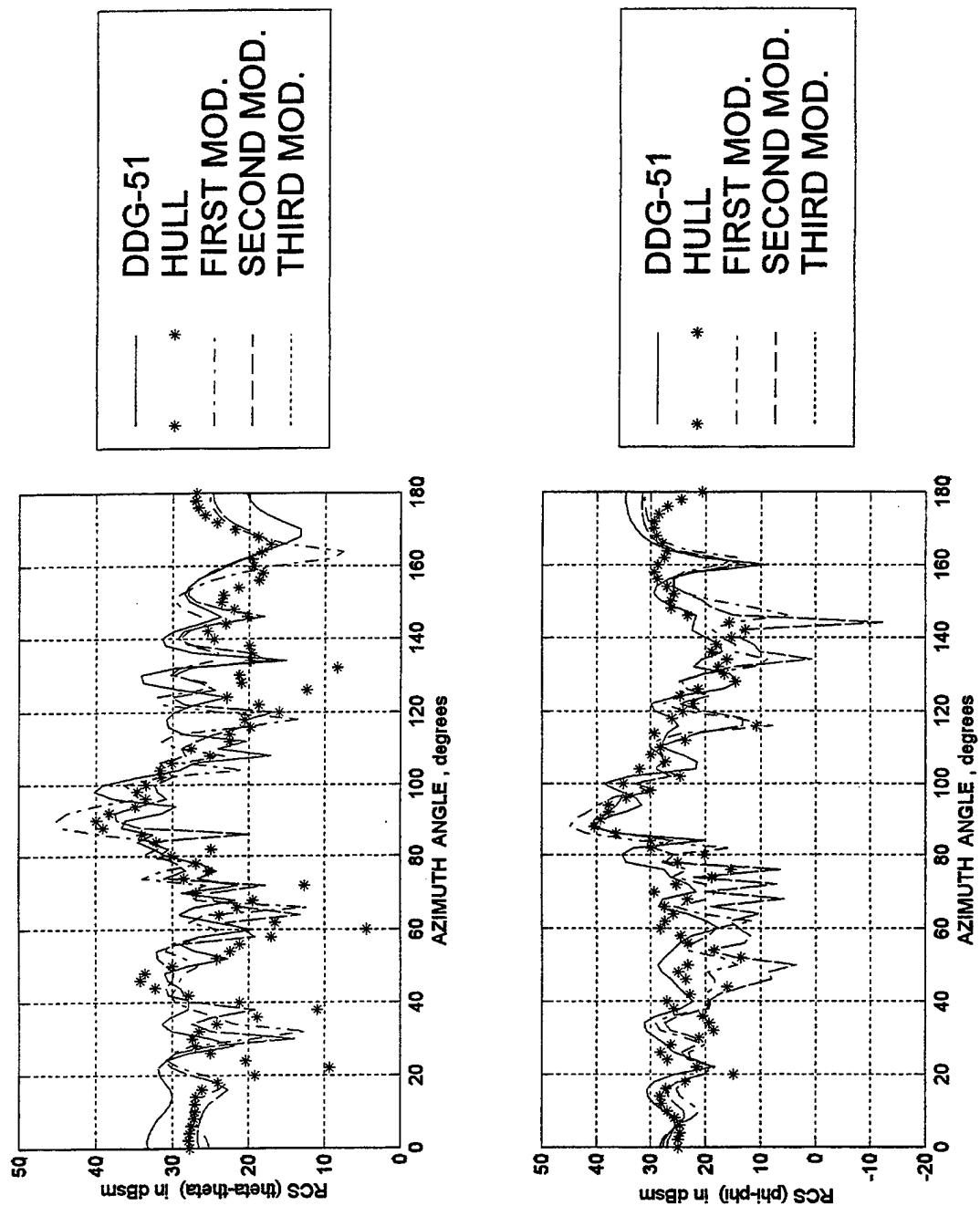
Figure A-3. Computed RCS for frequency of 15 MHz and elevation angle of 10 degrees in free space.

91
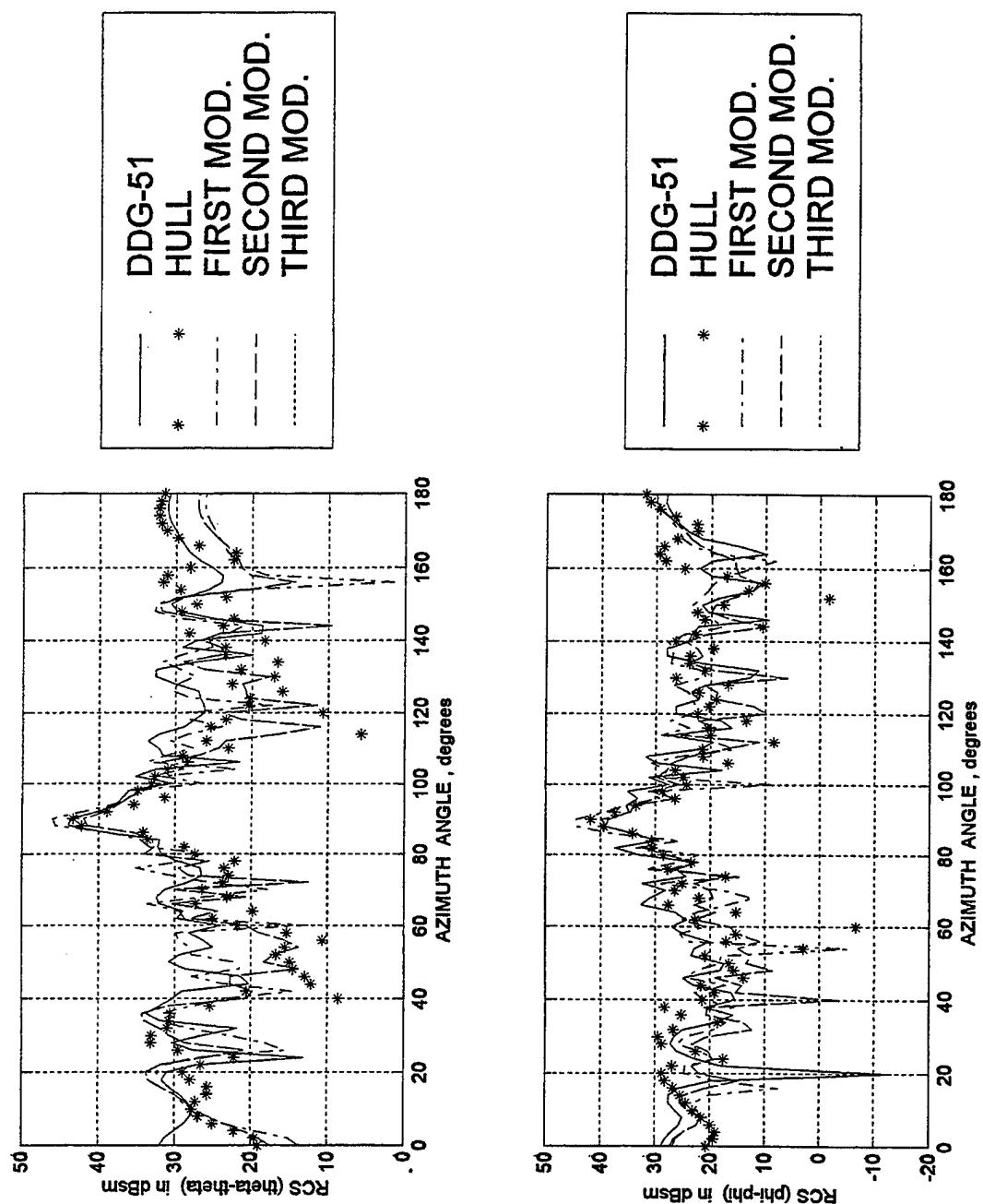
Figure A-4. Computed RCS for frequency of 20 MHz and elevation angle of 10 degrees in free space.

92
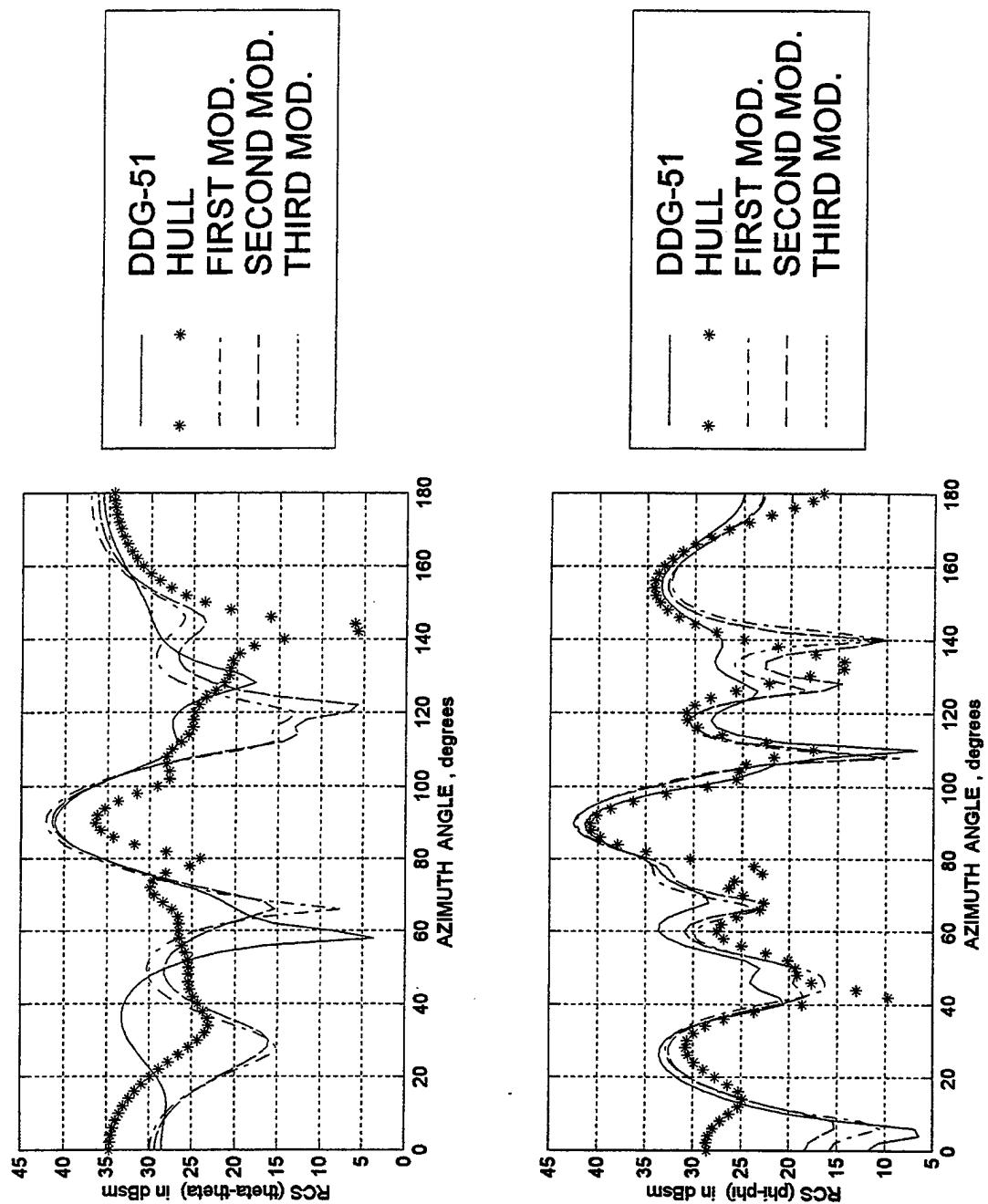
Figure A-5. Computed RCS for frequency of 5 MHz and elevation angle of 20 degrees in free space.

93
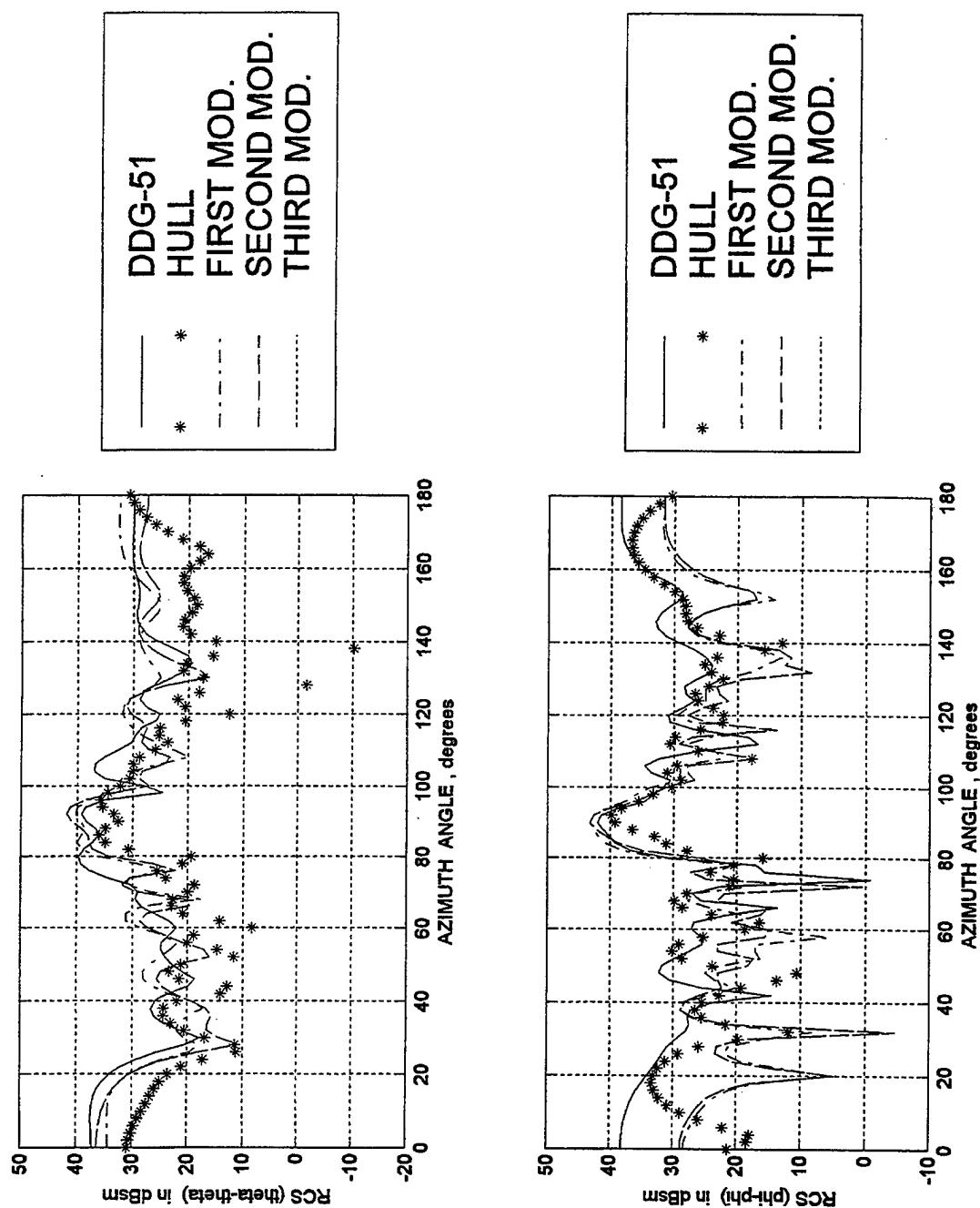
Figure A-6. Computed RCS for frequency of 10 MHz and elevation angle of 20 degrees in free space.

94
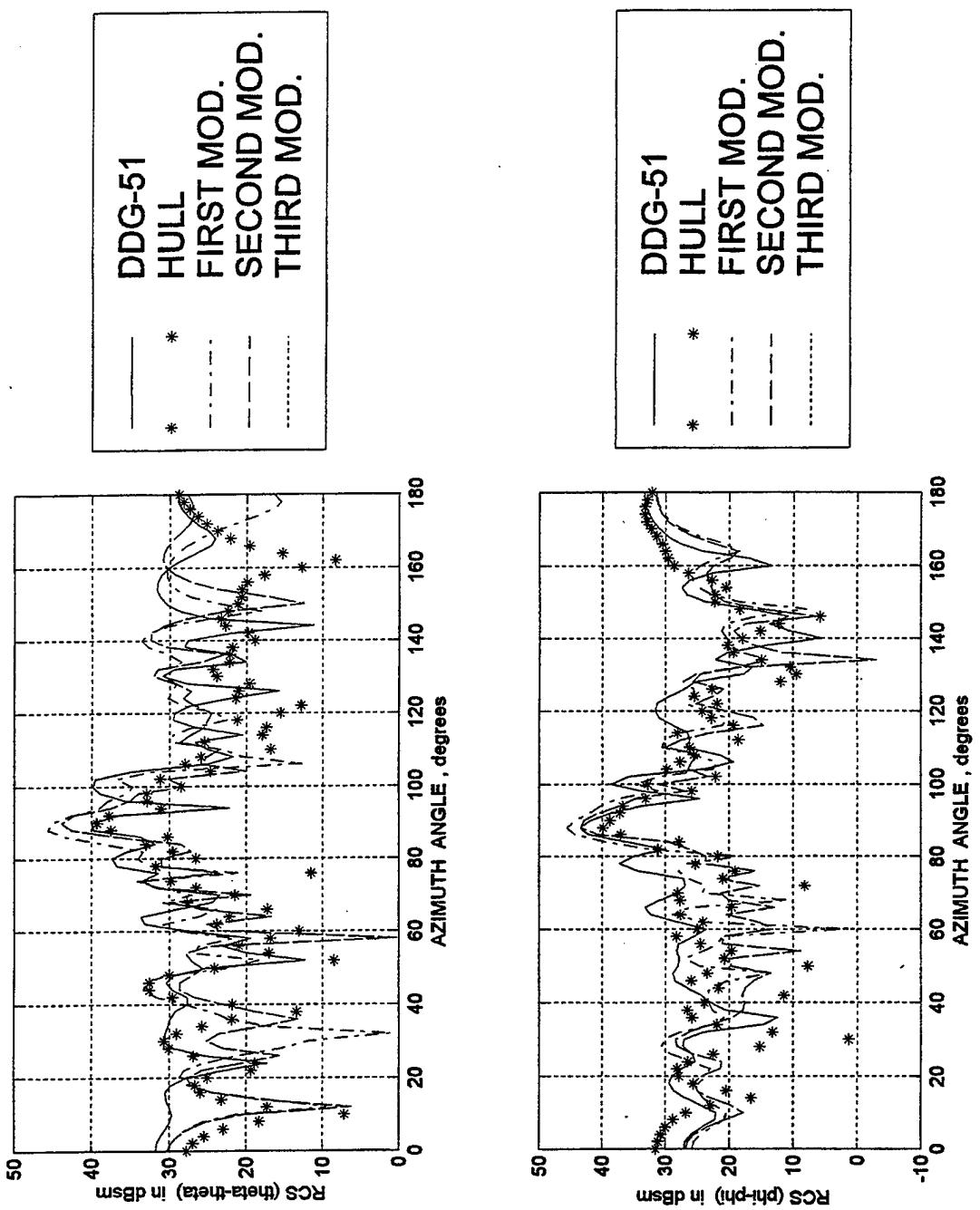
Figure A-7. Computed RCS for frequency of 15 MHz and elevation angle of 20 degrees in free space.
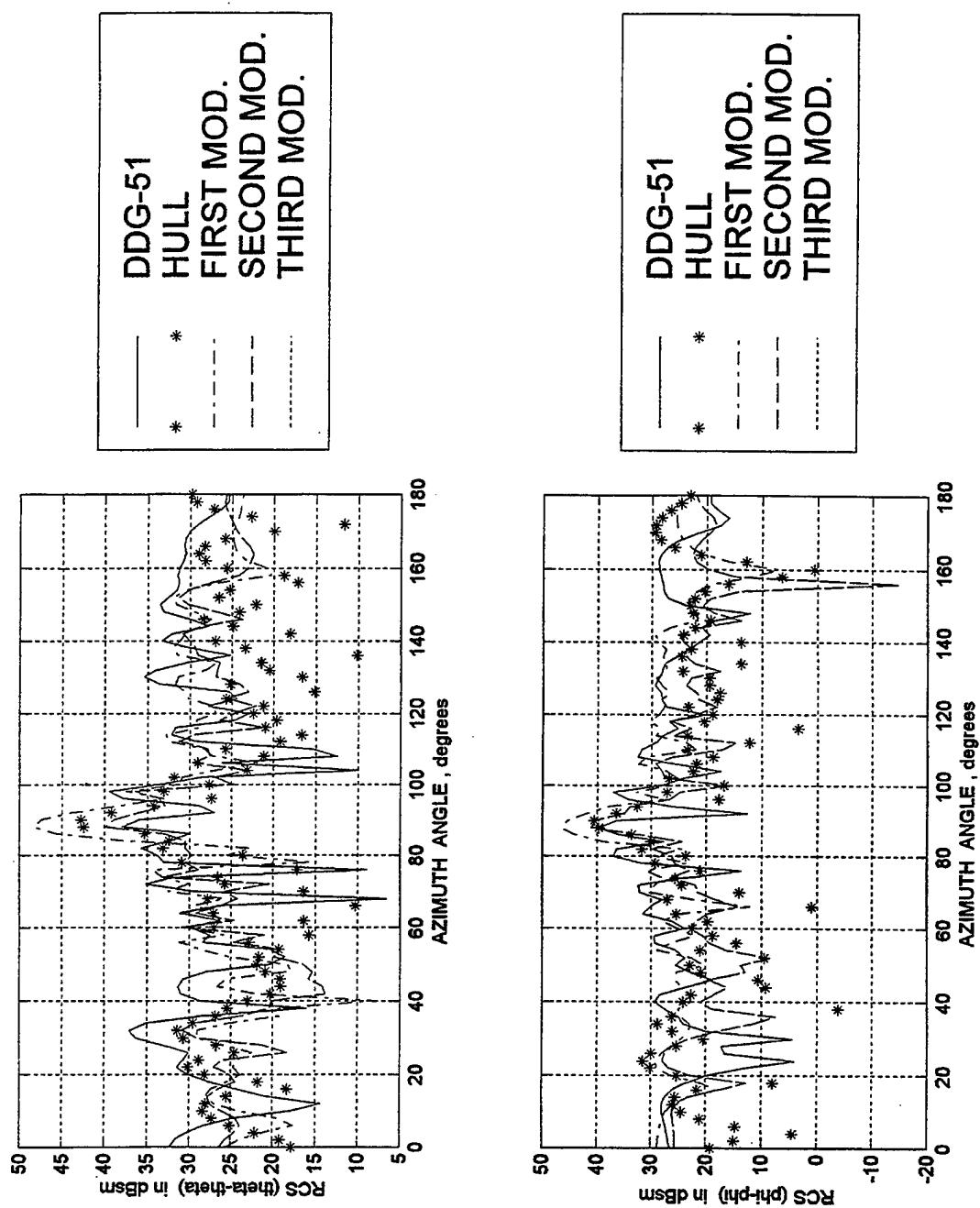
Figure A-8. Computed RCS for frequency of 20 MHz and elevation angle of 20 degrees in free space.

96
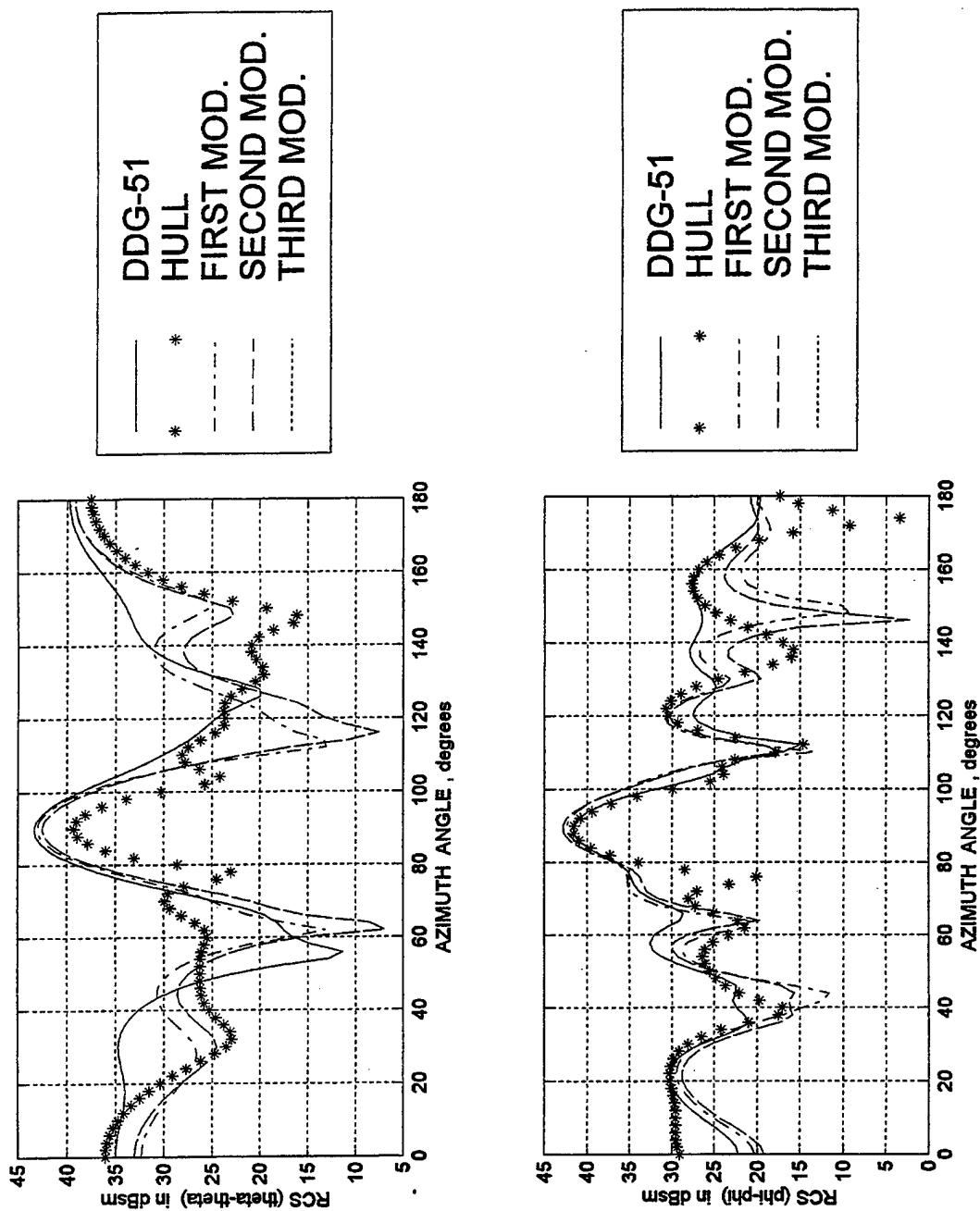
Figure A-9. Computed RCS for frequency of 5 MHz and elevation angle of 30 degrees in free space.
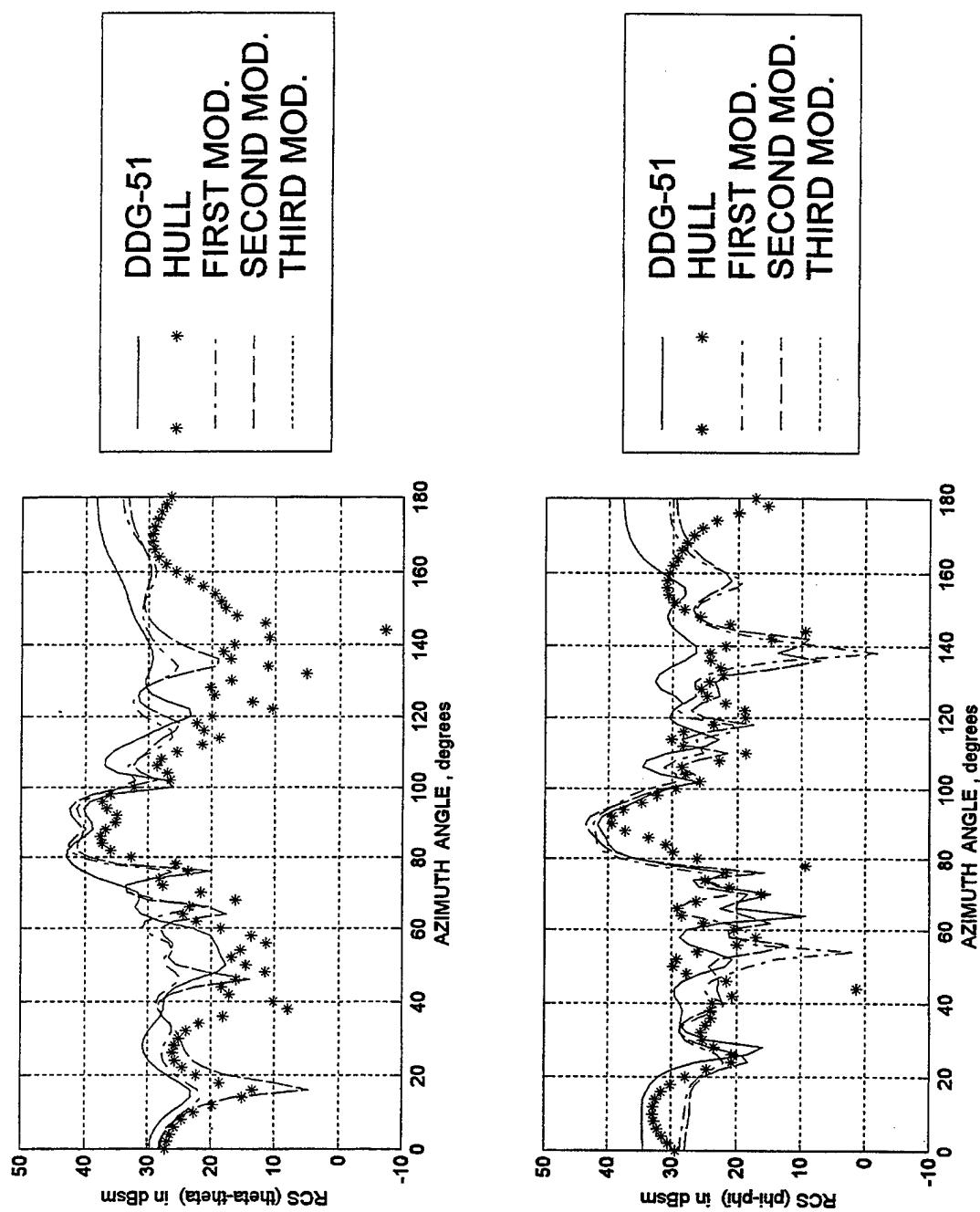
Figure A-10. Computed RCS for frequency of 10 MHz and elevation angle of 30 degrees in free space.
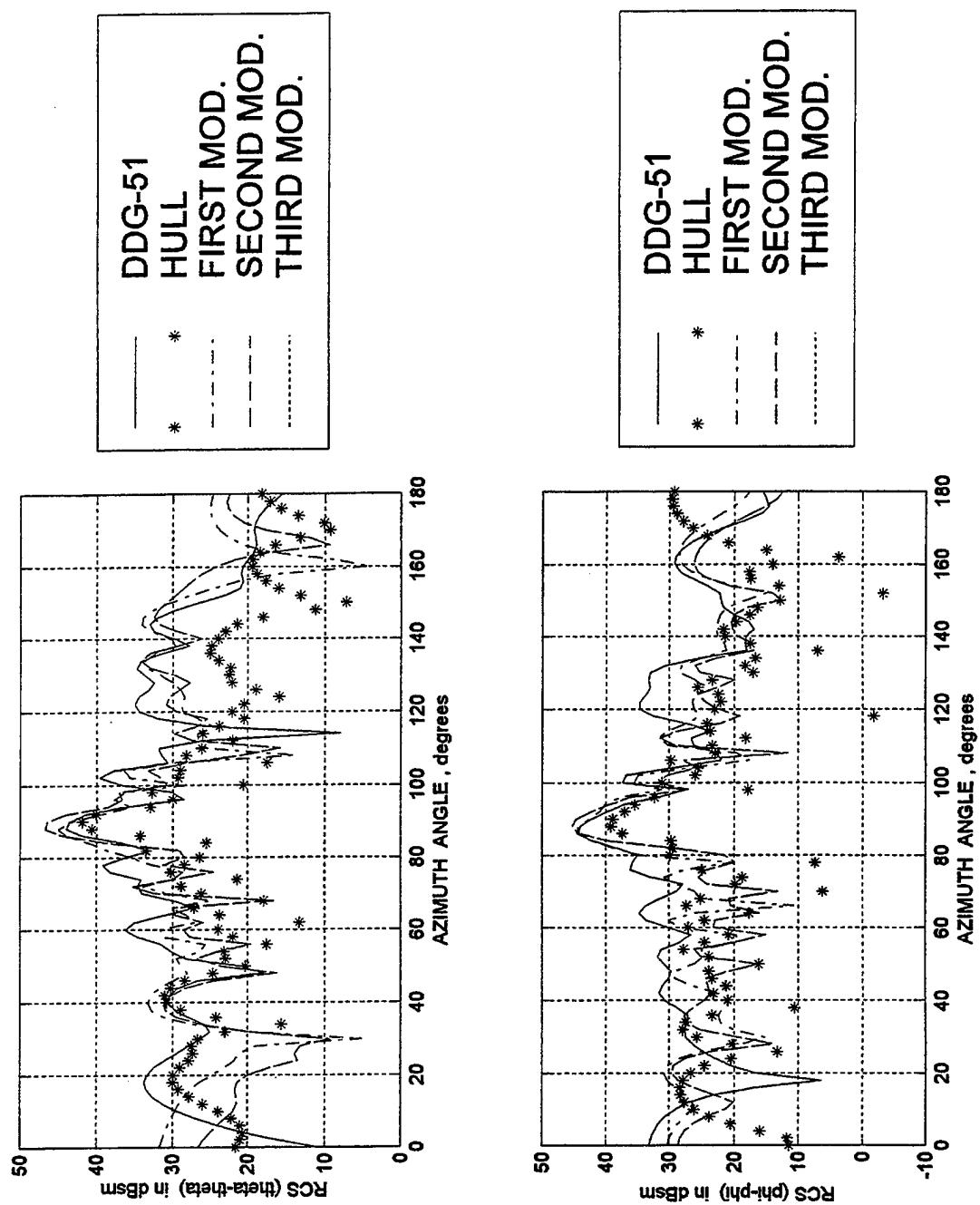
Figure A-11. Computed RCS for frequency of 15 MHz and elevation angle of 30 degrees in free space.
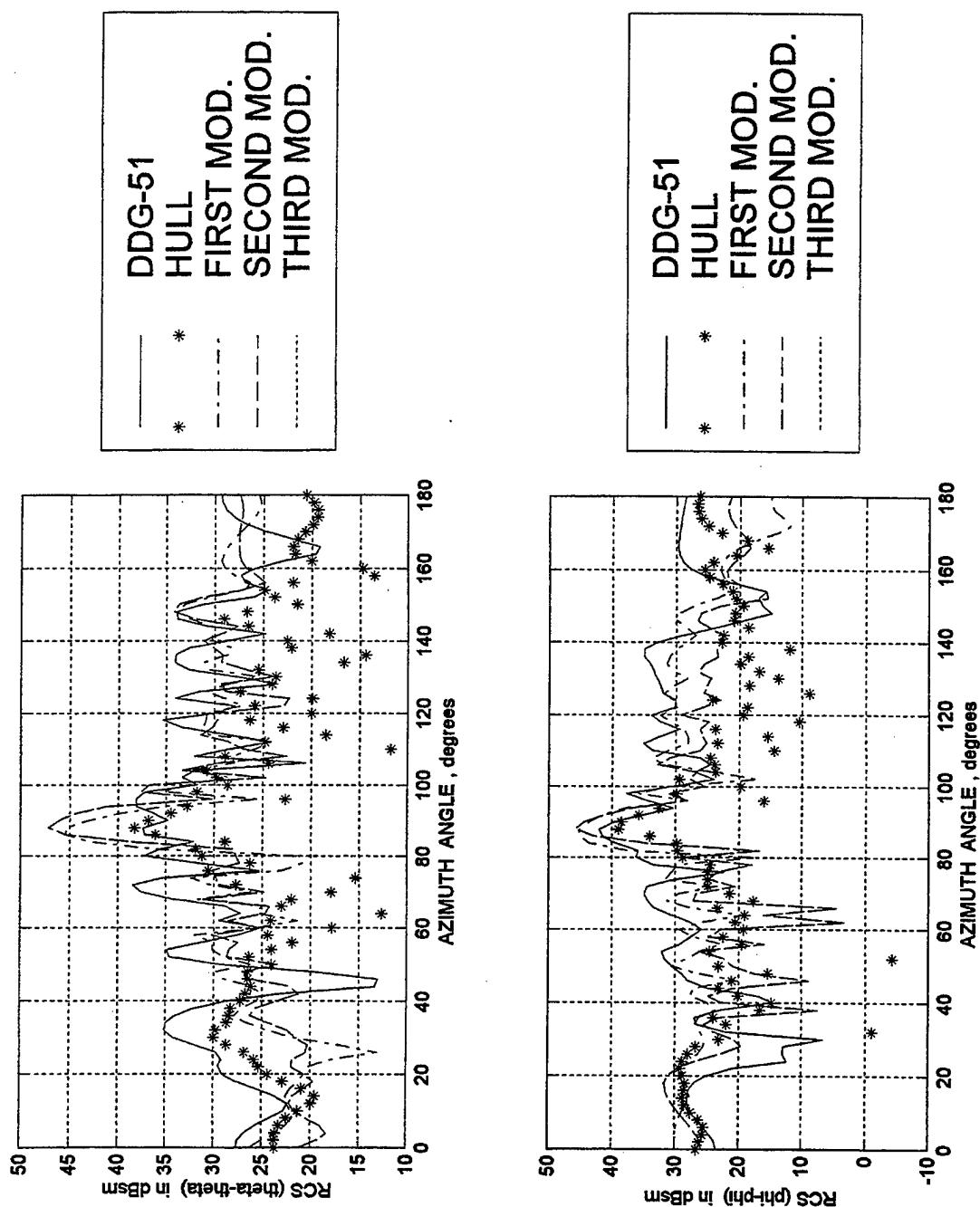
Figure A-12. Computed RCS for frequency of 20 MHz and elevation angle of 30 degrees in free space.

100

LIST OF REFERENCES

1. Jenn, D. C., *Radar and Laser Cross Section Engineering,* AIAA Education Series, AIAA, Washington, DC, 1995.

2. The Lockheed Martin Skunk Works [http://star.pst.qub.ac.uk/~rsir/seashadow.html]. April 1998.

3. "Stealth ship Ytstridsfartyg 2000 (Surface Combatant 2000)." [http://www.geocities.com/CapeCanaveral/Lab/2323/ys2000.htm]. April 1998.

4. "HMS Smyge, Swedish stealth ship." [http://www.geocities.com/CapeCanaveral/Lab/2323/ys2000.htm]. April 1998.

5. Headrick, J. M. and Skolnik, M. I. "Over-the- Horizon Radar in the HF Band," *Proceedings of the IEEE*, Vol. 62, June 1974, pp. 664-673.

6. Skolnik, M. I., *Radar Handbook*, McGraw-Hill Inc, New York.

7. Skolnik, M. I., *Introduction to Radar Systems*, McGraw-Hill Inc, New York.

8. Jenn, D. C., "Microwave Devices and Radar", Lecture Notes for EO4612, Vol IV.

9. Eaves, J. L. and Reedy, E. K. *Principles of Modern Radar,* Van Nostrand Reinhold, New York.

10. Jay, F., (editor in chief), *IEEE Standard Dictionary of Electrical and Electronic Terms*, ANSI/IEEE Std 100-1984, 3rd edition, IEEE Press, New York, 1984.

11. Knott, E. F., Shaeffer, J. F. and Tuley, M. T. *Radar Cross Section,* Artech House, Boston, 1993.

12. Johnson, W., *Patch Code Users' Manual,* Sandia Report SAND87-2991, May 1988.

13. *The ACAD User's Manual,* Lockheed Martin Corp., Ft. Worth, April 1995.

14. *ACAD Reference Set - Volume 1*, Lockheed Martin Corp., Ft. Worth, April 1995.

15. CAPT. Ken Webb and CDR. Al Greco, "Operational, Performance, and Technical Challenges of the DD-21 Program," presentation of American Society of Naval Engineers, NPS, April 1998.

16. Keller, J. B., "Diffraction by an Aperture," *J. App. Phys.*, Vol. 28, No. 4, April 1957, pp. 426-444.

INITIAL DISTRIBUTION LIST

No. of Copies

1. Defense Technical Information Center 2
   8725 John J. Kingman Rd., STE 0944
   Ft. Belvoir, Virginia 22060-6218

2. Dudley Knox Library................................2
   Naval Postgraduate School
   411 Dyer Rd.
   Monterey, California 93943-5101

3. Chairman, Code EC.................................1
   Department of Electrical and Computer Engineering
   Naval Postgraduate School
   Monterey, California 93943-5101

4. Chairman, Code PH/Mw..............................1
   Department of Physics
   Naval Postgraduate School
   Monterey, California 93943-5101

5. Professor David C. Jenn, Code EC/Jn...............1
   Department of Electrical and Computer Engineering
   Naval Postgraduate School
   Monterey, California 93943-5101

6. Professor David D. Cleary, Code PH/Cl.............1
   Department of Physics
   Naval Postgraduate School
   Monterey, California 93943-5101

7. Professor Jeffrey B. Knorr, Code EC/Ko............1
   Department of Electrical and Computer Engineering
   Naval Postgraduate School
   Monterey, California 93943-5101

8. Embassy of Greece................................ 1
   Naval Attache
   Ministry of Defence
   2228 Massachusetts Av., NW
   Washington, DC 20008

9. Dimitrios Kouteas.................................. 2
    Melpomenis 26 St.
    155-61 Cholargos
    Athens
    Greece